GLOBAL MODELING STUDY OF AEROSOL INDIRECT EFFECTS IN MIXED-PHASE CLOUDS

by

Yuxing Yun

A dissertation submitted in partial fulfillment

of the requirements for the degree of

Doctor of Philosophy

(Atmospheric and Space Sciences)

in The University of Michigan

2013

Doctoral Committee:

Professor Joyce E. Penner, Chair

Associate Professor Xianglei Huang

Associate Professor Allison L. Steiner

Assistant Professor Gregory James Dick

Assistant Professor Mark G. Flanner

Assistant Professor Derek J. Posselt

Acknowledgements

I would like to express my gratitude to all the people who helped me to complete this thesis. First of all, I would like to thank my advisor, Prof. Joyce E. Penner. Without her support, this work could not even be possible. Her patience and encouragement was vital in my growth from a fresh college graduate to a young researcher. I'm grateful that she gave me ample freedom to pursue the scientific questions that intrigue me. Her sharp vision and broad knowledge inspires me to reach higher goals. Her scientific attitude and working ethics set a great example in my future career. She also gave me many opportunities to attend scientific conferences, which was a great benefit.

I would also like to say thank you to my dissertation committee, Prof. Xianglei Huang, Prof. Allison L. Steiner, Prof. Mark Flanner, Prof. Derek J. Posselt, and Prof. Gregory J. Dick. I sincerely appreciate the constructive comments that you provided to my thesis work, and your help in many aspects of my career. I'm grateful to Dr. Minghuai Wang at PNNL for the valuable scientific discussions and Roy Chen at University of Michigan for the instructive coding advice that helped me tremendously during the early years of my research here. I'd like to thank Dr. Olga Popovicheva at Moscow State University who collaborated with me in the second part of my PhD research.

It was a great experience to work with many talented people in our group: Yang, Huan, Li, Luis, Cheng, Guangxing, Xi, and Erika. I appreciate the constructive comments that you provided during our group meetings, and also for the friendship and companionship that you shared with me. I'm grateful to all my friends at AOSS and University of Michigan, who made my memory of here a fond and loving one.

Last but not least, I would like to thank my family. I can never be where I am now without you. Especially, I would like to thank my mom for her selfless support and sacrifice during all these years. I'm also grateful for my boyfriend for his understanding and support.

Table of Contents

List of Figures

List of Tables

Abstract

Aerosol indirect effects (AIE) remains one of the largest uncertainties in understanding and projecting anthropogenic climate change. This study aims to improve the understanding of the aerosol indirect effect in mixed-phase clouds by studying the heterogeneous ice nucleation parameterization and aerosol-cloud interactions.

The first part of the dissertation enabled the assessment of aerosol indirect effects in mixed-phase clouds by implementing aerosol-dependent heterogeneous ice nucleation parameterizations into coupled CAM3+ and aerosol transport model IMPACT (CAM-IMPACT). An improvement to current parameterization to make it consistent with observation was also suggested. The effect of different parameterizations on cloud liquid/ice water amount, cloud radiative forcing and anthropogenic aerosol forcing were compared. Model results were evaluated against satellite observations (ISCCP, CERES, and MODIS) of cloud fraction, liquid/ice water path, and cloud forcing, as well as in-situ observation of statistical distributions of cloud ice fraction. The aerosol-dependent freezing parameterization predicts less ice water path (IWP) than the original formulation, especially in the Southern Hemisphere. The net solar flux at top of atmosphere (FSNT), and net long-wave flux at the top of the atmosphere (FLNT) changes by up to 8.73 W/m^2

and 3.52 W/m^2, respectively, due to the use of different parameterizations in mixed-phase clouds.

In the second part of the dissertation, a 3-(hydrophobic, hydrophilic, and hygroscopic) soot scheme is developed, which provides a link between sulfuric acid coating, hygroscopicity, and ice nucleation efficiencies, according to laboratory observation. The distribution and burden of soot with different hygroscopicity were analyzed and presented. An offline radiation model was updated to include ice nucleation and liquid-ice interaction for mixed-phase cloud, and used to compare mixed-phase cloud AIE using with 3-soot scheme and 1-soot scheme. The new scheme results in significant changes to anthropogenic forcing in mixed-phase clouds. The net forcing in off-line studies varies from 0.111 to 1.059 W/m^2 depending on the ice nucleation capability of hygroscopic soot particles. The total anthropogenic cloud forcing and whole-sky forcing with the new scheme is 0.06 W/m^2 and -2.45 W/m^2, respectively.

The third part of this study is an assessment of the effect of marine organic aerosol (MOA) as ice nuclei on a global scale. The emission, transport, deposition, and ice nucleation for MOA were implemented into the coupled CAM-IMPACT model. Multiple sensitivity experiments were designed to test the effect of sea-spray emission functions, organic enrichment functions, and MOA ice nucleation efficiencies. The distribution and burden of MOA were analyzed. The modeled ice water path and cloud radiative forcing were evaluated against various satellite observations. The changes to anthropogenic AIE with

the addition of the natural marine organic ice nuclei were assessed. MOA is found to be

the dominant ice nuclei species compared to dust and soot. The comparison of ice water

path to ISCCP observation improves when MOA is included as ice nuclei.

CHAPTER 1

Introduction

1.1   The global climate system

The global climate system is an internally coupled system between the atmosphere, the lithosphere, the hydrosphere, the biosphere, and the cryosphere. Fluxes of mass, heat, and momentum are exchanged between them on a variety of space and time scales. The atmosphere is the most unstable and rapidly changing part of the system. In common notion, "weather" is the fluctuating state of the atmosphere, while "climate" is the average state of weather. Climate is not only determined by the atmosphere circulation and composition, but also by the interaction with ocean currents, land albedo, soil moisture, sea ice coverage, etc. Therefore, to understand climate and its variations, we must understand the climate system.

The climate system receives energy from the sun on average of 340.2 ± 0.1 W/m^2 at the top of the atmosphere [*Kiehl and Treberth*, 1997]. This is the ultimate source of energy that drives the various activities in the system. Among this energy, 100.0 ± 2 W/m^2 is immediately reflected back to space by the Earth's surface, clouds, and the atmosphere.

The remaining 240.2 W/m^2 is partially absorbed by the atmosphere, but most by the Earth's surface. To maintain energy balance, the earth emits energy partially as infrared radiation, partially as sensible heat, and partially as water vapor which releases latent heat when it condenses. There is a small energy imbalance at the top of the atmosphere (0.6±0.4 W/m^2). Figure 1.1 illustrates the earth annual global energy balance. The left hand side shows what happens with the incoming solar radiation, and the right hand side shows what happens with the outgoing longwave radiation. According to Planck's Law, any physical object radiates energy of an amount and at wavelengths typical for the temperature of the object. For the Earth to radiate 240.2 W/m^2, it should radiate at an effective emission temperature of −19°C. This is 33°C lower than the average Earth surface temperature (14°C). To understand this, one must take into account of the greenhouse effect.
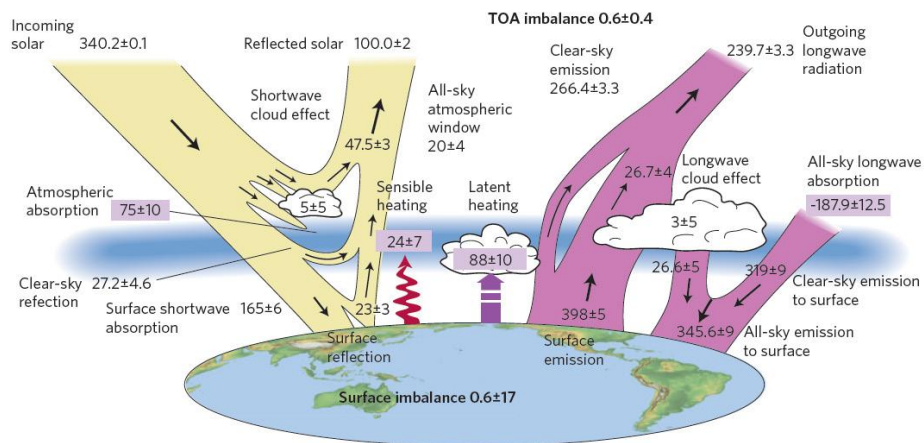
Figure 1.1: The Earth's radiation and energy balance (IPCC TAR)

Greenhouse gases (GHG) absorb the infrared radiation emitted by the Earth's surface and the atmosphere, and re-emit them in all directions, including downwards to the Earth's surface. Due to the presence of the greenhouse gases, only a small fraction of the total thermal radiation from the Earth escapes to the space, while the remaining is trapped within the atmosphere. This leads to a global mean temperature (14ºC) which is 33ºC higher than it would be if there were no greenhouse gases (-19ºC). This is the so called greenhouse effect.

1.2   Anthropogenic climate change

The radiation balance of the climate system can be perturbed by external forces. These perturbations will cause an energy imbalance and may potentially lead to climate change. Climate change is referred to as the statistically significant variations of the mean state of the climate or of its variability, persisting for decades or longer (IPCC TAR).

The external forces that cause the perturbation to the energy balance can be natural such as the variation of solar irradiance, the Earth orbit changes, and ejection of a large amount of aerosols by volcano eruption. Since the industrial revolution in the mid-18th century, human activities have significantly changed the atmospheric constituents by releasing greenhouse gases and aerosol particles through fossil fuel burning, biomass burning, and other activities. This causes the anthropogenic climate change. Their effect

to climate changes has been described by the Intergovernmental Panel on Climate Change (IPCC) as:

"Greenhouse gases and aerosols affect climate by altering incoming solar radiation and out- going infrared (thermal) radiation that are part of Earth's energy balance. Changing the atmospheric abundance or properties of these gases and particles can lead to a warming or cooling of the climate system. Since the start of the industrial era (about 1750), the overall effect of human activities on climate has been a warming influence. The human impact on climate during this era greatly exceeds that due to known changes in natural processes, such as solar changes and volcanic eruptions."

As Figure 1.2 shows, the observed global mean surface temperature has increased by 0.74ºC over the last 100 years. Figure 1.2 a compares the observed surface temperature increase to that simulated with both natural and anthropogenic forcing. Figure 1.2 b compares the same observation to that simulated with only natural forcing. It is clear that this observed temperature increase cannot be reproduced by including natural perturbations only, such as variations in solar radiance and volcano eruptions. Anthropogenic perturbations need to be taken into account of to reproduce the observed temperature change.

This warming produced by anthropogenic activities gives rise to a series of problems, e.g. sea level rise, reduction of snow and ice coverage, thawing of permafrost, searing heat waves, and more intensive precipitation. These consequences pose significant threats to our society and challenge the climate research community to explore the underlying physical mechanisms and offer accurate predictions of future climate change.

1.3   Radiative forcing and its uncertainty

The magnitude of the external perturbation from natural or anthropogenic sources is measured in terms of radiative forcing, which is defined as the net radiative imbalance at the tropopause caused by the external forcing agent. A positive forcing tends to warm the surface, while a negative forcing tends to cool it. Radiative forcing can be related to the global mean equilibrium temperature change at the surface through the follow relationship:

$$\Delta T_s = \lambda \Delta F$$

Here ΔF is the radiative forcing, ΔT_s is the global mean surface temperature change, and λ is the climate sensitivity. Radiative forcing is a simple measure for both quantifying and ranking the many different influences on climate change. Since introduced in early studies of the climate response to change in solar irradiance and CO_2 [*Manabe and*
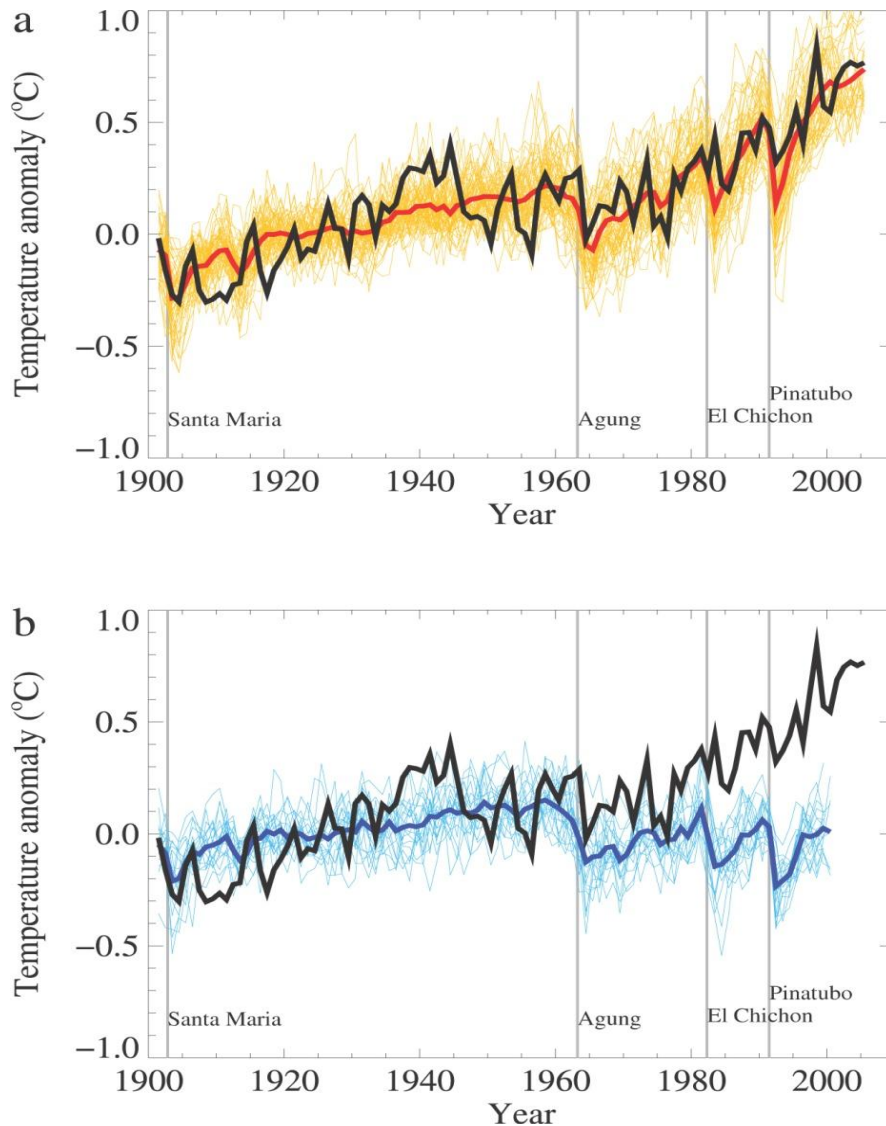
Figure 1.2: Comparison between global mean surface temperature anomalies (°C) from observations (black) and AOGCM simulations forced with (a) both anthropogenic and natural forcings and (b) natural forcings only. All data are shown as global mean temperature anomalies relative to the period 1901 to 1950, as observed (black, Hadley Centre/Climatic Research Unit gridded surface temperature data set (HadCRUT3); Brohan et al., 2006) and, in (a) as obtained from 58 simulations produced by 14 models with both anthropogenic and natural forcings. The multi-model ensemble mean is shown as a thick red curve and individual simulations are shown as thin yellow curves. Vertical grey lines indicate the timing of major volcanic events. The simulated global mean temperature anomalies in (b) are from 19 simulations produced by five models with natural forcings only. The multi-model ensemble mean is shown as a thick blue curve and individual simulations are shown as thin blue curves. (Adopted from IPCC AR4)

Moller, 1961; *Manabe and Wetherald*, 1967], radiative forcing has been widely used to assess and compare the natural and anthropogenic drivers of climate change.

Figure 1.3 shows the contribution to radiative forcing from both natural and human-induced changes between 1750 and 2005. The long-lived greenhouse gases cause the largest warming (2.63 ± 0.24 W/m^2). However, their forcing is well defined with an uncertainty of only about 10% because of their long lifetime and homogeneous distribution. Among the greenhouse gases, CO_2 has the largest contribution. Tropospheric ozone, stratospheric water vapor, contrail, and black carbon on snow all cause a warming effect. Stratospheric ozone, land use change, and aerosol cause cooling effects. In all, total anthropogenic forcing has a best estimate of 1.6 W/m^2, with an uncertainty range from 0.6 to 2.4 W/m^2. The largest source of uncertainty comes from the effect of aerosols. The total radiative forcing of aerosols is -1.2 W/m^2, with a large uncertainty range from -0.2 to -2.3 W/m^2. The largest estimate is almost enough to offset the warming produced by greenhouse gases. So the reduction in the uncertainty of aerosol forcing is essential to better understand the anthropogenic climate change, and in improve the projection of future climate change.

Figure 1.3: Summary of the principal components of the radiative forcing of climate change. All these radiative forcings result from one or more factors that affect climate and are associated with human activities or natural processes as discussed in the text. The values represent the forcings in 2005 relative to the start of the industrial era (about 1750). The thin black line attached to each colored bar represents the range of uncertainty for the respective value. (Figure adapted from IPCC AR4.)

1.4   Aerosol direct and indirect effects

Aerosols are liquid or solid particles suspended in the air. They can be of natural origin such as windborne dust, sea spray, volcano emission, pollen, spore, and bacteria. They can also be from anthropogenic origin such as sulfate, black carbon (BC) and organic carbon (OC) that are generated from fossil fuel and biomass burning. Another useful distinction is between primary and secondary aerosols. Primary aerosols are directly emitted from the sources, while secondary aerosols are generated through chemical reactions within the atmosphere. The size of the aerosol particles can range from a few nanometers to around 100 μm. They go through a life cycle in the atmosphere which includes emission, chemical reactions, nucleation, coagulation, condensation, cloud processing, dry deposition, and wet deposition.

Despite their small sizes, aerosols particles can affect the climate in a number of ways. Figure 1.4 is a schematic diagram showing the various mechanisms. Aerosols can scatter and absorb shortwave and longwave radiation, thereby altering the radiative balance of the Earth-atmosphere system. This is the so-called aerosol direct effects (ADE). Aerosols can also act as cloud condensation nuclei (CCN), and through that modify the microphysical and hence the radiative properties, amount and lifetime of clouds. This is the so called aerosol indirect effects (AIE). The aerosol indirect effect can be split into the first indirect effect and the second indirect effect. The first indirect effect, the "cloud albedo effect", or the "Twomey effect", refers to the increase of cloud droplet number

and decrease of cloud droplet size induced by the anthropogenic aerosol emission increase, with the liquid water content held fixed. The second indirect effect, the "cloud lifetime effect", or the "Albrecht effect", refers to the suppression of drizzle with decreased cloud droplet size, thereby the increase of liquid water content (LWC), the increase of cloud height and cloud lifetime. Aerosols can also cause indirect effect on ice clouds, mix-phase clouds, and contrails by acting as ice nuclei (IN). Absorbing aerosols can heat the atmosphere, and causes cloud burn-off which reduces large-scale cloud fraction. This is term as semi-direct effect. Besides these, aerosols can also change snow albedo by depositing dark particles (soot, dust) on snow surfaces, and affect the biogeochemical cycles by providing nutrients such as nitrate and iron to the land and ocean biological communities, among others.

Global modeling is the primary tool for estimating the aerosol indirect effects. The anthropogenic aerosol indirect effect is usually estimated using a General Circulation Model (GCM), by conducting a present-day simulation and a pre-industrial simulation, with fixed sea surface temperature and CO_2 concentration. However, there are large uncertainties in model estimates. The current scientific understanding for aerosol direct effect is classified as "medium to low" and that for the cloud albedo effect is "low" by IPCC AR4. No best estimate even exists for aerosol indirect effects in ice cloud, mixed-phase clouds, and contrails, due to the uncertainty and unknowns surrounding ice cloud nucleation and physics. This dissertation tackles the aerosol indirect effect in mixed-phase clouds.
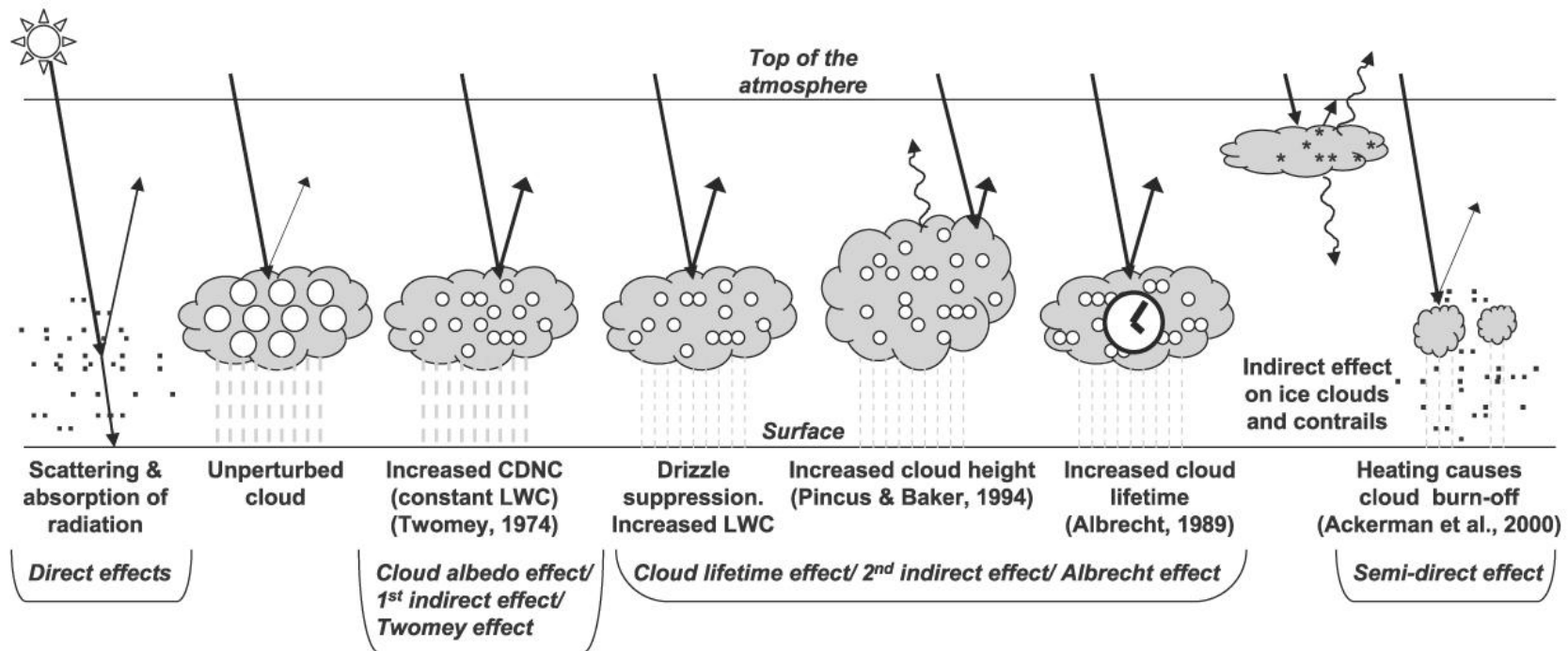
Figure 1.4: Schematic diagram showing the various radiative mechanisms associated with cloud effects that have been identified as significant in relation to aerosols (modified from Haywood and Boucher, 2000). The small black dots represent aerosol particles; the larger open circles cloud droplets. Straight lines represent the incident and reflected solar radiation, and wavy lines represent terrestrial radiation. The filled white circles indicate cloud droplet number concentration (CDNC). The vertical grey dashes represent rainfall, and LWC refers to the liquid water content. (adopted from IPCC AR4)

1.5   Aerosol indirect effects in mixed-phase clouds

Mixed-phase clouds (clouds that typically occur between 0°C and -40°C and contain both ice particles and supercooled liquid droplets) cover about 22% of the earth [*Warren et al.,* 1988 a, b] and have a substantial influence on climate. The aerosol indirect effect in mixed-phase clouds is more complex than that in pure warm or ice clouds, due to the coexistence and interaction of liquid and ice particles. The increased anthropogenic aerosol emission will not only affect the mixed-phase cloud microphysics as cloud condensation nuclei, but also as ice nuclei. At the same subfreezing temperature, the saturation vapor pressure over ice is smaller than that over water. As a result, water vapor will condense onto existing ice crystals, while liquid droplets will evaporate to compensate for the depleted water vapor. This is the so-called Bergeron-Findeisen process (Figure 1.5). This will cause rapid growth of the ice crystals and depletion of liquid droplets, and is sometimes termed "cloud glaciation effect" [*Lohmann and Feichter*, 2005]. Therefore, the increase of ice nuclei concentration will dramatically change the cloud phase and cloud radiative forcing. Liquid droplets tend to be smaller and much more numerous than ice crystals, so the optical depth of a liquid cloud will be larger than that of an ice cloud with the same amount of condensed water. The anthropogenic AIE in mixed-phase clouds are determined by the changes in their cloud liquid water content, ice water content, as well as the number concentrations in each condensate type [*Xie et al.*, 2008].
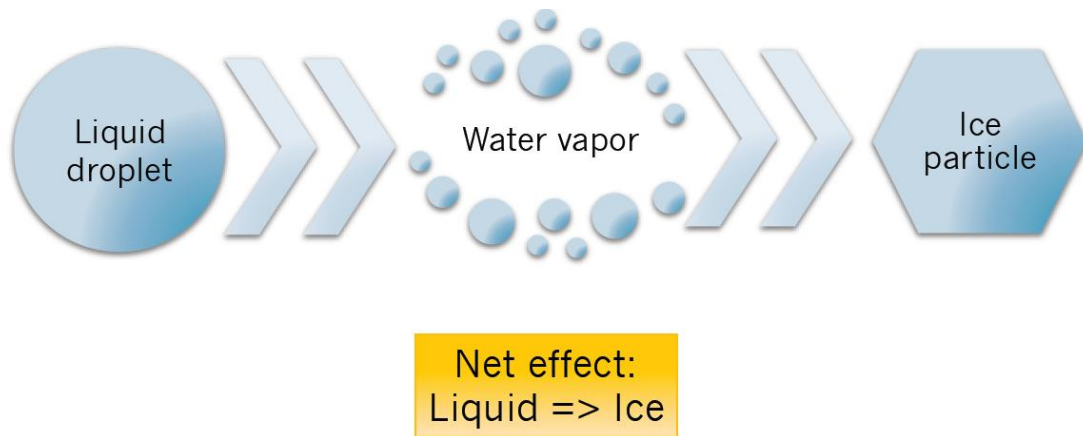
Figure 1.5: Bergeron-Findeisen process

The research on aerosol indirect effect in mixed-phase clouds is still in its infancy, due to the lack of understanding of the ice nucleation processes, and how it depends on the aerosol properties. There are two kinds of ice nucleation mechanisms in general, homogeneous ice nucleation and heterogeneous ice nucleation. To put into simple words, homogeneous ice nucleation is the freezing of pure liquid drops, while heterogeneous ice nucleation requires the presence of a foreign particle. This foreign particle is the so-called "ice nuclei". Homogeneous freezing require very high ice supersaturation that can only be reached at very low temperatures typically for cirrus clouds [*Pruppacher and Klett*, 1997]. At the warm temperatures in mixed-phase clouds, ice particles are formed by various heterogeneous freezing processes. Heterogeneous freezing occurs by four different mechanisms: condensation freezing, immersion freezing, deposition nucleation, and contact freezing. Condensation freezing occurs when a nucleus acts first as a cloud condensation nucleus and later as a freezing nucleus. Immersion freezing occurs when ice nucleates on a solid particle, which is immersed in a droplet. Deposition nucleation refers to the process by which water vapor directly deposits on a solid surface and freezes.

Contact freezing refers to the freezing of a supercooled droplet when it collides with a freezing nucleus by Brownian diffusion, thermophoresis, or diffusiophoresis [*Vali*, 1985]. Figure 1.6 is a schematic description of the heterogeneous ice nucleation mechanisms. Currently, there is no means to distinguish the different freezing mechanisms, except contact freezing in laboratory observations.
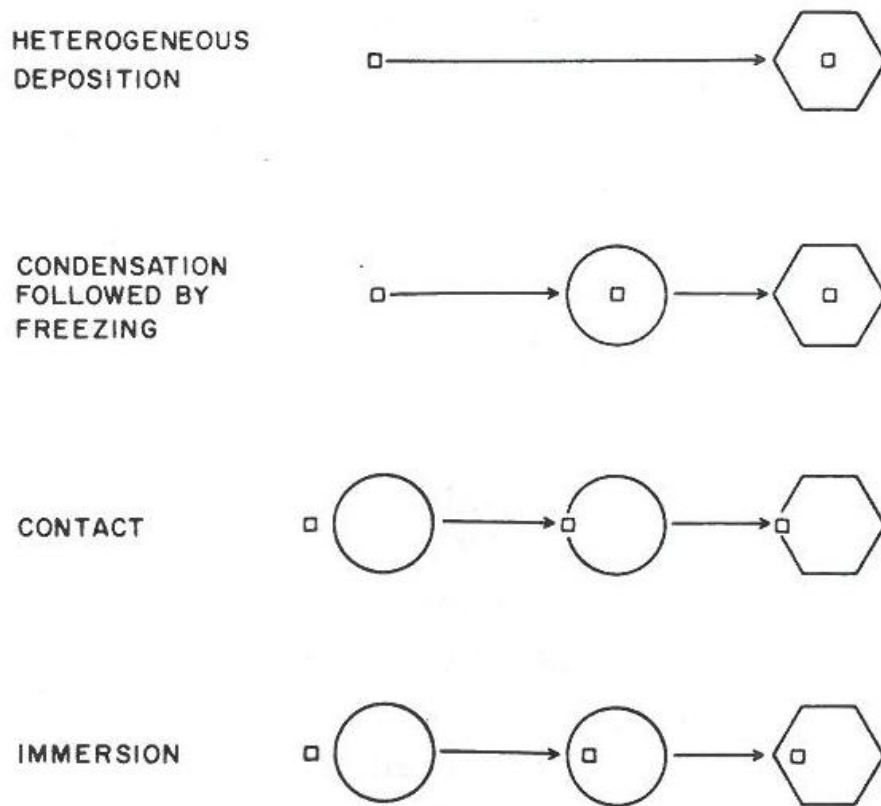
Figure 1.6: Heterogeneous ice nucleation mechanisms (adopted from Rogers and Yau, 1989)

Not all aerosols can be ice nuclei. In fact, only about 1 in 10^7 of them does, assuming 10^4 cm^{-3} as a typical concentration of aerosol particles, and an ice nuclei concentration of 1/L

at -20°C [*Rogers and Yau*, 1989]. What kinds of aerosols can act as ice nuclei on what condition is still an area of active research. In situ measurements [*Demott et al.*, 2003; *Targino et al.*, 2006; *Richardson et al.*, 2007; *Kamphus et al.*, 2010] and laboratory observations have found dust, black carbon, and certain kinds of biological organics acting as ice nuclei. [*Field et al.*, 2006; *Archuleta et al.*, 2005; *Zuberi et al.*, 2002; *Kanji and Abbatt*, 2006; *Cozic et al.*, 2008; *Koehler et al.*, 2009; *DeMott et al.*, 1999; *Pratt et al.*, 2009; *Prenni et al.*, 2009; *Pöschl et al.*, 2010]

It is highly unknown what characteristics of the aerosol particles determine their ice nucleating ability. However, it is generally thought that there are certain areas on the aerosol surface that are capable of forming critical ice embryos on the nanometer scale. Those areas are termed "active sites" [*Pruppacher and Klett*, 1997]. They are determined by the surface feature of the aerosols and have a high compatibility with the lattice structure of the ice embryo. The occurrences of these sites are rare, and are proportional to the surface area of an aerosol particle. This is consistent with observations that show larger aerosol particles have higher ice nucleating efficiency [e.g. *Demott*, 1990].

1.6   Overview of this thesis

The challenge with modeling ice nucleation in global climate models is difference between the scale size that the model can resolve (100 - 400km), and the scale size that ice nucleation takes place (0.01 – 1000 μm). Therefore, ice nucleation in mixed-phase

clouds needs to be parameterized. The main focus of this dissertation is on improving the estimate of aerosol indirect effect in mixed-phase clouds by improving the representation of ice nucleation treatment.

At any given temperature, the amount of ice nucleating activity increases with ice supersaturation [*Fletcher*, 1962; *Meyers*, 1992; *Al-Naimi and Saunders*, 1985; *Hussain and Saunders*, 1984]. Traditional ice nucleation parameterization is only a function of ice supersaturation [*Meyers*, 1992] or temperature [*Cooper*, 1986; *Fletcher*, 1962]. In order to study the aerosol effect on ice nucleation, improvements need to be made on these parameterizations, introducing the dependency on aerosols properties. Therefore, in Chapter 2, we implement an aerosol-dependent heterogeneous ice nucleation and address the following question:

1. How does an aerosol-dependent ice nucleation parameterization change the predicted distribution of the cloud ice and water field, the cloud radiative forcing, and anthropogenic aerosol effect?

To address it, we extend the previous studies by implementing the two aerosol dependent parameterizations in the coupled CAM and IMPACT aerosol transport model [*Wang and Penner*, 2010; *Wang et al.*, 2009], and compare these formulations to the previously used *Meyers* et al. [1992] parameterization and *Young* [1974] parameterization. This new set

of heterogeneous freezing parameterizations has empirically-derived dependencies on the chemistry and surface area of multiple aerosol species. This allows us to examine the climate forcing of anthropogenic aerosols on mixed-phase clouds. Ice nuclei number concentration, cloud liquid water path, ice water path, and the Earth's radiation budget from the different simulations are compared among themselves and to satellite observations. We also present an estimate of the anthropogenic aerosol effect in mixed-phase clouds in the two simulations with the aerosol-dependent deposition/condensation/immersion freezing parameterization and each of the two contact freezing parameterizations.

With a typical lifetime of a week, ice nucleating aerosols, such as dust and black carbon often go through long range transport in the atmosphere, having sufficient time to interact with soluble materials such as sulfuric acid. The ice nucleating ability of these aerosols may also change as a result of these interactions. For example, fossil fuel black carbon and organic matter (ffBC/OM) are often emitted together with sulfate, which coats the surface of these particles and changes their hygroscopicity. Observational studies show that the hygroscopicity of soot particles can modulate their ice nucleation ability. However, most climate models treat BC as a single group of aerosol with uniform ice nucleation properties. Improved ice nucleation parameterization of fossil fuel burning aerosols that considers the effect of hygroscopicity is need for more accurate assessment of the anthropogenic AIE. Therefore, the question to be addressed in Chapter 3 is:

2. How does consideration of hygroscopicity of fossil fuel combustion aerosols during the ice nucleation process change the fossil fuel combustion aerosol forcing in mixed-phase clouds?

To address it, we implemented a scheme that uses 3 levels of soot hygroscopicity (hydrophobic, hydrophilic and hygroscopic) and used laboratory data to specify their ice nuclei abilities, in place of a single category scheme (1-ffBC/OM) [*Wang et al.*, 2009]. We present the hydrophobic, hydrophilic and hygroscopic ffBC/OM aerosol fields, as well as the cloud water field and radiative forcing from the original and the new scheme. Finally, an updated total anthropogenic forcing is presented with the new 3-ffBC/OM scheme.

Ocean covers about 70% of the Earth's surface. Marine aerosols are thus an important component in the global aerosol field. There have been several observational studies on the ice nucleation activities of marine aerosols. Due to the considerable contribution of MOA to total marine aerosol and their ice nucleation properties, they have the potential to effectively influence marine cloud microphysics, and through that the cloud phase, cloud optical depth, and cloud radiative forcing. However, the effects of the marine organic aerosols as ice nuclei have not yet been evaluated on a global scale. This is important not only for simulation of the current climate state, but also for anthropogenic aerosol effect since it reshapes the back ground natural aerosol effect. Therefore, the question to be addressed in Chapter 4 is:

3. How the inclusion of the marine organic ice nuclei changes the predicted ice water field, liquid water field, and anthropogenic aerosol forcing?

To address it, we implement the aerosol microphysics and ice nucleation for marine organic aerosol into CAM-IMPACT. The emission of the marine biogenic aerosols is parameterized as a function of the sea salt emissions. The ice nucleation efficiency of the marine biogenic aerosols is constrained by measurement by *Bigg* [1973]. Two sea salt emission parameterizations and two marine organic fraction parameterizations are tested. To test the uncertainty in the derived ice nucleation efficiency of marine biogenic aerosols, the ice nucleation efficiency is decreased and increased by a factor of 10 in two separated sensitivity tests. The resulting cloud ice/liquid water field and cloud radiative forcing is compared to satellite observations. Anthropogenic aerosol forcing with and without the marine biogenic ice nuclei are also compared.

The dissertation concludes with a summary of the main results and an outlook for future work in the final chapter.

References

Al-Naimi, R., and C. P. R. Saunders (1985), Measurements of natural deposition and condensation-freezing ice nuclei with a continuous flow chamber, *Atmospheric Environment*, 19(11), 1871-1882.

Archuleta, C. M., P. J. DeMott, and S. M. Kreidenweis (2005), Ice nucleation by surrogates for atmospheric mineral dust and mineral dust/sulfate particles at cirrus temperatures, *Atmospheric Chemistry and Physics*, *5*, 2617-2634.

Bigg, E. K. (1973), Ice nucleus concentrations in remote areas, *Journal of the Atmospheric Sciences*, *30*(6), 1153-1157.

Cooper, W. A. (1986), *Ice initiation in natural clouds, in Precipitation Enhancement—A Scientific Challenge,* Meteorol. Monogr., vol. 21, edited by R. G. Braham Jr., pp. 29–32, Am. Meteorol. Soc., Boston, Mass.

Cozic, J., S. Mertes, B. Verheggen, D. J. Cziczo, S. J. Gallavardin, S. Walter, U. Baltensperger, and E. Weingartner (2008), Black carbon enrichment in atmospheric ice particle residuals observed in lower tropospheric mixed phase clouds, *Journal of Geophysical Research-Atmospheres*, *113*(D15), 11, doi:D15209 10.1029/2007jd009266.

Demott, P. J. (1990), AN EXPLORATORY-STUDY OF ICE NUCLEATION BY SOOT AEROSOLS, *Journal of Applied Meteorology*, *29*(10), 1072-1079.

DeMott, P. J., Y. Chen, S. M. Kreidenweis, D. C. Rogers, and D. E. Sherman (1999), Ice formation by black carbon particles, *Geophysical Research Letters*, *26*(16), 2429-2432.

DeMott, P. J., D. J. Cziczo, A. J. Prenni, D. M. Murphy, S. M. Kreidenweis, D. S. Thomson, R. Borys, and D. C. Rogers (2003a), Measurements of the concentration and composition of nuclei for cirrus formation, *Proceedings of the National Academy of Sciences of the United States of America*, *100*(25), 14655-14660, doi:10.1073/pnas.2532677100.

DeMott, P. J., K. Sassen, M. R. Poellot, D. Baumgardner, D. C. Rogers, S. D. Brooks, A. J. Prenni, and S. M. Kreidenweis (2003b), African dust aerosols as atmospheric ice nuclei, *Geophysical Research Letters*, *30*(14), doi:10.1029/2003gl017410.

Fletcher, N. H. (1962), *The Physics of Rain Clouds*, 386 pp., Cambridge Univ. Press, New York.

Field, P. R., O. Mohler, P. Connolly, M. Kramer, R. Cotton, A. J. Heymsfield, H. Saathoff, and M. Schnaiter (2006), Some ice nucleation characteristics of Asian and Saharan desert dust, *Atmospheric Chemistry and Physics*, *6*, 2991-3006.

Hussain, K., and C. P. R. Saunders (1984), Ice nucleus measurement with a continuous flow chamber, *Quarterly Journal of the Royal Meteorological Society*, 110(463), 75-84.

IPCC, 2001: *Climate Change 2001: The Scientific Basis. Contribution of Working Group I to the Third Assessment Report of the Intergovernmental Panel on Climate Change* [Houghton, J.T.,Y. Ding, D.J. Griggs, M. Noguer, P.J. van der Linden, X. Dai, K. Maskell, and C.A. Johnson (eds.)]. Cambridge University Press, Cambridge, United Kingdom and New York, NY, USA, 881pp.

IPCC, 2007*: Climate Change 2007: The Physical Science Basis. Contribution of Working Group I to the Fourth Assessment Report of the Intergovernmental Panel on Climate Change* [Solomon, S., D. Qin, M. Manning, Z. Chen, M. Marquis, K.B. Averyt, M. Tignor and H.L. Miller (eds.)]. Cambridge University Press, Cambridge, United Kingdom and New York, NY, USA, 996 pp.

Kamphus, M., M. Ettner-Mahl, T. Klimach, F. Drewnick, L. Keller, D. J. Cziczo, S. Mertes, S. Borrmann, and J. Curtius (2010), Chemical composition of ambient aerosol, ice residues and cloud droplet residues in mixed-phase clouds: single particle analysis during the Cloud and Aerosol Characterization Experiment (CLACE 6), *Atmospheric Chemistry and Physics*, *10*(16), 8077-8095.

Kanji, Z. A., O. Florea, and J. P. D. Abbatt (2008), Ice formation via deposition nucleation on mineral dust and organics: dependence of onset relative humidity on total particulate surface area, *Environmental Research Letters*, *3*(2), doi:10.1088/1748-9326/3/2/025004.

Kiehl, J. T., and K. E. Trenberth (1997), Earth's annual global mean energy budget, *Bulletin of the American Meteorological Society*, *78*(2), 197-208, doi:10.1175/1520-0477(1997)078<0197:eagmeb>2.0.co;2.

Koehler, K. A., P. J. DeMott, S. M. Kreidenweis, O. B. Popovicheva, M. D. Petters, C. M. Carrico, E. D. Kireeva, T. D. Khokhlova, and N. K. Shonija (2009), Cloud condensation nuclei and ice nucleation activity of hydrophobic and hydrophilic soot particles, *Phys Chem Chem Phys*, *11*(36), 7906-7920.

Lohmann, U., and J. Feichter (2005), Global indirect aerosol effects: a review, *Atmospheric Chemistry and Physics*, *5*, 715-737.

Manabe, S., and F. Moller (1961), One the radiative equilibrium and heat balance of the atmosphere, *Monthly Weather Review*, 503-532.

Manabe, S., and R. Wetherald (1967), Thermal equilibrium of the atmosphere with a given distribution of relative humidity, *Journal of Atmospheric Sciences*, 24, 241-259.

Meyers, M. P., P. J. DeMott, and W. R. Cotton (1992), New primary ice-nucleation parameterizations in an explicit cloud model, *Journal of Applied. Meteorolory,* 31(7), 708–721.

Poschl, U., et al. (2010), Rainforest Aerosols as Biogenic Nuclei of Clouds and Precipitation in the Amazon, *Science*, *329*(5998), 1513-1516.

Pratt, K. A., P. J. DeMott, J. R. French, Z. Wang, D. L. Westphal, A. J. Heymsfield, C. H. Twohy, A. J. Prenni, and K. A. Prather (2009), In situ detection of biological particles in cloud ice-crystals, *Nature Geoscience*, *2*(6), doi:10.1038/ngeo521.

Prenni, A. J., M. D. Petters, S. M. Kreidenweis, C. L. Heald, S. T. Martin, P. Artaxo, R. M. Garland, A. G. Wollny, and U. Poschl (2009), Relative roles of biogenic emissions and Saharan dust as ice nuclei in the Amazon basin, *Nature Geoscience*, *2*(6), 401-404, doi:10.1038/ngeo517.

Pruppacher, H. R., and J. D. Klett (1997), *Microphysics of Clouds and Precipitation*, 2nd ed. Kluwer Academic, AA Dordrecht, The Netherlands.

Richardson, M. S., et al. (2007), Measurements of heterogeneous ice nuclei in the western United States in springtime and their relation to aerosol characteristics, *Journal of Geophysical Research-Atmospheres*, *112*(D2), doi:10.1029/2006jd007500.

Rogers R. R., and M. K. Yau (1989), *A short course in cloud physics*, 3rd edition, Elsevier Science, Oxford, UK.

Targino, A. C., R. Krejci, K. J. Noone, and P. Glantz (2006), Single particle analysis of ice crystal residuals observed in orographic wave clouds over Scandinavia during INTACC experiment, *Atmospheric Chemistry and Physics*, *6*, 1977-1990.

Vali, G. (1985), Nucleation Terminiology, *Bulletin of the American Meteorological Society*, 66(11), 1426-1427.

Wang, M., and J. E. Penner (2010), Cirrus clouds in a global climate model with a statistical cirrus cloud scheme, *Atmospheric Chemistry and Physics*, *10*(12), 5449-5474.

Wang, M. H., J. E. Penner, and X. H. Liu (2009), Coupled IMPACT aerosol and NCAR CAM3 model: Evaluation of predicted aerosol number and size distribution, *Journal of Geophysical Research-Atmospheres*, *114*, doi:10.1029/2008JD010459

Warren, S.G., C.J. Hahn, J. London, R.M. Chervin and R.L. Jenne, 1986: Global distribution of total cloud cover and cloud type amounts over land. NCAR Tech. Note, *NCAR/TN-273+STR*, 29 pp. + 200 maps.

Warren, S.G., C.J. Hahn, J. London, R.M. Chervin and R.L. Jenne, 1988: Global distribution of total cloud cover and cloud type amounts over the ocean. NCAR Tech. Note, *NCAR/TN-317+STR*, 41 pp. + 170 maps.

Xie, S. C., J. Boyle, S. A. Klein, X. H. Liu, and S. Ghan (2008), Simulations of Arctic mixed-phase clouds in forecasts with CAM3 and AM2 for M-PACE, *Journal of Geophysical Research-Atmospheres*, *113*(D4), 16, doi:D0421110.1029/2007jd009225.

Young, K. C. (1974), Numerical-simulation of wintertime, orographic precipitation .1.Description of model microphysics and numerical techniques, *Journal of the Atmospheric Sciences*, *31*(7), 1735-1748.

Zuberi, B., A. K. Bertram, C. A. Cassa, L. T. Molina, and M. J. Molina (2002), Heterogeneous nucleation of ice in (NH4)(2)SO4-H2O particles with mineral dust immersions, *Geophysical Research Letters*, *29*(10), doi:10.1029/2001gl014289.

CHAPTER 2

Global model comparison of heterogeneous ice nucleation

parameterizations in mixed-phase clouds

2.1   Introduction

Mixed-phase clouds (clouds that typically occur between 0°C and -40°C and contain both ice particles and supercooled liquid droplets) cover about 22% of the earth [*Warren et al.*, 1988 a, b] and have a substantial influence on climate. The radiative properties of mixed-phase clouds are largely determined by their cloud liquid water content, ice water content, as well as the number concentrations in each condensate type [*Xie et al.*, 2008]. Liquid droplets tend to be smaller and much more numerous than ice crystals, so the optical depth of a liquid cloud will be larger than an ice cloud with the same amount of condensed water. *Penner et al*. [2001] showed that the difference in forcing associated with changing all clouds between 0°C and -40°C from liquid to ice was $+13W/m^2$. This forcing estimate included the effect of precipitation rate changes through their impacts on the ice and liquid water path changes [*Lohmann et al.,* 2002].

At the warm temperatures in mixed-phase clouds, ice particles are formed by various heterogeneous freezing processes, since homogeneous freezing requires high ice supersaturations, and is usually limited to temperatures below -40°C [*Pruppacher and Klett*, 1997]. During heterogeneous freezing (as opposed to homogeneous freezing), a so-called ice nucleus (IN) facilitates the phase transition from vapor or liquid to ice [*Pruppacher and Klett*, 1997]. Heterogeneous freezing occurs by four different mechanisms: condensation freezing, immersion freezing, deposition nucleation, and contact freezing. Condensation freezing occurs when a nucleus acts first as a cloud condensation nucleus and later as a freezing nucleus. Immersion freezing occurs when ice nucleates on a solid particle, which is immersed in a droplet. Deposition nucleation refers to the process by which water vapor directly deposits on a solid surface and freezes. Contact freezing refers to the freezing of a supercooled droplet when it collides with a freezing nucleus by Brownian diffusion, thermophoresis, or diffusiophoresis. These heterogeneous freezing mechanisms are described in more detail in *Vali* [1985].

Variations in the number concentration and chemical properties of ice-forming nuclei in space and time should be taken into account when predicting ice number concentrations in mixed-phase clouds. However, the ice nucleation parameterization in mixed-phase clouds in most GCMs does not depend on the aerosol properties. For example, the *Cooper* [1986] and *Fletcher* [1962] parameterizations are only a function of temperature. The *Meyers et al.* [1992] parameterization that is often used for deposition and condensation freezing only depends on supersaturation. Also, the *Meyers et al.* [1992] parameterization was derived from measurements near the surface and thus will over-

predict the ice crystal concentrations, if adjustments are not made to account for the decrease in aerosol particles with altitude. Due to these limitations one cannot use these ice nucleation parameterizations to study the effects of aerosols on mixed-phase clouds.

Recently, several heterogeneous freezing parameterizations have been developed to take into account the effects of different aerosol types on ice nucleation. Some of these are based on laboratory observations [*Lohmann and Diehl*, 2006; *Diehl and Wurzler*, 2004; *Diehl et al.*, 2006; *Marcolli et al.,* 2007; *Connolly et al.,* 2009; *Murray et al.,* 2011]. Some of the laboratory observations used artificially generated surrogates for atmospheric particles [*DeMott,* 1990; *Diehl and Mitra,* 1998; *Gorbunov et al.,* 2001; *Murray et al.,* 2011], while others used natural aerosol samples [*Schaefer*, 1949; *Isono and Ibeke*, 1960; *Field et al.,* 2006; *Connolly et al.* 2009; *Koehler et al.,* 2007, 2010; *Kulkarni and Dobbie* 2010; *Kanji et al.,* 2011]. Another group of heterogeneous freezing parameterizations are based on classical nucleation theory. The problem with using classical nucleation theory is that the freezing ability of an aerosol particle is characterized by the contact angle parameter, which is hard to measure and validate. In addition, the use of a single contact angle for differentiating the freezing properties of different particle types also assumes that the substrate surface is energetically homogeneous. In reality, it is thought that freezing preferentially starts at certain active sites on certain particles [*Pruppacher and Klett*, 1997 (pp. 330)]. Several studies have utilized the classical nucleation theory and made various improvements [*Kärcher and Lohmann*, 2003; *Chen et al.,* 2008; *Marcolli et al.,* 2007; *Khvorostyanov and Curry*, 2004; *Liu and Penner*, 2005; *Pruppacher and Klett*, 1997 (pp. 341-344)]. A third method for

deriving heterogeneous freezing parameterizations is to develop an empirically derived in-situ observation-based parameterization. This was the method used by *Phillips et al.* [2008], who proposed a parameterization for deposition/condensation/immersion freezing that was constrained by in-situ measurements of IN number concentration. In this parameterization, the number concentration of ice nuclei not only depends on ice supersaturation, but also on the surface area concentration, and the proportion of dust, black carbon, and organics. *Eidhammer et al.* [2009] compared three heterogeneous ice nucleation parameterizations in a parcel model including the in-situ observation-based method of *Phillips et al.* [2008], the *Khvorostyanov and Curry* [2004] parameterization which is based on classical theory, and the *Diehl and Wurzler* [2004] parameterization which is based on laboratory observations, and concluded that the *Phillips et al.* [2008] parameterization compares well with most ice nucleation measurements included in their study. They recommended that it be used in cloud and global-scale models in preference to the other two parameterizations. Recent implementations of the *Phillips et al.* [2008] parameterization include *Seifert et al.* [2011] who implemented the *Phillips et al.* [2008] parameterization in a convective-scale weather prediction model, *Wang et al.* [2011] who implemented it in a regional climate model, and *Barahona et al.* [2010] who implemented it for cirrus clouds in a global model. *DeMott et al.* [2010] proposed a simplified version of *Phillips et al.* [2008] parameterization, which depends on the total non-sea-salt aerosol number concentration with diameter larger than 0.5 µm, instead of relying on the surface area of dust, black carbon, and organics separately. However, here we choose to implement the *Phillips et al.* [2008] parameterization since it specifically includes the separate effects of organics, BC, and dust particles.

For contact freezing, there is no parameterization available that is constrained by in-situ measurements. The commonly applied *Young* [1974] parameterization predicts contact ice nuclei number concentrations based on temperature and was derived from the experimental data of *Blanchard* [1957]. It does not consider the specific properties of the aerosols that may affect contact freezing. In this parameterization, the number concentration of contact ice nuclei below -4°C is calculated as a temperature scaling of a specified number concentration of active ice nuclei at -4°C. *Phillips et al.* [2008] proposed a contact freezing parameterization based on the assumption that each IN particle can nucleate ice at a freezing temperature that is 4.5 °C higher than the freezing temperature associated with immersion or condensation freezing. This assumption was based on laboratory observations reported by *Shaw et al.* [2005]. Using this method, one is able to use the aerosol-dependent Phillips deposition/condensation/immersion freezing parameterization to treat contact freezing by specific aerosol types. However, the drawback of not being constrained by in-situ observations still exists.

Several recent studies have focused on heterogeneous ice nucleation in mixed-phase clouds using General Circulation Models (GCM). *Salzmann et al.,* [2010] and *Gettelman et al.,* [2010] improved the microphysics scheme in GFDL AM3 and CAM, respectively, and found that the simulated cloud forcing is sensitive to the formulation of the ice microphysics. *Hoose et al.,* [2010] implemented a classical-theory-based heterogeneous freezing parameterization in CAM-Oslo, and found that immersion freezing by dust is the

dominant ice formation processes, while the contribution of biological aerosols is marginal. *Lohmann et al.,* [2007], *Lohmann and Hoose*, [2009], and *Storelvmo et al.,* [2008, 2011] investigated the aerosol indirect effect in general, or in mixed-phase clouds only, and found that mixed-phase cloud processes have a major effect on the anthropogenic aerosol effect.

In this study, we extend the previous studies by implementing the two *Phillips et al.* [2008] parameterizations in the coupled CAM and IMPACT aerosol transport model [*Wang and Penner*, 2010; *Wang et al.*, 2009], and compare these formulations to the previously used *Meyers* et al. [1992] parameterization and *Young* [1974] parameterization. This new set of heterogeneous freezing parameterizations has empirically-derived dependencies on the chemistry and surface area of multiple aerosol species. This allows us to examine the climate forcing of anthropogenic aerosols on mixed-phase clouds. A total of 6 model simulations are presented. Ice nuclei number concentration, cloud liquid water path, ice water path, and the Earth's radiation budget from the different simulations are compared among themselves and to satellite observations. We also present an estimate of the anthropogenic aerosol effect in mixed-phase clouds in the two simulations with the aerosol-dependent deposition/condensation/immersion freezing parameterization and each of the two contact freezing parameterizations. In the next section, we describe the coupled model set-up in detail, as well as the four heterogeneous freezing parameterizations we test. Sections 3.1 – 3.7 discuss results for the ice nuclei concentrations, the cloud liquid/ice fields, the top of the atmosphere (TOA) radiation fields, as well as the comparison to satellite observations. We present the effects of

anthropogenic black carbon/organic matter on mixed-phase clouds in section 3.8. A sensitivity test that examines the effect of tuning the reference contact IN to that assumed in the *Young* [1974] parameterization is discussed in section 3.9. The last section concludes the study and provides an outlook for future developments.

2.2   Methods

2.2.1   The CAM-IMPACT Model

In this study, we use the coupled CAM-IMPACT model. The coupled model consists of two components: the NCAR Community Atmospheric Model (CAM3) [*Collins et al.*, 2006a], and the University of Michigan (Umich) IMPACT aerosol model (which is derived from the Lawrence Livermore National Laboratory (LLNL) chemical transport model) [*Rotman et al.*, 2004; *Penner et al.*, 1998]. The two components are run concurrently in the multiple processors multiple data (MPMD) mode [*Wang et al.*, 2009].

2.2.1.A   The IMPACT Global Aerosol Model

Umich IMPACT aerosol model is developed to use massively parallel computer architectures. *Liu and Penner* [2002] modified the LLNL IMPACT atmospheric chemistry model to treat the mass of sulfate aerosol as a prognostic variable. The model was further extended by *Liu et al.* [2005] to simulate the microphysics of sulfate aerosol

30

and its interactions with primary non-sulfate aerosols based on the aerosol module developed by *Herzog et al.* [2004]. The primary non-sulfate aerosol components included in this study are natural organic matter (NOM), which is assumed to be formed from terpene emissions, fossil fuel burning black carbon and organic matter (FFBC/OM), biomass burning black carbon and organic matter (BBBC/OM), aircraft BC (ABC), dust, and sea salt. Dust, sea salt, black carbon/organic matter are internally mixed with sulfate. The internal mixtures are formed through coagulation with sulfate aerosols, condensation of sulfuric acid, and when sulfate is formed through aqueous reactions in cloud drops that contain non-sulfate aerosols. Although BC and OM from fossil fuel burning and biomass burning are treated as distinct species in the model, they are assumed to be internally mixed for both optical properties and their effects on ice [*Liu et al.*, 2005; *Wang and Penner*, 2010]. The *Herzog et al.* [2004] module is able to treat an arbitrary number of modes to describe the microphysical processes determining the distribution of sulfate aerosol and its mixing state with other aerosol types [*Herzog et al.*, 2004; *Liu et al.*, 2005].

Here we used the 3-mode version that describes the variation of pure sulfate in a nucleation mode (radius < 5nm), an Aitken mode (5nm < radius < 50nm), and an accumulation mode (radius > 50nm). Both the mass and number of the pure sulfate aerosol for the three modes are predicted. Mineral dust and sea salt are divided into four size bins with radii varying from 0.05-0.63 μm, 0.63-1.26 μm, 1.26-2.5 μm, and 2.5-10 μm. Carbonaceous aerosols (BC and OM) are represented by a single submicron size bin. For a complete list of the size distribution parameters for non-sulfate aerosols, please refer to Table 3 in *Liu et al.* [2005]. The other predicted species include: dimethylsulfide

(DMS), sulfur dioxide (SO_2), and hydrogen peroxide (H_2O_2). A detailed description of the formation of sulfate particles, their interaction with non-sulfate aerosols, dry deposition, wet deposition and the scavenging efficiencies, as well as comparisons with observations can be found in *Wang et al.* [2009]. The present aerosol module uses the sea salt emissions calculated online in the model based on *Monahan et al.* [1986], and anthropogenic emissions set to those for the year 2000 [*Penner et al.*, 2009]. In addition, natural emissions of dust, DMS from the oceans, OM from vegetation, and SO_2 from volcanoes are included. SO_2 and BC/OM from fossil fuel burning adjusted to represent the spatial distribution from land, ship, and aircraft transportation from QUANTIFY (www.pa.op.dlr.de/quantify) are included.

The IMPACT aerosol model can be driven by either the meteorological fields from a general circulation model or assimilated meteorological data. In this coupled model study, we drive the IMPACT model by the generated meteorological fields from NCAR CAM3 as updated by *Wang and Penner* [2010]. Thus, variables such as temperature, wind speed, humidity, cloud water, cloud fraction, pressure, convective mass flux, precipitation, boundary layer height, and detrainment rate are passed from CAM3 to IMPACT at each IMPACT advection time step.

2.2.1.B NCAR CAM3

The NCAR CAM3 is part of the Community Climate System Model 3 (CCSM3) [*Collins et al.*, 2006a, b]. The model predicts both cloud liquid water and cloud ice water [*Boville et al.*, 2006]. The standard CAM3 version was updated by *Liu et al.* [2007], by introducing a two-moment cloud microphysics scheme for ice clouds, in which cloud ice number concentrations as well as mass concentrations are predicted by a prognostic equation. The two-moment scheme treats ice nucleation, coagulation, evaporation, and melting. In addition, *Wang and Penner* [2010] added a prognostic cloud droplet number concentration equation for liquid clouds. The complete set of equations for the two-moment treatment of cloud microphysics for liquid, ice, and mixed-phase clouds can be found in the supplementary material of *Wang and Penner* [2010]. The cloud droplet activation parameterization is that of *Abdul-Razzak and Ghan* [2000, 2002]. The liquid/ice partitioning in mixed-phase clouds is accomplished by explicitly treating the liquid mass conversion to ice due to the depositional growth of cloud ice at the expense of liquid water (the Bergeron-Findeisen process) using the scheme of *Rotstayn et al.* [2000]. This replaces the simple temperature-dependent liquid/ice partitioning in the standard CAM3. The cloud condensation and evaporation (C-E) scheme of *Zhang et al.* [2003] which removes any supersaturation above that of liquid water in the standard CAM3 is used only for liquid water in warm and mixed-phase clouds.

In mixed-phase clouds, water saturation is assumed for simplicity. Under such conditions, it is hard to distinguish deposition nucleation, condensation freezing, and immersion freezing. So here we refer to deposition/condensation/immersion freezing in mixed-phase clouds. However, in reality deposition nucleation cannot happen if aerosols take up layers

of water when water saturation is approached. A statistical cirrus cloud scheme that accounts for mesoscale temperature and velocity perturbations is implemented as described in *Wang and Penner* [2010] to better represent both subgrid-scale supersaturation and cloud formation. The treatment of temperature fluctuations with altitude is based on the gravity wave parameterization from *Gary* [2006, 2008]. We follow the *Wang and Penner* [2010] estimates for IN in cirrus clouds, which treated homogeneous freezing of pure sulfate particles and assumed that 1% of dust, BC/OM, and aircraft soot are immersion freezing IN [*Wang and Penner*, 2010].

In CAM3, aerosol optical properties are calculated using a prescribed aerosol concentration from an off-line calculation constrained by an assimilation of satellite retrievals [*Collins et al.*, 2001; *Rasch et al.*, 2001]. In the coupled CAM-IMPACT model, the prescribed aerosol concentration from CAM3 is replaced with concentrations calculated in the IMPACT aerosol model.

2.2.2   Heterogeneous ice nucleation parameterizations

2.2.2.A   Deposition/condensation/immersion (DCI) freezing

2.2.2.A.a The Phillips DCI freezing parameterization

Phillips et al. [2008] introduced a versatile method for parameterizing ice crystal number concentration in mixed-phase as well as cirrus clouds. The fundamental assumption in this parameterization is that the number concentration of ice nuclei for each aerosol species is proportional to the surface area of its aerosol particle population. There is theoretical and observational evidence supporting this assumption [*Pruppacher and Klett* 1997, *DeMott* 1990]. Heterogeneous freezing is an interface phenomenon on the surface of the IN, initiated at specific "active sites". Given the same surface properties, the larger the IN particle, the more active sites it will have. *Georgii and Kleinjung* [1967], *Berezinski et al.* [1988], *Archuleta et al.* [2005] and *Santachiara et al.* [2010] examined the effect of size on ice nucleation and found that the nucleation efficiency at a given temperature and supersaturation increases with increasing particle size. The *Phillips et al.* [2008] parameterization is qualitatively consistent with these findings since the number of active IN of each aerosol species is assumed to be proportional to its total surface area. The ice nuclei number concentration resulting from each of the three species treated by *Phillips et al.* [2008] is calculated as:

$$IN_{DCI,X} = \int_{\log[0.1\mu m]}^{\infty} \left\{ 1 - \exp\left[-\mu_X \left(D_X, S_i, T \right) \right] \right\} \times \frac{dn_X}{d \log D_X} d \log D_X \qquad (2.1)$$

where X is the label for the aerosol type. In this study, X = Dust, or BC/OM (dust, and black carbon/organic matter, respectively). S_i is the saturation ratio of vapor with respect to ice, and T is the physical temperature of ambient air in degrees C. BC/OM from both

fossil fuel burning and biomass burning are included. A recent laboratory study [*Friedman et al.,* 2011] found out that bare and coated soot particles are poor deposition ice nuclei below water saturation. However, above water saturation, droplet and ice particles cannot be distinguished in their experiment. So the efficiency of deposition/condensation/immersion nucleation at water saturation cannot be inferred from their study. The mixed-phase clouds in our model are assumed to be at water saturation. Therefore, BC/OM are considered as deposition/condensation/immersion nuclei in our study.

The number mixing ratio of aerosols in group X is n_X. μ_X is the average of the number of activated ice embryos per insoluble aerosol particle in the size interval between D_X and $Dx + dlogDx$, and is calculated as:

$$\mu_X = H_X(S_i,T)\xi(T)(\frac{\alpha_X n_{IN,1,*}}{\Omega_{X,1,*}}) \times \frac{d\Omega_X}{dn_X} \tag{2.2}$$

where $n_{IN,1,*}$ is the number mixing ratio of ice nuclei for the reference conditions at water saturation. The reference condition for this parameterization is based on field observations made during the Ice Nuclei Spectroscopy (INSPECT) 1 campaign [*DeMott et al.*, 2003], which took place in Colorado and is thought to be representative of typical background free tropospheric conditions. However, the representativeness of this

background free troposphere condition is limited by the available data. n_X is the number mixing ratio of particles in aerosol group X. Ω_X is the total surface area mixing ratio of all aerosols with dry diameters larger than 0.1μm in group X, and $\Omega_{X,1,*}$ is the component of Ω_X in the background reference scenario. The values of $\Omega_{X,1,*}$ are taken from *Phillips et al.* [2008]. *Eidhammer et al.* [2010] published a revision of the $\Omega_{X,1,*}$ value for dust, changing it from 5.0×10^{-7} m^2 kg^{-1} to 2.0×10^{-6} m^2 kg^{-1}. Using the new value would predict fewer ice nuclei from dust because the denominator is larger in Equation (2). The size limit of 0.1μm is supported by measurements of snow residuals [*Pruppacher and Klett* 1997; *Chen et al.*, 1998; *Prenni et al.*, 2007; *Marcolli et al.*, 2007]. α_X is the fractional contribution from aerosol group X to the IN concentration which was inferred from several field campaigns. Dust contributes ⅔, and BC/OM contributes ⅓. For BC/OM, the contribution from the organic matter (OM) is assumed to be 0.06, based on the assumption (made by Phillips et al. 2008) that half of the residual organic aerosol particles sampled from ice crystals (which is 13%) [*Targino et al.*, 2006; *DeMott et al.*, 2003; *Cziczo et al.*, 2004; *Richardson et al.*, 2007; *Phillips et al.*, 2008] are ice nuclei. Please note that there are significant uncertainties associated with the use of this assumption. The contribution from BC for the reference condition in the *Phillips et al.* [2008] parameterization is therefore assigned the value of ⅓-0.06.

H_X, is a factor that ranges from 0 to 1, and represents the relative scarcity of nucleation seen at relative humidities well below water saturation at temperatures warmer than -40°C. Here, since we assume water saturation during ice formation for all mixed-phase clouds, $Hx = 1$ for all chemical compositions. The value of $\xi(T)$ in equation (2) is zero at

T > -2°C, and 1 for T < -5°C, and interpolated in between, in order to account for the fact that no droplets freeze at temperatures higher than -2°C. At conditions with low ice freezing fractions, $\mu_X \ll 1$, we have:

$$IN_{DCI,X} \approx H_X(S_i,T)\xi(T)(\frac{\alpha_X n_{IN,1,*}}{\Omega_{X,1,*}}) \times \Omega_X \tag{2.3}$$

Therefore, the ice nuclei concentrations from each group of aerosols are based on their contribution to the ice nuclei measurements at the reference condition, which are then adjusted by the calculated aerosol surface area concentration, temperature, and ice supersaturation to account for regional and seasonal variations.

2.2.2.A.b The Meyers parameterization

The Meyers parameterization has been used in both global and cloud resolving models [*Gettelman et al.*, 2010; *Lee and Penner*, 2010; *Muhlbauer et al.*, 2010; *Salzmann et al.*, 2010]. The number concentration of ice nuclei as a function of ice supersaturation (S_i) is formulated as:

$$IN_{DCI} = \exp\{a+b[100(S_i-1)]\} \times D \tag{2.4}$$

$$D = \begin{cases} 1.0 & (z \leq 1000m) \\ 10^{-(z-1000)/6700} & (1000m < z \leq 7000m) \\ 10^{-6000/6700} & (z > 7000m) \end{cases} \qquad (2.5)$$

where $a = -0.639$, and $b = 0.1296$. The vertical decay rate (D) [*Liu et al., 2007*] is based on the measured vertical profiles of nonvolatile particle number concentrations in the Northern Hemisphere at midlatitudes during the INCA campaign [*Minikin et al., 2003*] and accounts for the fact that the original Meyers formulation was based on surface measurements. It is about tenfold per 6.7 km from the boundary layer top to 7km with no variation above 7 km. Note that the Meyers parameterization is not dependent on aerosol characteristics, but only on supersaturation with respect to ice.

2.2.2.B Contact freezing

The contact freezing of cloud droplets is thought to occur through Brownian coagulation with insoluble IN. The production rate of ice number from contact freezing is based on *Liu et al.* [2007]:

$$J_{frz,cnt} = 4\pi r_v N_d IN_{CON} D_{cnt} / \rho_0 \qquad (2.6)$$

where r_v is the volume mean droplet radius, N_d the number concentration of cloud droplets, and ρ_0 the air density. D_{cnt} is the Brownian aerosol diffusivity, and is calculated as:

$$D_{cnt} = \frac{k_B T_k C_c}{6\pi\mu r_{cnt}} \tag{2.7}$$

where T_k is the physical temperature of ambient air in Kelvin, r_{cnt} is the aerosol number mean radius, C_c the Cunningham correction factor, k_B the Boltzmann constant, and μ the viscosity of air. The number concentration of contact IN, IN_{CON} is parameterized using either the Phillips contact IN parameterization or the Young contact IN parameterization.

2.2.2.B.a The Phillips contact IN parameterization

Phillips et al. [2008] proposed treating contact IN using the same representation as that for the immersion or condensation nuclei, but assuming that the contact freezing temperature of the same particle is 4.5°C higher than the immersion and condensation nucleation temperature, based on measurements by *Shaw et al.* [2005]. However, it should be noted that *Shaw et al.* [2005] used volcanic ash aerosol particles that were100-300 micrometer in size, which is larger than the size of most aerosol particles at mixed-

phase cloud altitudes. Nevertheless, if freezing is a surface phenomenon, and we make the assumption that the number of active sites is proportional to the particle surface area, then the freezing with a submicrometer particle inside the drop would be much less efficient than that with a particle of 100-300um size. However, contact freezing with the particle at the surface of the drop will probably be less affected by the size of the particle due to the limited area of contact with the drop surface. Therefore, the difference between the surface mode and bulk-water mode for submicrometer particles will probably be at least as large as that observed by *Shaw et al.* [2005], so we adopt the 4.5°C change in freezing temperature here. The number mixing ratio of potentially active contact IN is represented by:

$$IN_{CON,X} \cong \alpha_X \xi(T) \left\{ \frac{n_{IN,1,*}[T - \Delta T_{CIN}, S_i^w (T - \Delta T_{CIN})]}{\Omega_{X,1,*}} \right\} \Omega_{X,\text{int}} \qquad (2.8)$$

$\Omega_{X,int}$ is the component of Ω_X for interstitial IN and S_i^w is the value of ice saturation ratio at water saturation. A complete list of symbols and notations can be found in. The Phillips contact freezing parameterization thus preserves the surface area dependence of the Phillips DCI freezing parameterization.

In the current set-up, all of the three processes that remove aerosols from the interstitial phase (droplet nucleation, contact freezing, DCI freezing) are assumed to occur simultaneously, and the cloud droplet number and ice number formed during the time

step are based on the number of aerosol particles at the beginning of the present time step. Whether the cloud droplet number (or ice crystal number from DCI freezing) increases at the end of the time step depends on the difference between the cloud droplet number (or ice crystal number from DCI freezing) formed during this time step and the previous time step (Equation 4 in *Liu et al.,* [2007]). While it may be tempting to exclude the aerosols that are predicted to activate as CCN or DCI freezing nuclei during the current time step from being contact ice nuclei, this would be inaccurate, because it assumes that CCN or DCI activation always occurs prior to contact nucleation. Also the droplet number or ice crystal number from DCI freezing does not increase until the end of the time step. Furthermore, the GCM we use does not presently carry information about the contributions from different aerosol species to the droplet number increase at the current time step. A more appropriate method would be to carry a separate "interstitial" group for each of the aerosol species. However, doing so requires a substantial amount of work and would significantly increase the computer time associated with the model, so that adding this capability was beyond the scope of the present study. Thus, here we assume that all aerosols are interstitial and $\Omega_{X,int} = \Omega_X$. We nevertheless acknowledge that this may result in an over estimation of the Phillips contact freezing.

2.2.2.B.b The Young contact IN parameterization

The Young parameterization for contact nuclei is

$$IN_{CON} = N_{a0}(270.16 - T_k)^{1.3}$$ (2.9)

where N_{a0} is the number concentration of active ice nuclei at -4°C, which was determined to be 0.2 cm^{-3} by *Young* [1974]. However, this assumption cannot be used without adjustment, since it does not allow for regional differences in contact ice nuclei due to aerosol abundance, and cannot be used to study aerosol effects on mixed-phase clouds. Several studies have attempted to introduce aerosol dependence into contact freezing parameterizations by making various assumptions. *Liu et al.* [2007] assumed that all dust aerosols act as contact ice nuclei. *Gettlemann et al.* [2010] assumed that only coarse mode dust aerosols were contact ice nuclei. *Lohmann* [2002] made several assumptions: contact ice nuclei were assumed to be all dust aerosols, the dust aerosol mass was reduced by the mass of sulfate aerosol before calculating the contact IN, or all hydrophobic carbonaceous particles were contact IN. *Lohmann and Diehl* [2006] assumed that contact ice nuclei were hydrophilic black carbon and accumulation mode dust aerosols, multiplied by a temperature-dependent fraction. This linear temperature dependence function implies that 100% acts as contact IN at T < -17°C for dust, and at T < -26°C for black carbon. *Storelvmo et al.* [2008] assumed that if dust and BC aerosols were coated with less than one monolayer of soluble material, they would be contact freezing nuclei. Finally, *Lohmann et al.* [2007] assumed externally mixed dust and BC would act as contact freezing nuclei.

Table 2.1: Description of symbols and notations used.

Notation	Description	Value and units
a	Parameter used in Meyers parameterization	-0.639
b	Parameter used in Meyers parameterization	0.1296
C_c	Cunningham correction factor	
D	Vertical decay rate in Meyers parameterization	
D_{oa}	Brownian aerosol diffusivity	$m^2 \, s^{-1}$
D_X	Geometric mean diameter of aerosol in group X for X = {Dust, BC/OM}	μ m
H_X	Fraction-reducing IN activity at low S_i, warm T	
IN_{CON}	Ice nuclei number concentration for contact freezing	m^{-3}
$IN_{CON,X}$	Ice nuclei number concentration for contact freezing from group X for X = {Dust, BC/OM}	m^{-3}
IN_{DCI}	Ice nuclei number concentration for immersion/condensation freezing	l^{-1}
$IN_{DCI,X}$	Ice nuclei number concentration for immersion/condensation freezing from group X for X = {Dust, BC/OM}	kg^{-1}
$J_{frz,cnt}$	Ice Number increase rate from contact freezing	$10^{12} \, kg^{-1} \, s^{-1}$
k_B	Boltzmann constant	1.381×10^{-23}
$n_{IN,1,*}$	Number mixing ratio of reference activity spectrum for water saturation in background-troposphere scenario	kg^{-1}
n_X	Number mixing ratio of particles in aerosol group X	kg^{-1}
N_{a0}	Number concentration of active ice nuclei at -4°C	m^{-3}
N_d	Number concentration of cloud droplets	$10^{12} \, kg^{-1}$
r_{cnt}	Number mean radius of aerosols	m
r_v	Volume mean radius of droplets	m
S_i	Saturation ratio of vapor with respect to ice	
S_i^w	Value of S_i at water saturation	
T	Physical temperature of ambient air in degree C	°C
T_k	Physical temperature of ambient air in Kelvin	K
ΔT_{CIN}	Difference in freezing temperature between surface and bulk-water modes	4.5°C
X	Label for group of insoluble aerosol	
α_X	Fraction of $n_{IN,1,*}$ ($H_X = 1$) from IN activity of group X = {Dust, BC/OM}	$\{2/3, 1/3 - 0.06\}$
z	Altitude	m
μ	Viscosity of air	kg/m/s
μ_X	Average number of ice embryos per aerosol particle in group X	
ρ_0	Density of ambient air	$kg \, m^{-3}$
$\xi(T)$	Function that is 0 for $T > -2$°C and 1 for $T < -5$°C, being δ_0^1 $(T, -5, -2)$ for $-5 < T < -2$°C	
Ω_X	Total surface area of all aerosols larger than 0.1 μm in diameter from group X	[aerosol] m^2 [air] kg^{-1}
$\Omega_{X,int}$	Interstitial component of Ω_X	[aerosol] m^2 [air] kg^{-1}
$\Omega_{X,1,*}$	Component of Ω_X in background-troposphere scenario for aerosol diameters between 0.1 and 1 μm with X = {Dust, BC/OM}	[aerosol] m^2 [air] kg^{-1}

Here, we assume that all hydrophobic dust and black carbon/organic matter can act as contact IN at -4°C. Furthermore, we assumed that all dust was hydrophobic and that the hydrophobic fraction of BC/OM was 17%, which is the global average value from the general circulation model simulation of *Reddy and Boucher.* [2004]. The justification for BC/OM acting as contact ice nuclei can be found in *Pruppacher and Klett* [1997] who state that organic compounds as well as other compounds are considerably better IN when acting in the contact mode rather than in the freezing or deposition modes. In addition, *Gorbunov et al.* [2001] found that soot particles act as efficient ice nuclei and their result has been interpreted as contact freezing, though this is under debate [*Storelvmo et al.,* 2008]. Therefore, N_{a0} is given as the sum of the number concentration of dust and 17% of the number concentration of black carbon/organic matter. Assuming all hydrophobic dust and BC/OM as contact IN might be an overestimation. In section 3.9, we discuss a sensitivity simulation, where the percentage of dust and BC/OM that act as contact ice nuclei is greatly reduced to match the contact IN concentration (0.2 cm^{-3}) assumed in *Young* [1974]. The impact to the anthropogenic aerosol forcing in mixed-phase clouds is also discussed there.

2.2.3 Set-up of simulations and experimental design

We use 26 vertical levels and a horizontal resolution of 2×2.5 degrees for both the CAM3 and IMPACT models in this study. The time step for CAM3 is 30 minutes, and that for advection in IMPACT is 1 hour. The finite volume dynamical core for CAM3 is used.

Six model experiments are designed. Table 2.2 summarizes the set-up of the experiments. The Mey_YCT case employs the Meyers parameterization for DCI IN and the Young parameterization for contact IN, similar to the original set-up of the CAM-IMPACT model [*Wang and Penner*, 2010]. Therefore, we specified this as the reference case. Phi_YCT is similar to Mey_YCT, except that the DCI IN parameterization is replaced by

the Phillips parameterization. In Mey_PCT and Phi_PCT the contact IN parameterization is that of *Phillips et al.* [2008]. Two pre-industrial simulations Phi_PCT_PImix and Mey_PCT_PImix are performed, in order to gauge the overall impact of mixed-phase clouds on climate forcing.

All the six experiments were run for 5 years and 4 months with fixed present-day sea surface temperatures. The first 4 months are treated as model spin-up and are excluded from the analysis presented below. Assessments are made of the changes of ice nuclei number concentration, cloud liquid/ice amount, the global radiation budget, and the effect of anthropogenic aerosols in mixed-phase clouds.

2.3   Results and Discussion

2.3.1   Comparison of deposition/condensation/immersion ice nuclei distributions

Figure 2.1 a, b, and c show the zonal and annual mean plots of DCI IN predicted in the

Mey_YCT and Phi_YCT simulations (Table 2.2) and their differences. Distinct features

Table 2.2: Sensitivity Simulations

Simulation	Description
Mey_YCT	Reference simulation using: Meyers (1992) parameterization for DCI freezing Young (1974) parameterization for contact freezing
Phi_YCT	Phillips et al. (2008) parameterization for DCI freezing Young (1974) parameterization for contact freezing
Mey_PCT	Meyers (1992) parameterization for DCI freezing Phillips et al. (2008) parameterization for contact freezing
Phi_PCT	Phillips et al. (2008) parameterization for DCI freezing Phillips et al. (2008) parameterization for contact freezing
Phi_PCT_PImix	Same as Phi_PCT, but with pre-industrial black carbon and organic matter for mixed-phase clouds ice nucleation.
Phi_YCT_PImix	Same as Phi_YCT, but with pre-industrial black carbon and organic matter for mixed-phase clouds ice nucleation.
Phi_YCT_Less	Same as Phi_YCT but with a reduced fraction of BC/OM and dust as contact IN to match the original *Young* (1974) assumption.

are seen using the two different parameterizations. In Mey_YCT, the ice nuclei

concentration in the Southern and Northern Hemispheres generally follows the

temperature distribution. This is caused by the assumption that mixed-phase clouds are at

water saturation, so that the ice saturation ratio follows the temperature distribution.

However, in Phi_YCT, there is a peak in the DCI IN concentrations near 400 hPa at 60

degrees latitude in both Hemispheres, with the peak in the Northern Hemisphere larger

than that in the Southern Hemisphere. The peak in the DCI IN concentration can be

attributed to the combined effects of the aerosol availability and the temperature that is
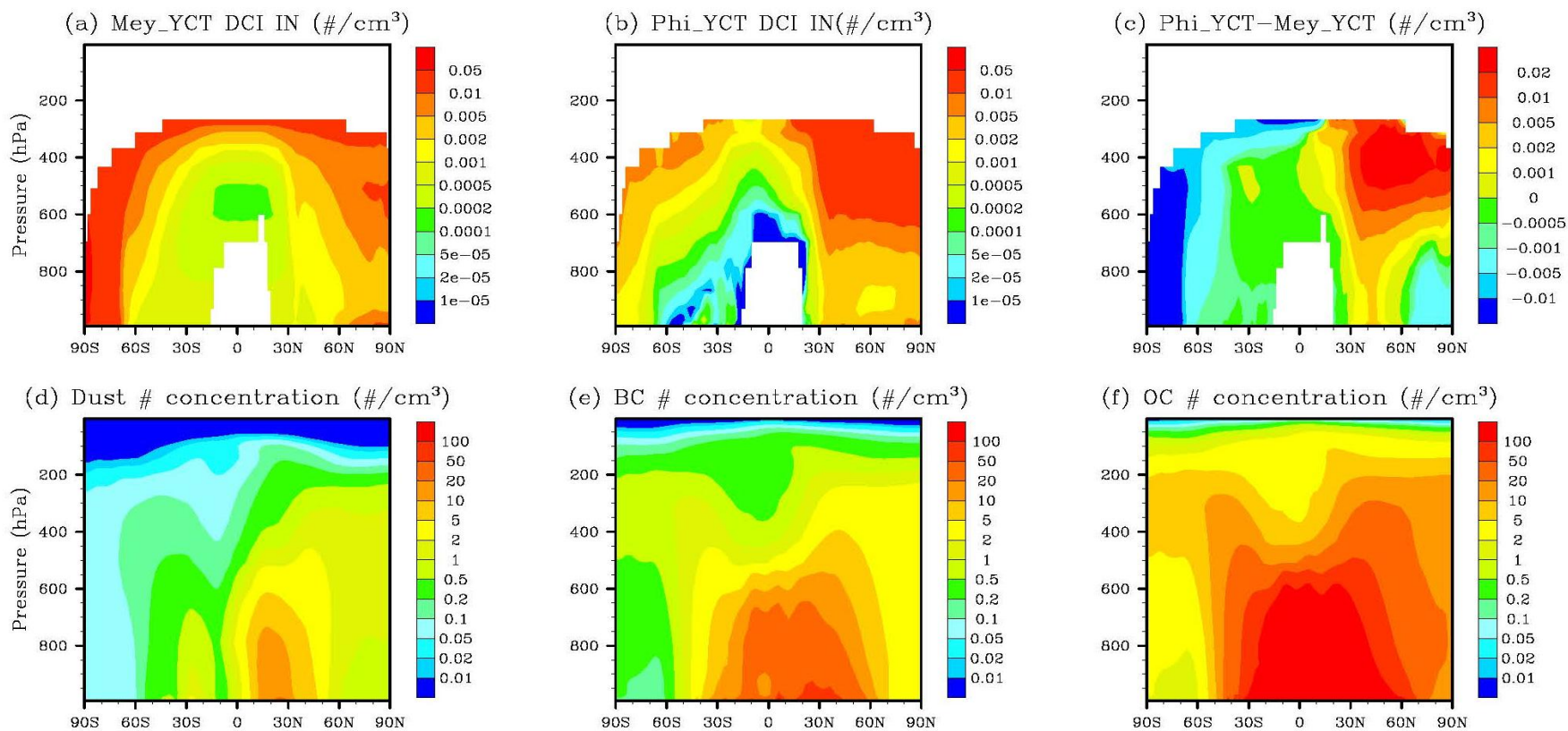
Figure 2.1: Zonal and annual mean latitude versus pressure plots of deposition/condensation/immersion freezing ice nuclei in Mey_YCT, Phi_YCT, and their differences (plot a, b, and c). Zonal and annual mean latitude versus pressure plots of dust, black carbon, and organic carbon (plot d, e, and f).

most suitable for producing DCI IN, which can be shown by comparing with the aerosol distributions (Figure 2.1 d, e, and f) and the temperature distribution (not shown). The larger peak in the Northern Hemisphere is due to the larger aerosol concentrations in the Northern Hemisphere.

One can also notice that there is a "pipeline" of DCI IN near 40N from the surface up towards the middle troposphere, which may correspond to the upward transport of dust from eastern China/Mongolia and BC/OM from Northern Hemisphere (NH) industrial regions (Figure 2.2). This is consistent with the hypothesis proposed by *Isono et al.* [1970] and *Hobbs et al.* [1971a, b] that the dust storms in Northern China and Mongolia can be advected by strong tropospheric winds and create an IN storm. The region above the equator is found to be deficient in IN which is similar to the summary given in *Pruppacher and Klett* [1997]. The other two cases, Phi_PCT and Mey_PCT show similar features in the predicted DCI IN concentrations, so their figures are not included here. In the Southern Hemisphere (SH), the Phillips DCI freezing parameterization generally produces smaller DCI IN concentrations than the Meyers parameterization (see Figure 2.1 c). In the NH, the Phillips DCI freezing parameterization produces larger DCI IN concentrations than the Meyers parameterization at altitudes around 400~600 hPa. At lower altitudes in the NH, the relative differences between the two parameterizations depend on latitude. Between 30°N and 60°N, due to higher aerosol concentrations, the DCI IN concentration predicted by the Phillips DCI freezing parameterization is larger than that from the Meyers parameterization. However, from 60°N onwards, the Meyers
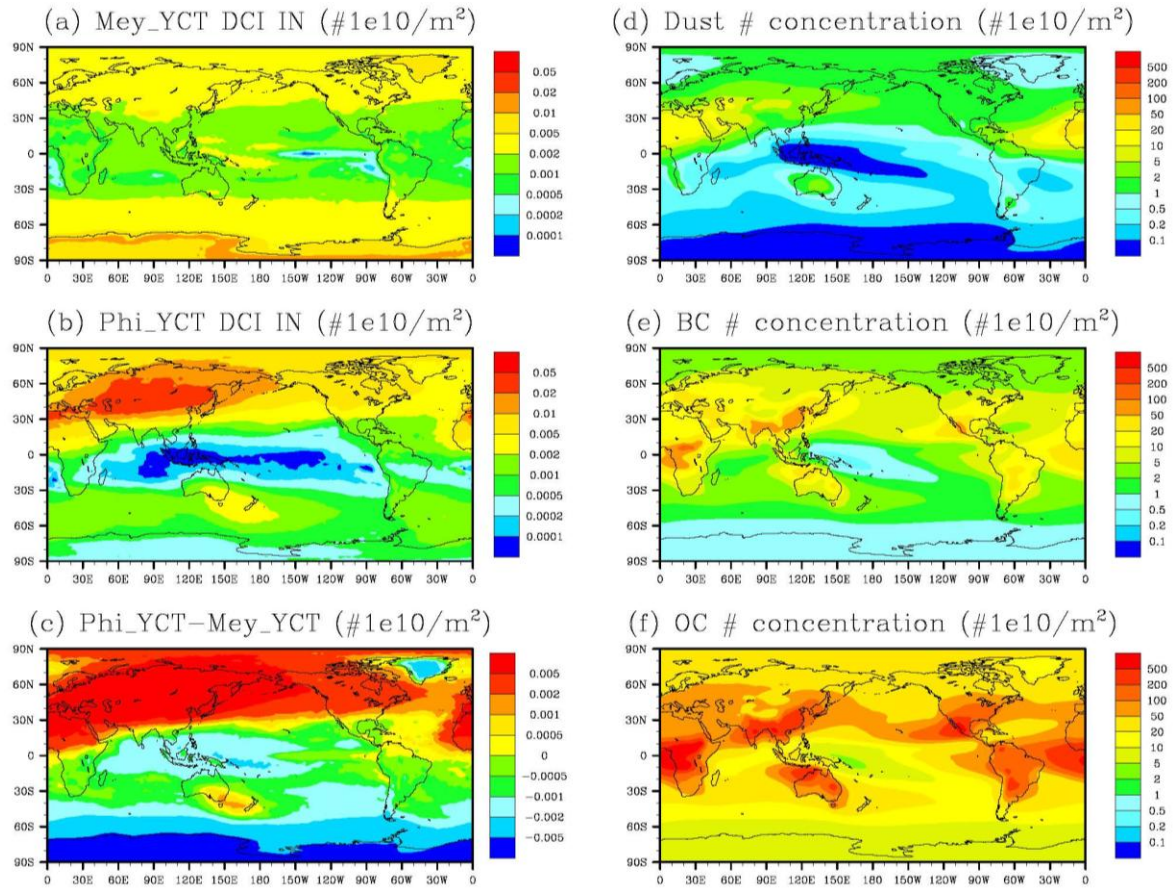
Figure 2.2: Vertically integrated latitude versus longitude plots of annually averaged deposition/condensation/immersion freezing ice nuclei in Mey_YCT and Phi_YCT, and their differences (plot a, b, and c). Vertically integrated annually averaged latitude versus longitude plots of dust, black carbon, and organic carbon (plot d, e, and f).

parameterization predicts larger DCI IN concentration than the Phillips DCI freezing parameterization.

Figure 2.2 a and b show the horizontal distribution of the vertically integrated DCI ice nuclei concentration for the Mey_YCT and Phi_YCT simulations. The simulation Phi_YCT shows a clear North-South contrast in the DCI IN concentration distribution patterns, which is not present in the Mey_YCT simulation. This North-South contrast is due to the differences in the aerosol distributions between the two hemispheres (see Figure 2.2 d, e, and f). The maximum of the DCI IN concentration in the Phi_YCT simulation is above the eastern China/Mongolia region, due to the high concentration of dust aerosol and the low temperatures there. Dust emissions from the Saharan desert and Australia are clearly seen in the DCI IN predicted from Phi_YCT. Fossil fuel burning BC/OM in the industrialized regions of southeast Asia, Europe, and North America; biomass burning BC/OM in South America and middle Africa do not have a significant impact on the distribution of DCI IN, because BC and OM together contribute only about ⅓ of the total DCI IN in the Phillips parameterization. In general, the DCI ice nuclei distribution predicted by Phi_YCT is larger in regions with higher aerosol emissions, and vice versa. Whereas the Meyers parameterization only tends to increase with decreasing temperature and does not include, for example, variations associated with dust. In the following sections, we will discuss how the correlation of the IN concentrations with the aerosol fields in the simulations using Phillips DCI freezing parameterization changes the spatial variations of the cloud ice field, the cloud fractions, and the global radiation budget.
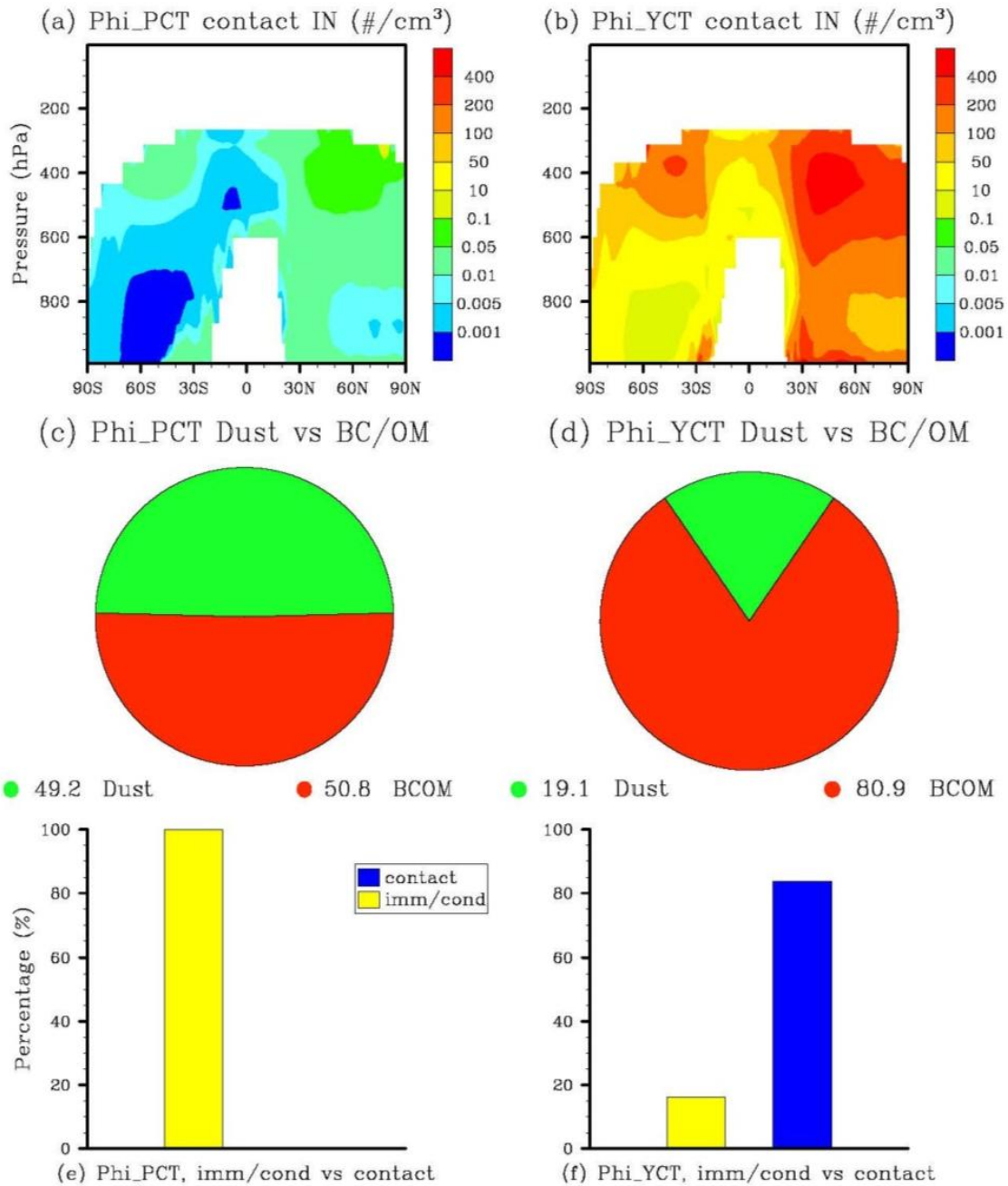
Figure 2.3: Zonal and annual mean latitude versus pressure plots of contact freezing ice nuclei for the (a) Phi_PCT simulation and the (b) Phi_YCT simulation. (c) and (d): global and annual average fraction of dust and BC/OM contact IN in mixed phase clouds for the two simulations, and (e) and (f): global and annual average relative contribution of contact freezing and DCI freezing to newly formed ice crystals.

2.3.2   Comparison of contact ice nuclei distributions

Figure 2.3 (upper panel) shows the contact IN predicted by the Phi_PCT and Phi_YCT cases. The contact IN predicted by Mey_PCT and Mey_YCT are not shown because they are very similar to the Phi_PCT and Phi_YCT cases. As shown in the figure, using the Phillips contact freezing parameterization decreases the contact IN concentration by three orders of magnitude. The spatial distribution of contact IN predicted from the two parameterizations is, however, very similar. There are two peaks of contact IN number concentrations around 400 hPa at mid-latitudes of both hemispheres, with the peak in the NH larger than that in the SH. The number concentration and spatial distribution of contact IN in the YCT cases are very similar to those shown in *Lohmann* [2002] where the contact nuclei are assumed to be insoluble carbonaceous particles (sum of hydrophobic black carbon and organic carbon). The middle panel of Figure 2.3 shows the percentage contribution from dust and BC/OM to the contact ice nuclei predicted from the two cases. For the Phi_PCT case, the contributions from dust and BC/OM are relatively equal, while for the Phi_YCT case, the contribution from BC/OM is much larger than that from dust. The reason is that the Phillips contact freezing parameterization prescribes the fractional contribution of dust to total ice nuclei at the reference condition to be ⅔, and the fractional contribution of BC/OM to be ⅓. Thus, even though the BC/OM surface and number concentrations are much larger than those of dust, the contribution from dust remains large. The lower panel in Figure 2.3 compares the relative contribution of contact freezing and DCI freezing to newly formed ice crystals. The contribution of contact freezing is minimal in the Phi_PCT case, with DCI

53

freezing contributing almost 100%. However in the Phi_YCT case, contact freezing contributes more than DCI freezing, with the relative contribution of the two being 83.81% and 16.19%, respectively.
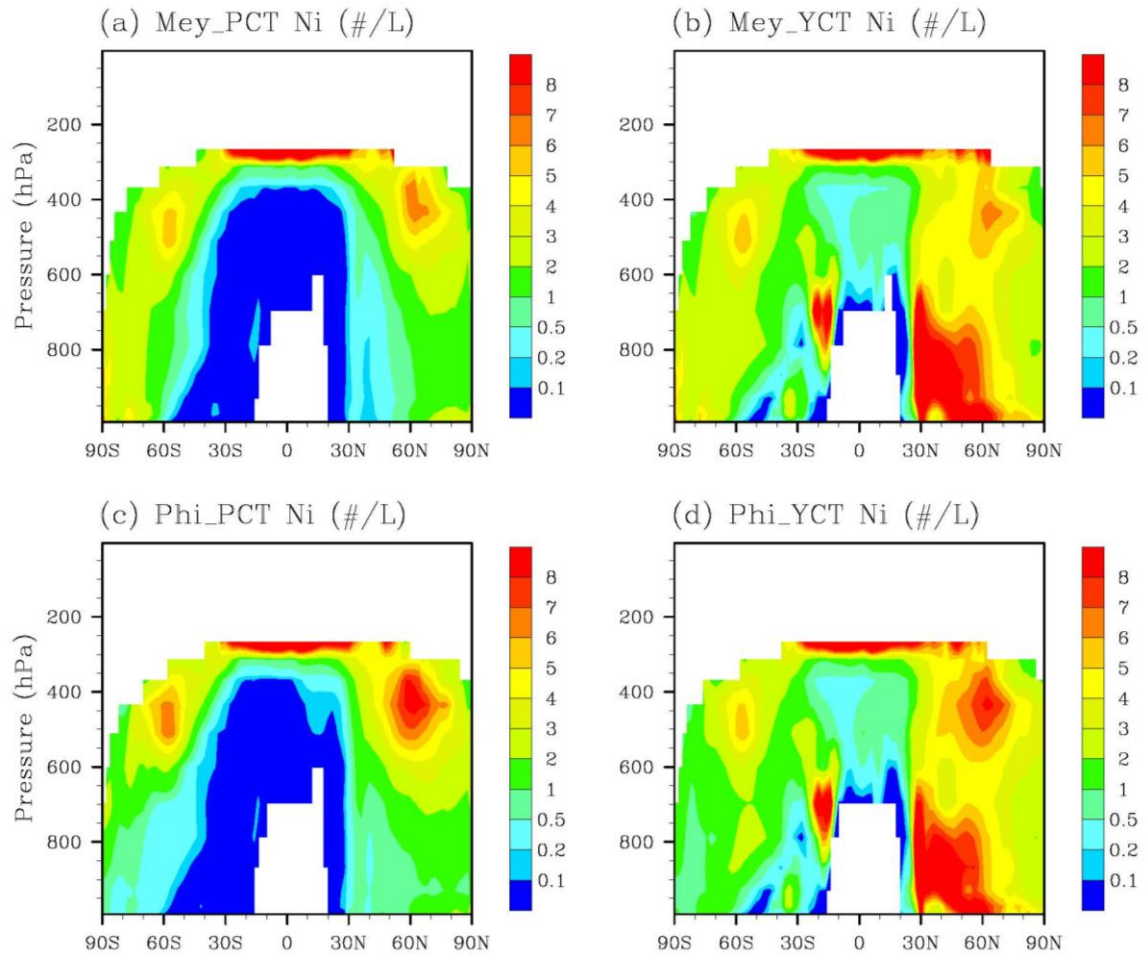
Figure 2.4: Zonal and annual mean latitude versus pressure plots of ice crystal number concentration in mixed-phase clouds from the four simulations.

2.3.3 Zonal mean latitude-pressure cross sections of ice and liquid cloud properties in mixed-phase clouds

Figure 2.4 shows zonal and annual average plots of the grid-average ice crystal number concentrations (Ni) in mixed-phase clouds from the four present-day simulations. A comparison of Mey_PCT with Phi_PCT, and of Mey_YCT with Phi_YCT shows that the use of the Phillips DCI freezing parameterization predicts more ice crystals in the middle troposphere of the NH, and fewer ice crystals in almost all of the SH. This is consistent with the comparison of the DCI ice nuclei distributions. Where ice crystal number concentrations increase, the effective ice crystal radius decreases and vice versa (figure not shown), because the limitation of the available water vapor will hinder the growth of the more numerous ice crystals. This is consistent with the findings of *Storelvmo et al.* [2011]. In addition, we expect that smaller ice crystal sizes decrease gravitational settling and lead to longer cloud lifetimes and larger ice water mixing ratios. This is demonstrated by the increase in ice water mixing ratio between 400 hPa and 600 hPa in the NH and the decrease in ice water mixing ratio in the SH with the Phi cases compared to the Mey cases (Figure 2.5).

At the same subfreezing temperature, the saturation vapor pressure over ice is smaller than that over water. Therefore, water vapor will condense onto existing ice crystals, while liquid droplets will evaporate to compensate for the depleted water vapor. This is the so-called Bergeron-Findeisen process. In places where we see an increase in ice water and ice number, the radius of cloud droplets is decreased (Figure 2.6), and vice versa,

because of the stronger Bergeron-Findeisen process. For example, the cloud droplet effective radius is smaller in Phi_PCT than in Mey_PCT in the NH between 400 and 600 hPa, and larger in the SH. The change in the cloud droplet effective radius in the NH between Mey_YCT and Phi_YCT is not very apparent because of the dominant effect of the Young contact freezing parameterization (Figure 2.3 f). Droplet evaporation in the model is represented by assuming that the loss rate of cloud liquid droplet number from the Bergeron-Findeisen process is half of the loss rate of the cloud liquid mass in the model. The changes of cloud droplet number and cloud liquid water mixing ratio are similar to that of the cloud droplet radius in these regions (figures not shown).

The Young contact freezing parameterization predicts more ice crystals at all latitudes and heights than does the Phillips contact freezing parameterization (Figure 2.4). Although the number concentration of contact ice nuclei decreases by three orders of magnitude from the YCT to the PCT cases (compare Figure 2.3 a to Figure 2.3 b), the number concentration of ice crystals changes by less than one order of magnitude (compare Figure 2.4 a to Figure 2.4 b, or Figure 2.4 c to Figure 2.4 d). This is because the contact-freezing rate also depends on the number concentration of cloud droplets, which is larger in the PCT cases where contact freezing is less efficient, and thus has a buffering effect on the change of contact freezing rate. This buffering effect was also pointed out in *Lohmann* [2002]. The ice crystal number concentration is significantly larger in the YCT cases in the region below 800hPa at NH mid-latitudes (between 30N and 60N). This is probably associated with fossil fuel BC and OM emissions in this region. *Lohmann* [2002] showed a similar increase between a case where contact ice nuclei was assumed to

56
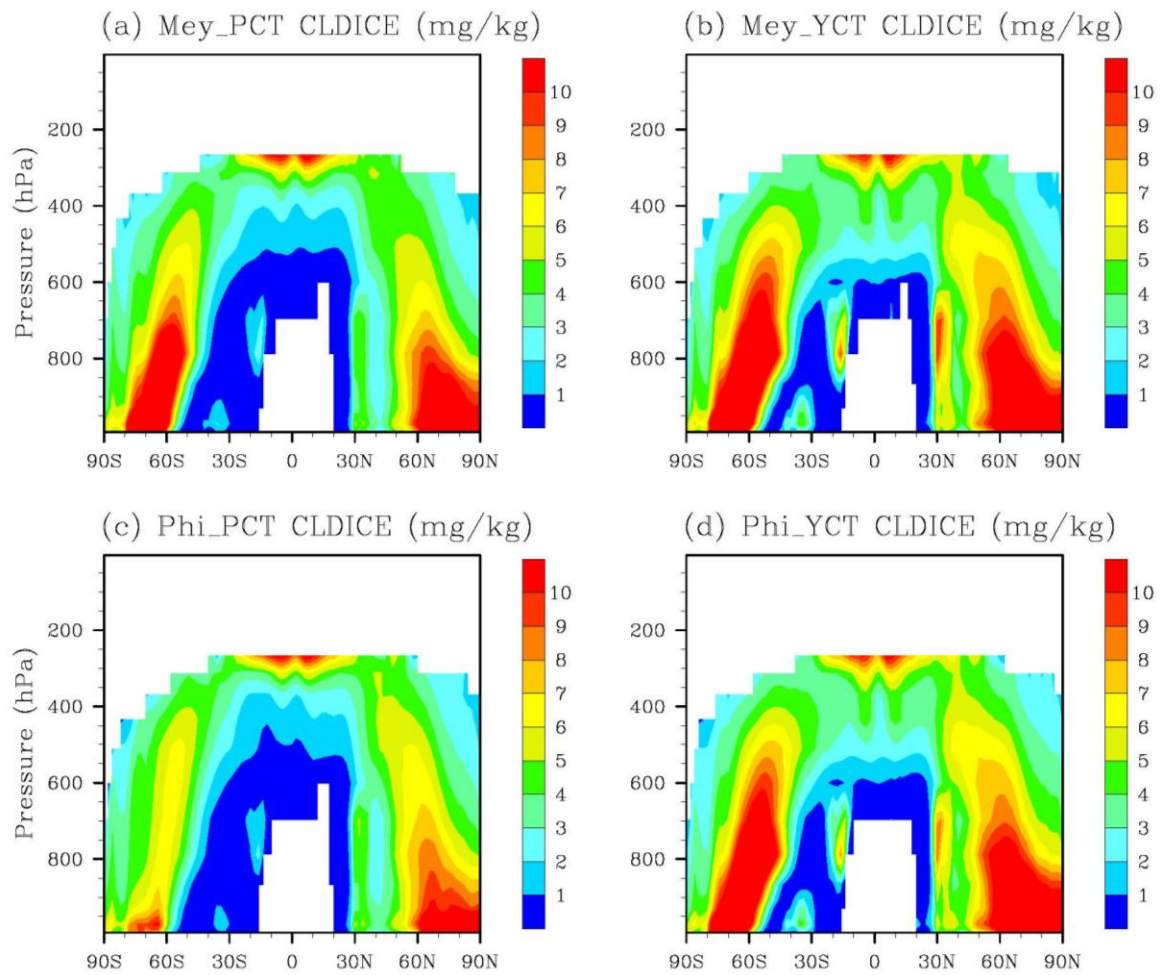
Figure 2.5: Zonal and annual mean latitude versus pressure plots of ice water mixing ratio in mixed-phase clouds from the four simulations.

be both dust and black carbon and a case where only dust acted as contact nuclei (Figure

3 in *Lohmann*, 2002). The larger ice crystal number concentration in the YCT cases leads

to smaller effective ice crystal radii and higher cloud ice water mixing ratios. For

example, the cloud ice water mixing ratio is larger in the Phi_YCT simulation (Figure 2.5

d) than in the Phi_PCT simulation (Figure 2.5 c). Because of the more efficient Bergeron-

Findeisen process, the effective droplet radius (Figure 2.6), droplet number concentration,

and cloud liquid content are smaller in all regions in the YCT cases. Overall, the effect of

changing the contact freezing parameterization from Young to Phillips on the cloud liquid

and ice field is more pronounced than that of changing the DCI parameterization from

Meyers to Phillips.

2.3.4   Probability distributions of in-cloud ice fraction

Figure 2.7 shows the probability distributions of in-cloud ice fraction (in-cloud ice water

content divided by in-cloud total water content) in different temperature ranges from the

four present-day simulations as well as observations from *Korolev et al.* [2003]. Model

output is calculated in the same way as described in *Gettelman et al.* [2010]. Ice fraction

is calculated only for grid points in mixed-phase conditions between 1000-100 hPa and

90°S-90°N. All of the four simulations show a high probability of pure liquid and ice

cloud conditions, and a low probability for mixed-phase clouds. The probability

distributions of ice fraction for all temperature intervals shift towards lower ice fractions

when going from the Mey_PCT case to the Phi_PCT case. There is also a decrease in the
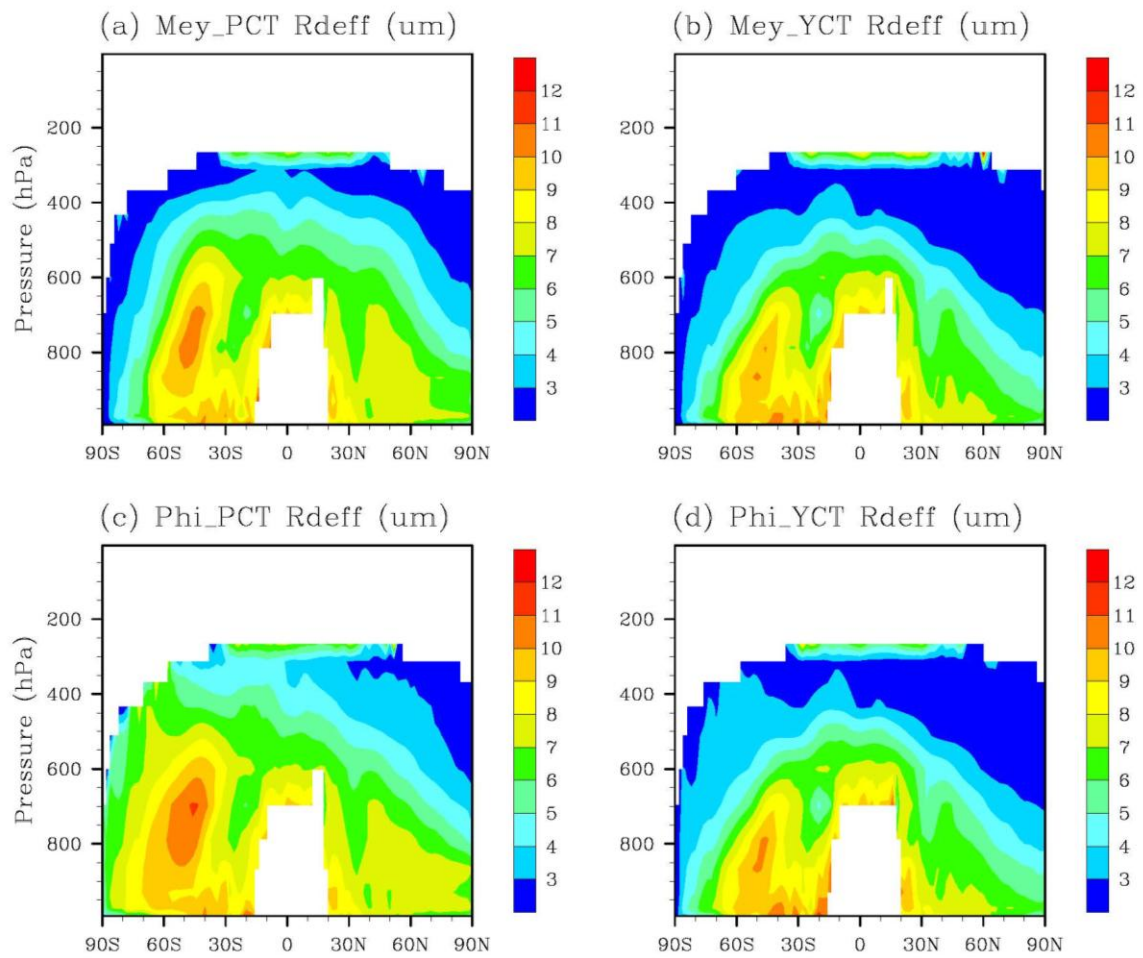
Figure 2.6: Zonal and annual mean latitude versus pressure plots of effective cloud droplet radius in mixed-phase clouds from the four simulations.

frequency of occurrence of intermediate ice fractions. This means, when using the Phillips DCI freezing parameterization, the possibility for a given grid box to have a low ice fraction and high liquid fraction is increased, while the chance of having a mixture of ice and liquid is decreased. Since the model output is calculated from grid boxes ranging from -90 to 90 latitudes, this change in the in-cloud ice fraction is an average result from local changes in cloud ice mass mixing ratio and cloud liquid mass mixing ratio. The difference between the Mey_YCT and Phi_YCT cases are very small, because of the dominant effect of contact freezing (Figure 2.3 f).

Comparing the Phillips contact freezing parameterization to the Young contact freezing parameterization (Mey_PCT vs. Mey_YCT, and Phi_PCT vs. Phi_YCT) shows that there is a significant change in the probability distribution of ice fractions. At all temperatures, the probability is decreased for low and intermediate ice fractions, and increased for high ice fractions in the simulations using the Young parameterization. This means, for any given grid box, there is a higher probability that it contains pure ice cloud than a mixed-phase or a supercooled liquid cloud when using the Young contact freezing parameterization. This result is consistent with the larger grid mean ice mass mixing ratio and smaller grid mean liquid mass mixing ratio from the YCT cases compared to the PCT cases (Section 3.3). The above changes to the probability distribution of ice fractions will have an effect on the cloud optical depth observed for middle altitudes clouds, and therefore affects the cloud fraction comparison to ISCCP observations (discussed in the next section).
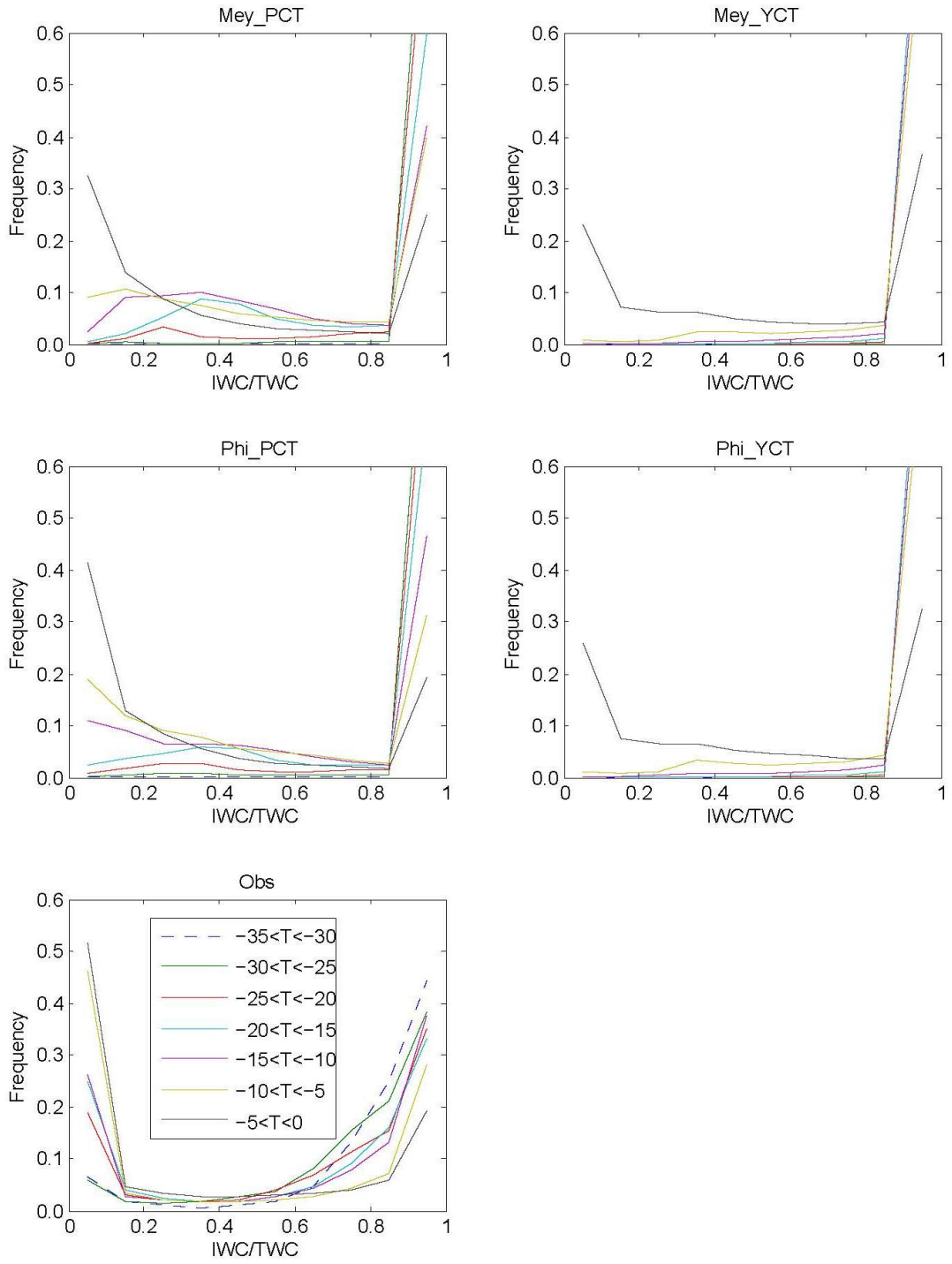
Figure 2.7: (a) – (d): Probability distributions of ice fraction at different temperature ranges predicted by the four present-day simulations. (e) observations from *Korolev et al.* [2003].

The frequency of occurrence of nearly pure liquid clouds is too low for all simulations compared to the observations, while the frequency of occurrence of mixed-phase conditions is high compared to observations. This might be due to the treatment of vapor deposition to ice simultaneously with the Bergeron-Findeisen process in the model, because the net loss of vapor to ice should only occur when liquid water is used up and saturation with respect to water can no longer be maintained. The current treatment might lead to more cloud ice, which in turn leads to a stronger depletion of cloud liquid by the Bergeron-Findeisen process. An adjustment of the scheme to account for the complete removal of liquid water prior to vapor deposition might improve the comparison. Under the current set-up, the Phi_PCT simulation is closer to the observations than the other three cases.

2.3.5 Comparison of middle cloud fractions to ISCCP observations

Figure 2.8 compares the amount of middle cloud (%) predicted from the four present-day model simulations to that observed in ISCCP. The model outputs are sampled using the ISCCP cloud simulator (http://cfmip.metoffice.com/ISCCP.html), so as to emulate the scenes observed by the satellites. The cloud type is determined by the combination of cloud optical thickness and cloud top pressure using the same criteria as that for the ISCCP satellite observations. For middle clouds, the cloud top pressure criterion is set to be between 680 and 440 hPa. Within the middle cloud category, altocumulus clouds are assumed to have an optical thickness of 0-3.6, altostratus clouds are assumed to have an optical thickness of 3.6-23, and nimbostratus clouds are assumed to have an optical

62

thickness of 23-379. As shown in Figure 2.8, all of the four model simulations significantly under-predict the optically thin and intermediate middle clouds (altocumulus and altostratus). There is also an under-prediction of the optically thick nimbostratus clouds, but to a lesser extent. *Lin and Zhang* [2004] did similar comparisons between the CAM2 cloud fractions and ISCCP observations. They also found a significant underestimation of middle clouds and proposed that "drier atmosphere in the subsidence regime, and lack of cloud formation in shallow convection scheme" are two possible causes [*Lin and Zhang*, 2004, page 3310]. Comparing the simulation Mey_PCT and the simulation Phi_PCT shows that the cloud fraction of the optically thin altocumulus clouds is decreased from Mey_PCT to Phi_PCT, while the amount of the optically intermediate altostratus clouds, and the optically thick nimbostratus clouds are increased. The latitude-longitude middle cloud distributions (not shown) show that the increases in altostratus and nimbostratus clouds in the Phi_PCT case mainly occur in the SH. This is where we observed a decrease in the cloud ice mixing ratio (Figure 2.5), and an increase of cloud liquid mixing ratio in the Phi_PCT case. With the same amount of condensed water, liquid water tends to be smaller and more numerous, and thus optically thicker. So having a smaller ice fraction (Figure 2.7) and a larger liquid fraction increases the cloud optical thickness in the Phi_PCT simulation. Therefore, more middle clouds will be classified as optically intermediate altostratus and optically thick nimbostratus, and less will fall into the altocumulus group.
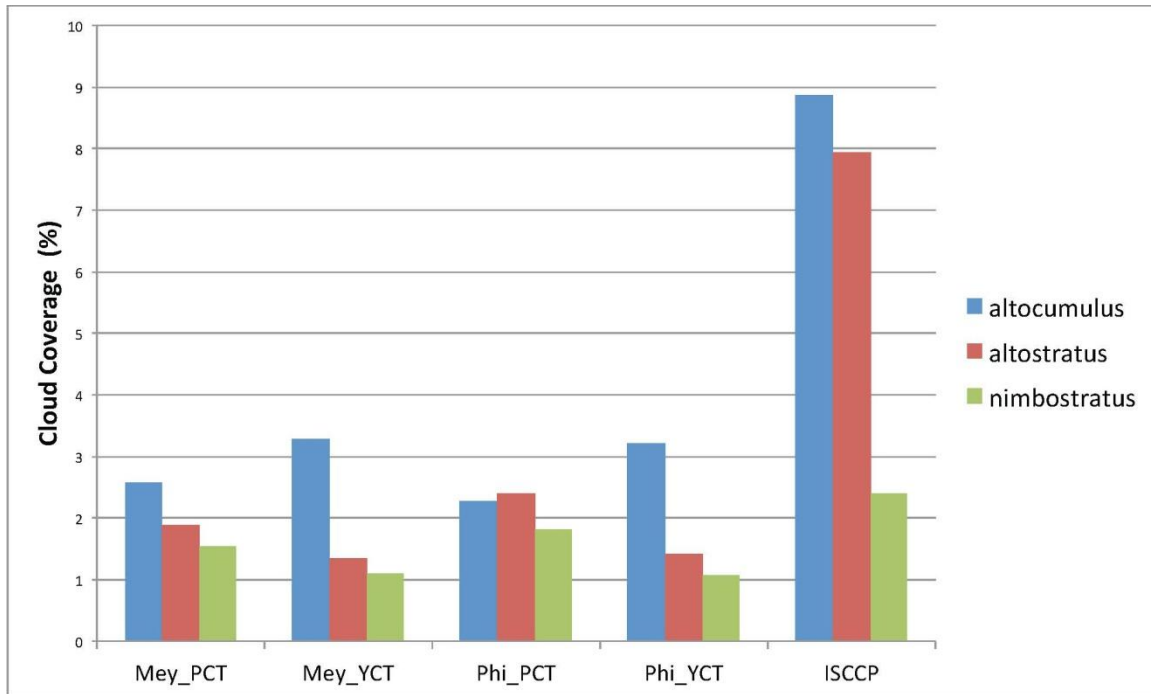
Figure 2.8: Middle cloud (altocumulus, altostratus, and nimbostratus) fraction (%) predicted from the four simulations and observed in ISCCP.

The Phillips contact freezing parameterization leads to smaller ice fractions than the Young parameterization (Figure 2.7). So the optical thickness of middle clouds is larger in the simulations using the Phillips contact freezing parameterization compared to those using the Young parameterization for the same reasons as explained above. Therefore, the amount of optically thin altocumulus clouds is smaller in the PCT cases, and the amount of altostratus and nimbostratus clouds are larger. The use of the Phillips DCI freezing parameterization and contact freezing parameterization improves the agreement of altostratus and nimbostratus clouds with ISCCP, at the expense of the agreement of altocumulus clouds.

2.3.6 Zonal means of radiation and vertically integrated mixed-phase cloud properties

Figure 2.9 a shows the zonal average distribution of vertically integrated ice crystal number concentration in mixed-phase clouds. As anticipated from the latitude-pressure cross section plots, higher ice crystal concentrations occur in cases in which the Young contact freezing parameterization is used, and in cases using the Phillips DCI freezing parameterization in the NH. In the SH, the Meyers parameterization predicts slightly more ice crystals in mixed-phase clouds.

The differences in cloud water content and ice crystal number concentration between Mey_YCT and Phi_YCT are small because of the dominant contribution of contact freezing. Therefore, we focus our discussion on the differences between Phi_PCT (red solid line) and Mey_PCT (blue solid line) to reveal the effects of using different DCI freezing parameterizations. The effective ice crystal radius (Figure 2.9 c) in the Mey_PCT simulation is larger than in the Phi_PCT simulation in the NH mid-latitudes, and smaller in the SH due the change in ice crystal number concentration and the limitation of water vapor. The effective cloud droplet radius (Figure 2.9 d) change between Mey_PCT and Phi_PCT is opposite that of the ice crystal number concentration because of the Bergeron-Findeisen process . The smaller IWP in the SH from Phi_PCT compared to that from Mey_PCT leads to more cloud droplets (Figure 2.9 b) and a larger LWP (Figure 2.9 f) because of the less efficient Bergeron-Findeisen process. Since liquid
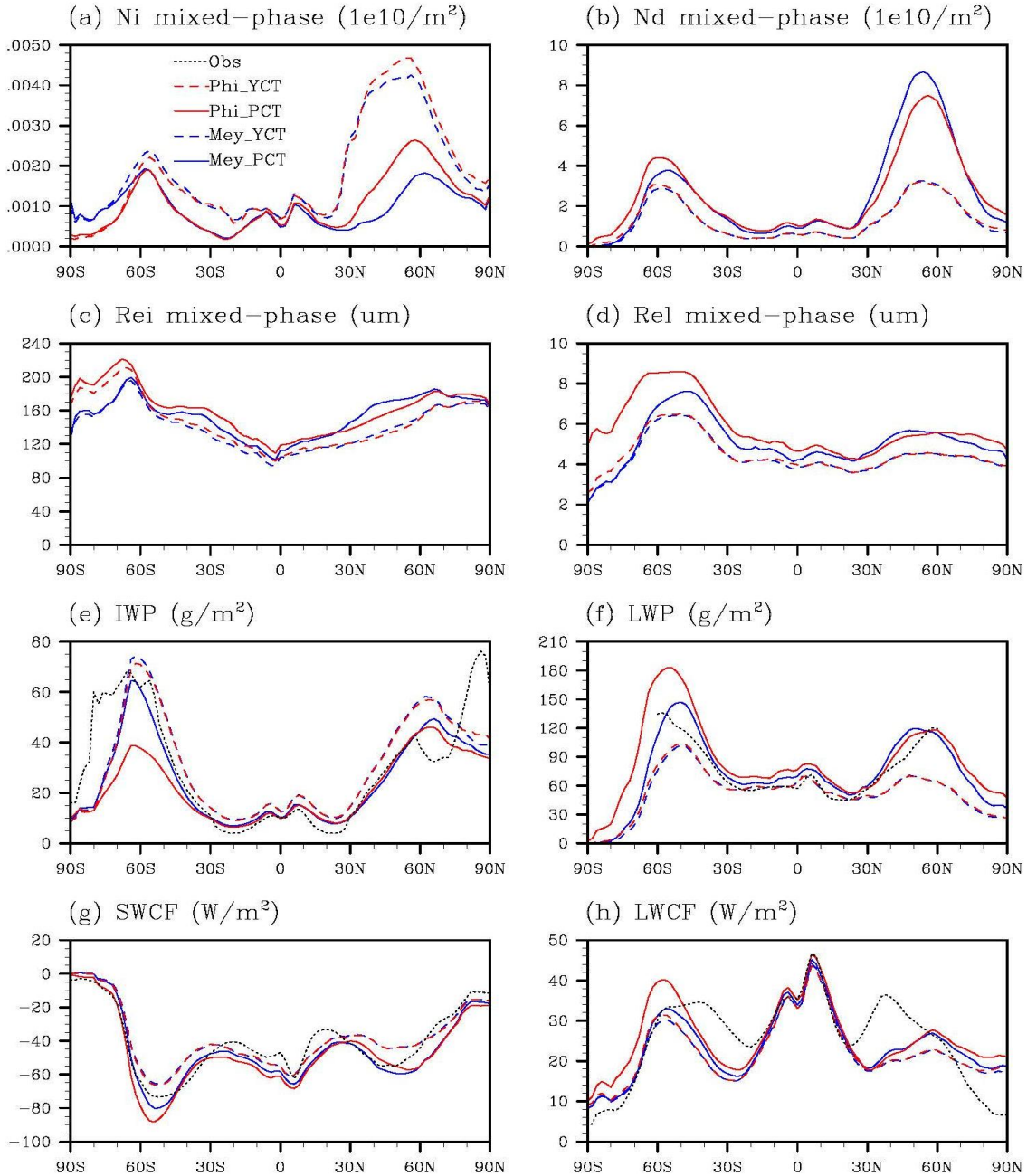
Figure 2.9: Zonal and annual mean shortwave cloud forcing (SWCF), longwave cloud forcing (LWCF), liquid water path (LWP), ice water path (IWP), vertically integrated mixed-phase cloud droplet number concentration (Nd) and ice crystal number concentration (Ni), effective cloud droplet radius (Rel) and ice crystal radius (Rei) in mixed-phase clouds from the four Present-Day model experiments described in Table 2.2. Black dotted lines refer to CERES data for LWCF and SWCF (http://ceres.larc.nasa.gov), MODIS data for LWP (http://modis.gsfc.nasa.gov/), and ISCCP data for IWP (http://isccp.giss.nasa.gov/).

droplets are generally smaller than ice crystals (and because the LWP is larger than the IWP), they tend to produce a larger forcing, so that the shortwave cloud forcing (SWCF) and longwave cloud forcing (LWCF) (defined as the difference in the top-of-atmosphere (TOA) shortwave and longwave radiation between all-sky and clear-sky conditions) are larger in magnitude in Phi_PCT parameterization than in the Mey_PCT parameterization in the SH. It should be noted here that the use of SWCF to evaluate the changes in clouds could also include changes in the surface albedo, which would then be wrongly associated with clouds. However, the top-of-atmosphere clear-sky net solar flux change is only $1.69 - 5.78\%$ of the top-of-atmosphere full-sky net solar flux change among the model simulations. Since the aerosol field used for different model simulations is very similar, we can assume that the clear-sky net solar flux change mainly comes from clear-sky albedo change. So the effect of clear-sky albedo change on SWCF is small.

DeMott et al. [2010] compared a global climate model simulation using the Meyers parameterization and the *DeMott et al.* [2010] IN parameterization that depends both on temperature, and on the number concentration of aerosols exceeding 0.5 μm in diameter. They also observed a decrease in IWP, and increases in LWP, SWCF, and LWCF from the simulation using Meyers to the simulation using the new aerosol dependent parameterization. The reason for this change was attributed to the reduced IN concentration of non-sea-salt particles larger than 0.5 μm. This is consistent with our finding that the use of the aerosol dependent IN parameterization decreases IWP, and increases LWP, SWCF, and LWCF.

The Phillips contact freezing parameterization predicts less Ni in mixed-phase clouds than the Young contact freezing parameterization. The fewer ice crystals produced using the Phillips contact freezing parameterization leads to larger effective ice crystal radius (compare the red solid line to the red dotted line, and blue solid line to blue dotted line in Figure 2.9 c). It also leaves more water droplets, produces larger effective cloud droplet radius, and LWPs at all latitudes (Figure 2.9 b, d, and f). Therefore, the SWCF and LWCF are larger in magnitude for the cases that use the Phillips contact freezing parameterization (Figure 2.9 g, h).

The global cloud properties predicted by the four present-day model simulations are compared to satellite observations in Figure 2.9. Since the differences in the SWCF and LWCF field are mainly due to changes in the LWP, which in turn is modified through changes in IWP, we focus our discussion on differences in the IWP here. The IWP data from ISCCP is constructed in the same way as in *Storelvmo et al.* [2008]. Thus, the IWP from 1983 to 2000 from nine cloud types (cirrus, cirrostratus, and deep convective clouds, in addition to the ice fraction of altostratus, altocumulus, nimbostratus, cumulus, stratocumulus, and stratus clouds) are added together to produce the total IWP. Cirrus cloud is defined by ISCCP to have a cloud top pressure higher than 440 hPa. However, in the tropics, liquid water may exist above 440 hPa. To take this fact into account, in the tropics (30°S to 30°N), ⅓ of the cloud water in cirrus, cirrostratus, and deep convective clouds is assumed to be liquid. Beyond this region, all cloud water in cirrus, cirrostratus,

and deep convective clouds is assumed to be in the ice phase. This approach is different from that adopted by *Eliasson et al.* [2011] since ice clouds in the tropics are not partially classified into liquid clouds by their method. The IWP from ISCCP is shown to be smaller than the newer estimates from CloudSat [*Eliasson et al.,* 2011]. Generally, the IWP from the PCT cases compares well with observations in the NH, while the YCT cases all over-predict the IWP in the NH. In the SH, all cases compare well with the ISCCP IWP, except for Phi_PCT, which under-predicts IWP by nearly $20g/m^2$ around 60S. The fact that the IWP predicted in the Phi_PCT and Mey_PCT cases agree fairly well with satellite observations in the NH shows that the Phillips DCI parameterization is able to correctly predict ice water contents with an online calculation of the aerosol fields. The Mey_PCT simulation compares well with satellite observations of IWP in the SH, which implies that the under-prediction of IWP in the Phi_PCT simulation in the SH is due to the small amount of DCI IN predicted by the Phillips DCI freezing parameterization. The IWP predicted in the Phi_YCT simulation compares well to ISCCP observation, because of the more contact ice nuclei predicted from the Young parameterization. The under-prediction of IWP in the SH by Phi_PCT suggests the possibility that there are missing sources of ice nuclei in the SH. Although the YCT cases are in better agreement with the observed IWP in the SH, they over-predict IWP in the NH.

2.3.7 Global mean radiation budget and cloud parameters

The global mean radiation budget and cloud water paths are summarized in Table 2.3. The shortwave (SWCF) and longwave (LWCF) cloud forcing observations are taken from ERBE for the years 1985-1989 [*Kiehl and Trenberth*, 1997] and CERES for the years 2000-2005 (http://ceres.larc.nasa.gov). In addition the longwave (LWCF) cloud forcing from TOVS retrievals [*Susskind et al.*, 1997; *Scott et al.*, 1999] is included. The liquid water path (LWP) observations are from SSM/I [for the years 1987-1994, *Ferraro et al.*, 1996; for August 1993 and January 1994, *Weng and Grody*, 1994; and for August 1987 and February 1998, *Greenwald et al.*, 1993] and ISCCP for the year 1987 [*Han et al.*, 1994], and MODIS Terra data for 2001-2005 (http://modis.gsfc.nasa.gov/). The SSM/I data are restricted to the oceans. Ice water path (IWP) has been derived from ISCCP data for the years 1983-2000 (http://isccp.giss.nasa.gov/). Observation of Nd is obtained from ISCCP for the year 1987 [*Han et al.*, 1998]. Total cloud cover (TCC) is obtained from ISCCP D data for the years 1983-2001 [*Rossow and Schiffer,* 1999] and MODIS for the years 2001-2004 [*Platnick et al.*, 2003]. Total precipitation (Ptot) is taken from the Global Precipitation Data Set for the years 1979-2002 (http://precip.gsfc.nasa.gov).

Switching from the Meyers parameterization to the Phillips DCI freezing parameterization results in a net cloud forcing (NCF) change of 0.02 W/m^2 and -0.17 W/m^2, for the YCT and PCT cases, respectively. Switching from the YCT to the PCT contact freezing parameterization results in a NCF change of -4.99 W/m^2 and -5.18 W/m^2,

for the Mey and Phi cases, respectively. *DeMott et al.* [2010] reported a global net cloud forcing change of -1.3 W/m^2 associated with switching from the Meyers parameterization to the *DeMott et al.* [2010] parameterization. Our results indicate that the treatment of contact freezing in mixed-phase clouds can be even more important in radiation balance of the climate system. The net solar flux at top of atmosphere (FSNT) changes by as much as 8.73 W/m^2 due to the use of different heterogeneous ice nucleation parameterizations in mixed-phase clouds in our experiments (see Table 2.3). The net longwave flux at top of atmosphere changes by a smaller amount, with the largest difference being 3.52 W/m^2. The reason the long wave flux change is smaller than the short wave flux change is because of the height and temperature of mixed-phase clouds. Unlike cirrus clouds, which are higher and thus much cooler compared to the surface, mixed-phase clouds are lower, so do not have as large a long wave warming effect as cirrus clouds.

Table 2.3: Global mean shortwave cloud forcing (SWCF), longwave cloud forcing (LWCF), net cloud forcing (NCF), liquid water path (LWP), ice water path (IWP), vertically integrated cloud droplet number concentration (Nd) and ice crystal number concentration (Ni), vertically integrated DCI freezing ice nuclei (IN_DCI) and contact freezing ice nuclei (IN_CON) number concentration, total cloud cover (TCC), total precipitation (Ptot), net solar flux at top of atmosphere (FSNT), and net long wave radiation at top of atmosphere (FLNT) from the experiments described in **Table 2.2** and comparison with observation.

	Obs	Mey_YCT	Phi_YCT	Mey_PCT	Phi_PCT	Phi_PCT_PImix	PCT PD-PI	Phi_YCT_PImix	YCT PD-PI
SWCF (W/m^2)	-47 - -54	-45.16±0.14	-45.33±0.17	-51.88±0.22	-53.63±0.12	-53.90±0.19	0.27±0.18	-46.54±0.18	1.21±0.31
LWCF (W/m^2)	22-30	24.34±0.06	24.53±0.08	26.06±0.10	27.65±0.04	27.77±0.05	-0.11±0.05	24.91±0.08	-0.38±0.10
NCF (W/m^2)		-20.82±0.14	-20.80±0.12	-25.81±0.19	-25.98±0.08	-26.13±0.17	0.15±0.17	-21.63±0.18	0.83±0.26
LWP (g/m^2)	50-87	59.39±0.26	60.04±0.50	79.06±0.33	88.22±0.29	88.86±0.42	-0.64±0.31	63.47±0.35	-3.43±0.84
IWP (g/m^2)	21.2	26.42±0.10	26.05±0.06	20.62±0.07	18.32±0.06	18.09±0.06	0.23±0.10	24.82±0.16	1.23±0.14
Nd (10^{10}/m^2)	4	2.08±0.01	2.12±0.02	3.34±0.02	3.27±0.02	3.28±0.01	-0.01±0.02	2.23±0.01	-0.11±0.03
Ni (10^{10}/m^2)		0.028±0.008	0.03±0.01	0.02±0.003	0.03±0.01	0.028±0.004	0.0008±0.002	0.025±0.004	0.006±0.005
IN_DCI (10^{10}/m^2)		0.0022±7e-6	0.0035±1e-4	0.0023±1e-5	0.0036±1e-4	0.0033±1e-4	0.0003±2e-4	0.0032±2e-4	0.0003±2e-4
IN_CON (10^{10}/m^2)		79.78±2.17	78.15±2.41	0.0085±1e-4	0.0087±3e-4	0.0068±2e-4	0.0019±4e-4	44.41±1.14	33.74±2.11
TCC (%)	0.65-0.67	0.682±0.001	0.682±0.001	0.688±5e-4	0.689±6e-4	0.689±7e-4	-0.00005±1e-3	0.683±0.002	-0.001±0.002
Ptot (mm/d)	2.61	2.926±0.004	2.93±0.01	2.94±0.01	2.93±0.004	2.928±0.004	0.0005±0.001	2.93±0.01	-0.001±0.012
FSNT(W/m^2)		243.78±0.15	243.60±0.13	236.71±0.19	235.05±0.12	234.77±0.20	0.28±0.19	242.43±0.17	1.17±0.25
FLNT(W/m^2)		-238.47±0.09	-238.24±0.07	-236.228±0.14	-234.95±0.12	-234.83±0.15	-0.12±0.08	-237.99±0.15	-0.24±0.11

2.3.8 Anthropogenic aerosol effects in mixed-phase clouds

Two additional simulations, Phi_PCT_PImix, and Phi_YCT_PImix were performed, in order to estimate the overall impact of mixed-phase clouds on climate forcing. In these simulations, we carried separate PI BC/OM but we only allowed the PI concentrations to affect the heterogeneous freezing in mixed-phase clouds, in order to gauge only changes in these clouds. So although BC/OM particles contribute to droplet formation in the model, the amount of droplet activation should be close to the same between PD and PImix runs. We estimate the anthropogenic aerosol effects in mixed-phase clouds by taking the difference between the Phi_PCT and Phi_PCT_PImix simulations, and between the Phi_YCT and the Phi_YCT_PImix simulations.

The differences in the global average radiation fluxes are summarized in Table 2.3. The increase in BC/OM concentrations from pre-industrial to present day in mixed-phase clouds leads to increases of 9.1% and 27.9% in the DCI ice nuclei and contact ice nuclei, respectively, in the PCT simulations, and increases of 9.4% and 75% in the DCI ice nuclei and contact ice nuclei, respectively, in the YCT simulations. Ice crystal number concentrations increase by 7.14% between the Phi_PCT and Phi_PCT_PImix cases, and by 20% between the Phi_YCT and Phi_YCT_PImix cases. This also leads to a slight increase in IWP. At the same time, LWP and cloud droplet number are decreased because of the Bergeron-Findeisen process. This leads to smaller reflectivity of solar radiation and larger transitivity of long-wave radiation by mixed-phase clouds in the PD scenario.

Therefore, the SWCF and LWCF both decreased in absolute value from PI to PD. The net cloud forcing (NCF) change from pre-industrial to present-day is 0.15 W/m^2 in the PCT simulations, and 0.83 W/m^2 in the YCT simulations. Both of these changes are statistically significant. So the anthropogenic aerosol effect in mixed-phase clouds is a warming effect from our simulations. This NCF change is caused by changes in the number concentrations in mixed-phase clouds as well as changes due to feedbacks, since both cloud albedo and lifetime effects are included as well as other feedbacks within the cloud systems.

Storelvmo et al. [2011] also provided estimates of the effect of anthropogenic emissions of BC on mixed-phase clouds (-0.32 to 0.23 W/m^2). Their pre-industrial simulations are carried out with all aerosol emissions except BC the same as present-day simulations. They assume that the effects of BC on liquid clouds are negligible, because BC particles in their model are assumed to be largely hydrophobic. The NCF changes predicted from *Storelvmo et al.* [2011] with heterogeneous freezing parameterization of *Diehl et al.* [2006] and *Hoose et al.* [2010] are positive. The only negative NCF change (-0.32 W/m^2) is from the simulation where the *DeMott et al.* [2010] parameterization is used (Table 3 of *Storelvmo et al.*, 2011). They suggested that it is because the *DeMott et al.* [2010] parameterization is only based on large (> 0.5 μm) particle concentration, which is mostly from natural sources. The concentration of these natural particles decrease in PD because of more soluble coating, which leads to smaller ice nuclei concentration in PD. The 0.15 W/m^2 forcing predicted by the PCT simulation lies within the range of forcings

74

predicted by *Storelvmo et al.* [2011] (-0.32 to 0.23 W/m^2). The 0.83 W/m^2 forcing predicted by the YCT simulation is beyond that range.

The total short-wave forcing produced by heterogeneous freezing of anthropogenic BC in mixed-phase clouds is calculated by taking the difference between the net solar flux at top of model (FSNT) between the Phi_PCT and Phi_PCT_PImix cases, and between the Phi_YCT and Phi_YCT_PImix cases. These are estimated to be 0.28 W/m^2 for the PCT case, and 1.17 W/m^2 for the YCT case. This total forcing includes the net cloud forcing, as well as the forcing due to feedbacks in meteorology fields such as water vapor. However, the effect of water vapor on the short-wave radiation is small. The total long-wave forcing, which is calculated similarly, is smaller than the short-wave forcing for reasons explained in section 3.7. It is estimated to be -0.12 W/m^2 for the PCT cases, and -0.24 W/m^2 for the YCT cases. So the total climate forcing from anthropogenic BC/OM in mixed-phase clouds is estimated to be 0.16 – 0.93 W/m^2 using the aerosol-dependent parameterizations. These ranges of forcing changes reflects the uncertainty caused by different treatments of contact freezing in mixed-phase clouds, the narrowing of which deserves further research effort.

Here we caution that our comparison results are not meant to tell which of the parameterizations is the most realistic. Since these comparison results depend to a large extent on the fraction of BC/OM that is assumed to be contact IN. Due to the abundance of biomass burning and fossil fuel burning BC/OM particles, assuming only 1% versus

100% of BC/OM acting as contact IN would make a large difference. Here, we assumed that the hydrophobic fraction of fossil fuel BC/OM fraction that could act as contact IN was 17%. The smaller the hydrophobic fraction, the closer the Young parameterization will be to the Phillips contact freezing parameterization. Eventually, one can assume a hydrophobic fraction so that the two contact freezing parameterizations match each other. We confirm this supposition by adding a sensitivity test with a smaller percentage of dust and BC/OM acting as contact IN in the *Young* [1974] contact freezing parameterization in section 3.9. In a subsequent study, the number concentration of BC/OM that acts as contact IN will be predicted based on online calculations of the hygroscopicity.

2.3.9 Sensitivity to the contact ice nuclei assumed in the Young parameterization

Here we examine a sensitivity simulation Phi_YCT_Less, where the fractions of dust and BC/OM that act as contact ice nuclei in the *Young* [1974] parameterization are greatly reduced. The original *Young* [1974] parameterization was derived from the experimental data of *Blanchard* [1957], which was conducted in winter in Massachusetts. The number concentration of contact ice nuclei was determined by *Young* [1974] to be 0.2cm^{-3} at $-4°C$ at sea level. Here, we match this value based on adjusting the concentration of BC/OM and dust particles at $-4°C$ at sea level to obtain 0.2cm^{-3} at the same season and location as the *Blanchard* [1957] measurements. We also assume that the fraction of dust that act as contact ice nuclei is 10 times larger than the fraction of BC/OM, to take into account that dust is a better ice nuclei. The factor of 10 is taken from the prediction of the *Phillips et al.* [2008] parameterization, where the frozen fraction of dust is about 10 times larger

than soot from -3~ -40°C. The frozen fractions predicted by *Phillips et al.* [2008]

parameterization have been shown to match well with observations [*Phillips et al.,* 2008].
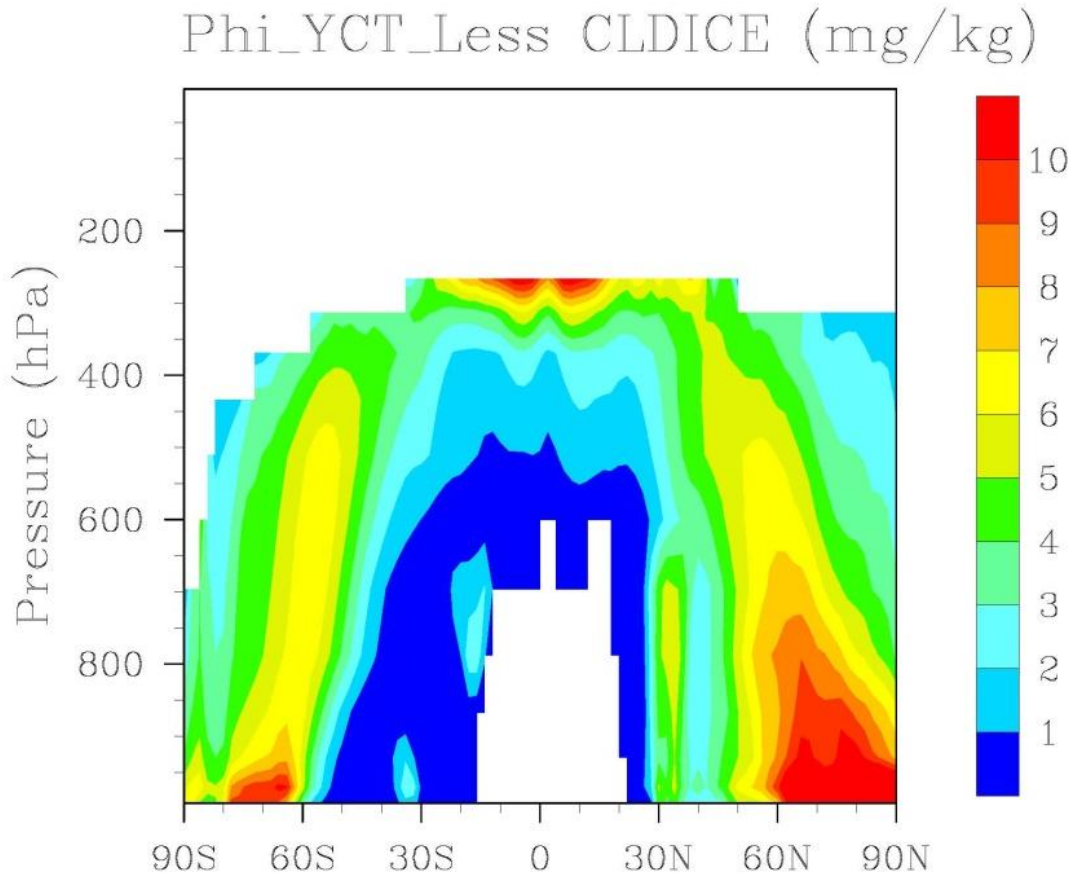
Figure 2.10: Zonal and annual mean latitude versus pressure plots of ice water mixing ratio in mixed-phase clouds for sensitivity test Phi_YCT_Less.

Thus, instead of 100% of dust and 17% of BC/OM acting as contact ice nuclei, in Phi_YCT_Less, we use 0.2% of dust and 0.02% of BC/OM. The mixed-phase cloud ice water mixing ratio for this sensitivity test is shown in Figure 10. Comparing this figure to Figure 2.5, one sees that the mixed-phase cloud ice water mixing ratio from this sensitivity test is very similar to the Phi_PCT case. The anthropogenic aerosol effect in mixed-phase clouds calculated using this case is 0.71 W/m^2, which lies within the range of 0.16 – 0.93 W/m^2 estimated using the Phi_PCT and Phi_YCT cases. The anthropogenic aerosol forcing is not very close to the Phi_PCT estimate, because the contribution of BC/OM to contact freezing in Phi_YCT_Less, similar to Phi_YCT, is still much larger than that from dust (figure not shown). In summary, if one assumes a smaller number concentration of, for example, hydrophobic BC/OM as contact ice nuclei, the ice concentrations in the YCT cases would decrease, becoming closer to the PCT cases, and there would be a smaller anthropogenic aerosol effect in mixed-phase clouds.

2.4 Summary

One parameterization for deposition/condensation/immersion ice nucleation and one for contact freezing in mixed-phase clouds that depend on the aerosol size distribution and chemical composition are introduced into a coupled general circulation model and aerosol transport model. The present-day cloud liquid and ice water fields and the top of the atmosphere cloud radiative forcing are analyzed and compared to observations to see the effect of different heterogeneous freezing treatments.

The DCI IN predicted using the Phillips parameterization shows a strong resemblance to the aerosol distribution. Compared to the Meyers parameterization, The Phillips DCI freezing parameterization predicts more ice crystals in the middle troposphere and lower troposphere mid-latitudes in the NH, and fewer ice crystals in the high-latitude NH and most of the SH. This leads to smaller IWP in the Phi DCI freezing cases especially in the SH. The smaller IWP in the SH from the Phi_PCT simulation leads to more cloud droplets and a larger LWP because of the less efficient Bergeron-Findeisen process. Therefore, the shortwave cloud forcing (SWCF) and longwave cloud forcing (LWCF) are larger in magnitude in the Phi_PCT simulation than in the Mey_PCT simulation in the SH. In the Mey_YCT and Phi_YCT cases, the effect of contact IN dominates in mixed-phase clouds, which makes the changes predicted from using different DCI freezing parameterizations unimportant.

The Phillips contact IN parameterization predicts three orders of magnitude less contact IN than the Young parameterization, and the contributions from dust and BC/OM are relatively equal. In the YCT cases, the contribution from BC/OM is much larger than that from dust. Deposition/condensation/immersion freezing dominates in the PCT cases, while contact freezing dominates in the YCT cases, unless the number of contact ice nuclei is reduced to the reference value on which the Young (1974) parameterization was based. Less cloud ice water and larger ice crystal effective radius are predicted in the PCT cases. The global average effective droplet radius, droplet number concentration and

cloud liquid mixing ratios and LWPs increase because of the less efficient Bergeron-Findeisen process. Therefore, the SWCF and LWCF are larger in magnitude for the cases that use the Phillips contact freezing parameterization. The influences of using different contact freezing parameterizations on the cloud liquid and ice field are more pronounced than that from changing the DCI parameterization from Meyers to Phillips.

When using the Phillips DCI freezing parameterization, the possibility for a given grid box to have low ice fraction is increased, while that for a given grid box to have a mixture of ice and liquid in decreased than when using Meyers parameterization. When using the Phillips contact freezing parameterization, the possibility for a given grid box to have low ice fraction is also increased compared to that using the Young parameterization. The above changes to the probability distribution of ice fractions further affect the cloud optical thickness observed at middle cloud altitudes.

When using the Phillips DCI freezing parameterization and contact freezing parameterization, the optical thickness of middle clouds is increased. As a result, the cloud fractions of altostratus and nimbostratus clouds are increased, and that of altocumulus clouds are decreased compared to using the Meyers parameterization, or the Young parameterization. Therefore, the comparison of altostratus and nimbostratus clouds to ISCCP is improved, while the comparison of altocumulus clouds to ISCCP is worsened.

In the SH, all cases except Phi_PCT are in reasonable agreement with observations of IWP. The IWP from the PCT cases compares well with observations in the NH, while the YCT cases over predict IWP in the NH. The fact that Phi_PCT and Mey_PCT agree fairly well with satellite observations in the NH shows that the Phillips DCI freezing parameterization is able to correctly predict ice water contents using an online calculation of aerosol fields. The under-prediction of IWP in the SH by Phi_PCT, however, suggests the possibility that there are missing sources of ice nuclei in the SH.

Switching from the Meyers parameterization to the Phillips DCI freezing parameterization results in an NCF change of 0.02 W/m^2 and -0.17 W/m^2, for the YCT and PCT cases, respectively. The net solar flux at top of atmosphere (FSNT), and net long-wave flux at top of atmosphere (FLNT) also changes by up to 8.73 W/m^2 and 3.52 W/m^2, respectively, due to the use of different heterogeneous ice nucleation parameterizations in mixed-phase clouds. This indicates that treatment of heterogeneous freezing in mixed-phase clouds is important for the radiation balance of the climate system.

The anthropogenic effects of BC/OM in mixed-phase clouds are estimated. A net cloud forcing of 0.15 W/m^2 is calculated for the PCT simulations and 0.83 W/m^2 for the YCT simulations. The total short-wave climate forcing of anthropogenic BC/OM in mixed-phase cloud is 0.28 W/m^2 for the PCT cases, and 1.17 W/m^2 for the YCT cases. The total long-wave climate forcing of anthropogenic BC/OM in mixed-phase cloud is estimated to

be -0.12 W/m^2 for the PCT cases, and -0.24 W/m^2 for the YCT cases. So the total climate forcing from anthropogenic BC/OM in mixed-phase clouds is $0.16 - 0.93$ W/m^2 using the aerosol-dependent freezing parameterizations. This range of forcing change reflects the uncertainty caused by different treatments of contact freezing in mixed-phase clouds, the narrowing of which deserves further research effort.

Our results are not intended to delineate which of the parameterizations is best, because of the uncertainties associated with the satellite data and comparison technique, as well as assumptions about which aerosol components act as contact freezing ice nuclei in the *Young* [1974] parameterization. When number concentration of dust and BC/OM contact ice nuclei is matched to the 0.2cm^{-3} assumed in the original *Young* [1974] parameterization, the cloud ice mixing ratio is close to that in the Phi_PCT cases, and produces a smaller anthropogenic aerosol effect of 0.71 W/m^2 in mixed-phase clouds.

References

Abdul-Razzak, H., and S. J. Ghan (2000), A parameterization of aerosol activation 2. Multiple aerosol types, *Journal of Geophysical Research-Atmospheres*, *105*(D5), 6837-6844.

Abdul-Razzak, H., and S. J. Ghan (2002), A parameterization of aerosol activation - 3. Sectional representation, *Journal of Geophysical Research-Atmospheres*, *107*(D3).

Archuleta, C. M., P. J. DeMott, and S. M. Kreidenweis (2005), Ice nucleation by surrogates for atmospheric mineral dust and mineral dust/sulfate particles at cirrus temperatures, *Atmospheric Chemistry and Physics*, *5*, 2617-2634.

Barahona, D., J. Rodriguez, and A. Nenes (2010), Sensitivity of the global distribution of cirrus ice crystal concentration to heterogeneous freezing, *Journal of Geophysical Research-Atmospheres*, *115*.

Berezinski N.A., G.V. Stepanov, V.G. Khorguani (1988) Ice-forming activity of atmospheric aerosol particles of different sizes, *Lecture Notes in Physics*, Vol. 309, Atmospheric aerosols and nucleation, Springer, 1988.

Blanchard, D.C., 1957: The supercooling, freezing and melting of giant waterdrops at terminal velocity in air, in *Artificial Simulation of Rain*, London, Pergamon Press, 233-249.

Boville, B. A., P. J. Rasch, J. J. Hack, and J. R. McCaa (2006), Representation of clouds and precipitation processes in the Community Atmosphere Model version 3 (CAM3), *Journal of Climate*, *19*(11), 2184-2198.

Chen, Y. L., S. M. Kreidenweis, L. M. McInnes, D. C. Rogers, and P. J. DeMott (1998), Single particle analyses of ice nucleating aerosols in the upper troposphere and lower stratosphere, *Geophysical Research Letters*, *25*(9), 1391-1394, doi:10.1029/97GL03261.

Collins, W. D., P. J. Rasch, B. E. Eaton, B. V. Khattatov, J. F. Lamarque, and C. S. Zender (2001), Simulating aerosols using a chemical transport model with assimilation of satellite aerosol retrievals: Methodology for INDOEX, *Journal of Geophysical Research-Atmospheres*, *106*(D7), 7313-7336, doi:10.1029/2000JD900507

Collins, W. D., P. J. Rasch, B. A. Boville, J. J. Hack, J. R. McCaa, D. L. Williamson, B. P. Briegleb, C. M. Bitz, S. J. Lin, and M. H. Zhang (2006a), The formulation and atmospheric simulation of the Community Atmosphere Model version 3 (CAM3), *Journal of Climate*, *19*(11), 2144-2161.

Collins, W. D., et al. (2006b), The Community Climate System Model version 3 (CCSM3), *Journal of Climate*, *19*(11), 2122-2143.

Connolly, P. J., O. Moehler, P. R. Field, H. Saathoff, R. Burgess, T. Choularton, and M. Gallagher (2009), Studies of heterogeneous freezing by three different desert dust samples, *Atmospheric Chemistry and Physics*, *9*(8), 2805-2824.

Cooper, W. A. (1986), *Ice initiation in natural clouds, in Precipitation Enhancement—A Scientific Challenge,* Meteorol. Monogr., vol. 21, edited by R. G. Braham Jr., pp. 29–32, Am. Meteorol. Soc., Boston, Mass.

Cziczo, D. J., D. M. Murphy, P. K. Hudson, and D. S. Thomson (2004), Single particle measurements of the chemical composition of cirrus ice residue during CRYSTAL-FACE, *Journal of Geophysical Research-Atmospheres*, *109*(D4), doi:10.1029/2003JD004032

DeMott, P. J. (1990), AN EXPLORATORY-STUDY OF ICE NUCLEATION BY SOOT AEROSOLS, *Journal of Applied Meteorology*, *29*(10), 1072-1079.

DeMott, P. J., D. J. Cziczo, A. J. Prenni, D. M. Murphy, S. M. Kreidenweis, D. S. Thomson, R. Borys, and D. C. Rogers (2003), Measurements of the concentration and composition of nuclei for cirrus formation, *Proceedings of the National Academy of Sciences of the United States of America*, *100*(25), 14655-14660.

DeMott, P. J., A. J. Prenni, X. Liu, S. M. Kreidenweis, M. D. Petters, C. H. Twohy, M. S. Richardson, T. Eidhammer, and D. C. Rogers (2010), Predicting global atmospheric ice nuclei distributions and their impacts on climate, *Proceedings of the National Academy of Sciences of the United States of America*, *107*(25), 11217-11222.

Diehl, K., and S. K. Mitra (1998), A laboratory study of the effects of a kerosene-burner exhaust on ice nucleation and the evaporation rate of ice crystals, *Atmospheric Environment*, *32*(18), 3145-3151.

Diehl, K., and S. Wurzler (2004), Heterogeneous drop freezing in the immersion mode: Model calculations considering soluble and insoluble particles in the drops, *Journal of the Atmospheric Sciences*, *61*(16), 2063-2072.

Diehl, K., M. Simmel, and S. Wurzler (2006), Numerical sensitivity studies on the impact of aerosol properties and drop freezing modes on the glaciation, microphysics, and dynamics of clouds, *Journal of Geophysical Research-Atmospheres*, *111*(D7), doi:10.1029/2005JD005884

Eliasson, S., S. A. Buehler, M. Milz, P. Eriksson, and V. O. John (2011), Assessing observed and modelled spatial distributions of ice water path using satellite data, *Atmospheric Chemistry and Physics*, *11*(1), 375-391.

Eidhammer, T., P. J. DeMott, and S. M. Kreidenweis (2009), A comparison of heterogeneous ice nucleation parameterizations using a parcel model framework, *Journal of Geophysical Research-Atmospheres*, *114*, 19, doi:10.1029/2008JD011095

Eidhammer, T., et al. (2010), Ice Initiation by Aerosol Particles: Measured and Predicted Ice Nuclei Concentrations versus Measured Ice Crystal Concentrations in an Orographic

Wave Cloud, *Journal of the Atmospheric Sciences*, *67*(8), 2417-2436, doi: 10.1175/2010JAS3266.1

Ferraro, R. R., F. Z. Weng, N. C. Grody, and A. Basist (1996), An eight-year (1987-1994) time series of rainfall, clouds, water vapor, snow cover, and sea ice derived from SSM/I measurements, *Bulletin of the American Meteorological Society*, *77*(5), 891-905.

Field, P. R., O. Mohler, P. Connolly, M. Kramer, R. Cotton, A. J. Heymsfield, H. Saathoff, and M. Schnaiter (2006), Some ice nucleation characteristics of Asian and Saharan desert dust, *Atmospheric Chemistry and Physics*, *6*, 2991-3006.

Fletcher, N. H. (1962), *The Physics of Rain Clouds*, 386 pp., Cambridge Univ. Press, New York.

Friedman, B., G. Kulkarni, J. Beranek, A. Zelenyuk, J. A. Thornton, and D. J. Cziczo (2011), Ice nucleation and droplet formation by bare and coated soot particles, *Journal of Geophysical Research-Atmospheres*, 116, 17203-17203.

Gary, B. L. (2006), Mesoscale temperature fluctuations in the stratosphere, *Atmospheric Chemistry and Physics*, *6*, 4577-4589.

Gary, B. L. (2008), Mesoscale temperature fluctuations in the Southern Hemisphere stratosphere, *Atmospheric Chemistry and Physics*, *8*(16), 4677-4681.

Georgii H.W. And Kleinjung E. (1967), Relations Between the chemical composition of atmospheric aerosol particles and the concentration of natural ice nuclei, *Journal de Recherches atmospheriques*, 145-156

Gettelman, A., X. Liu, S. J. Ghan, H. Morrison, S. Park, A. J. Conley, S. A. Klein, J. Boyle, D. L. Mitchell, and J. L. F. Li (2010), Global simulations of ice nucleation and ice supersaturation with an improved cloud scheme in the Community Atmosphere Model, *Journal of Geophysical Research-Atmospheres*, *115*, doi:10.1029/2009JD013797

Gorbunov, B., A. Baklanov, N. Kakutkina, H. L. Windsor, and R. Toumi (2001), Ice nucleation on soot particles, *Journal of Aerosol Science*, *32*(2), 199-215.

Greenwald, T. J., G. L. Stephens, T. H. Vonderhaar, and D. L. Jackson (1993), A physical retrieval of cloud liquid water over the global oceans using special sensor microwave imager (SSM/I) observations, *Journal of Geophysical Research-Atmospheres*, *98*(D10), 18471-18488, doi:10.1029/93JD00339

Han, Q. Y., W. B. Rossow, and A. A. Lacis (1994), Near-global survey of effective droplet radii in liquid water clouds using ISCCP data, *Journal of Climate*, *7*(4), 465-497.

Han, Q. Y., W. B. Rossow, J. Chou, and R. M. Welch (1998), Global variation of column droplet concentration in low-level clouds, *Geophysical Research Letters*, *25*(9), 1419-1422, doi:10.1029/98GL01095

Herzog, M., D. K. Weisenstein, and J. E. Penner (2004), A dynamic aerosol module for global chemical transport models: Model description, *Journal of Geophysical Research-Atmospheres*, *109*(D18), doi:10.1029/2003JD004405

Hobbs, P. V., G. C. Bluhm, and T. Ohtake (1971a), Transport of ice nuclei over north Pacific ocean, *Tellus*, *23*(1), 28-&.

Hobbs, P. V., Fullerto.Cm, and G. C. Bluhm (1971b), Ice nucleus storms in Hawaii, *Nature-Physical Science*, *230*(12), 90-&.

Hoose, C., J. E. Kristjansson, J. P. Chen, and A. Hazra (2010), A Classical-Theory-Based Parameterization of Heterogeneous Ice Nucleation by Mineral Dust, Soot, and Biological Particles in a Global Climate Model, *Journal of the Atmospheric Sciences*, *67*(8), 2483-2503.

Isono, K. and Y. Ibeke (1960), On the ice-nucleating ability of rockforming minerals and soil particles, *Journal of the Meteorological Society of Japan*, 38, 213-230.

Isono, K., M. Komabayasi, T. Takeda, T. Tanaka (1970), *Concentration and nature of ice nuclei in the rim of the North Pacific Ocean,* NWAP Rept., 70-R Water Resources Lab., Nagoya University, Nagoya, Japan.

Kanji, Z. A., P. J. DeMott, O. Mohler, and J. P. D. Abbatt (2011), Results from the University of Toronto continuous flow diffusion chamber at ICIS 2007: instrument intercomparison and ice onsets for different aerosol types, *Atmospheric Chemistry and Physics*, *11*(1), 31-41.

Kärcher, B., and U. Lohmann (2003), A parameterization of cirrus cloud formation: Heterogeneous freezing, *Journal of Geophysical Research-Atmospheres*, *108*(D14), doi:10.1029/2002JD003220

Khvorostyanov, V. I., and J. A. Curry (2004), The theory of ice nucleation by heterogeneous freezing of deliquescent mixed CCN. Part I: Critical radius, energy, and nucleation rate, *Journal of the Atmospheric Sciences*, *61*(22), 2676-2691.

Kiehl, J. T., and K. E. Trenberth (1997), Earth's annual global mean energy budget, *Bulletin of the American Meteorological Society*, *78*(2), 197-208.

Koehler, K. A., S. M. Kreidenweis, P. J. DeMott, A. J. Prenni, and M. D. Petters (2007), Potential impact of Owens (dry) Lake dust on warm and cold cloud formation, *Journal of Geophysical Research-Atmospheres*, *112*(D12).

Koehler, K. A., S. M. Kreidenweis, P. J. DeMott, M. D. Petters, A. J. Prenni, and O. Mohler (2010), Laboratory investigations of the impact of mineral dust aerosol on cold cloud formation, *Atmospheric Chemistry and Physics*, *10*(23), 11955-11968.

Korolev, A. V., and I. P. Mazin (2003), Supersaturation of water vapor in clouds, *Journal of the Atmospheric Sciences*, *60*(24), 2957-2974.

Korolev, A. V., G. A. Isaac, S. G. Cober, J. W. Strapp, and J. Hallett (2003), Microphysical characterization of mixed-phase clouds, *Quarterly Journal of the Royal Meteorological Society*, 129(587), 39-65.

Kulkarni, G., and S. Dobbie (2010), Ice nucleation properties of mineral dust particles: determination of onset RH(i), IN active fraction, nucleation time-lag, and the effect of active sites on contact angles, *Atmospheric Chemistry and Physics*, 10(1), 95-105.

Lee, S. S., and J. E. Penner (2010), Aerosol effects on ice clouds: can the traditional concept of aerosol indirect effects be applied to aerosol-cloud interactions in cirrus clouds?, *Atmospheric Chemistry and Physics*, 10(21), 10345-10358.

Lin, W. Y., and M. H. Zhang (2004), Evaluation of clouds and their radiative effects simulated by the NCAR Community Atmospheric Model against satellite observations, *Journal of Climate*, 17(17), 3302-3318.

Liu, X. H., and J. E. Penner (2002), Effect of Mount Pinatubo H2SO4/H2O aerosol on ice nucleation in the upper troposphere using a global chemistry and transport model, *Journal of Geophysical Research-Atmospheres*, 107(D12), doi:10.1029/2001JD000455

Liu, X. H., and J. E. Penner (2005), Ice nucleation parameterization for global models, *Meteorologische Zeitschrift*, 14(4), 499-514.

Liu, X. H., J. E. Penner, and M. Herzog (2005), Global modeling of aerosol dynamics: Model description, evaluation, and interactions between sulfate and nonsulfate aerosols, *Journal of Geophysical Research-Atmospheres*, 110(D18), doi:10.1029/2004JD005674

Liu, X., J. E. Penner, S. J. Ghan, and M. Wang (2007), Inclusion of ice microphysics in the NCAR community atmospheric model version 3 (CAM3), *Journal of Climate*, 20(18), 4526-4547.

Liu, X. H., J. E. Penner, and M. H. Wang (2009), Influence of anthropogenic sulfate and black carbon on upper tropospheric clouds in the NCAR CAM3 model coupled to the IMPACT global aerosol model, *Journal of Geophysical Research-Atmospheres*, 114, doi:10.1029/2008JD010492

Lohmann, U. (2002), Possible aerosol effects on ice clouds via contact nucleation, *Journal of the Atmospheric Sciences*, 59(3), 647-656.

Lohmann, U., and K. Diehl (2006), Sensitivity studies of the importance of dust ice nuclei for the indirect aerosol effect on stratiform mixed-phase clouds, *Journal of the Atmospheric Sciences*, 63(3), 968-982.

Lohmann, U., and C. Hoose (2009), Sensitivity studies of different aerosol indirect effects in mixed-phase clouds, *Atmospheric Chemistry and Physics*, 9(22), 8917-8934.

Lohmann, U., P. Stier, C. Hoose, S. Ferrachat, S. Kloster, E. Roeckner, and J. Zhang (2007), Cloud microphysics and aerosol indirect effects in the global climate model ECHAM5-HAM, *Atmospheric Chemistry and Physics*, 7, 3425-3446.

Marcolli, C., S. Gedamke, T. Peter, and B. Zobrist (2007), Efficiency of immersion mode ice nucleation on surrogates of mineral dust, *Atmospheric Chemistry and Physics*, *7*, 5081-5091.

Meyers, M. P., P. J. DeMott, and W. R. Cotton (1992), New primary ice-nucleation parameterizations in an explicit cloud model, *Journal of Applied. Meteorolory,* 31(7), 708–721.

Minikin, A., A. Petzold, J. Strom, R. Krejci, M. Seifert, P. van Velthoven, H. Schlager, and U. Schumann (2003), Aircraft observations of the upper tropospheric fine particle aerosol in the Northern and Southern Hemispheres at midlatitudes, *Geophysical Research Letters*, *30*(10), doi:10.1029/2002GL016458

Monahan, E. C., and I. G. Omuircheartaigh (1986), WHITECAPS AND THE PASSIVE REMOTE-SENSING OF THE OCEAN SURFACE, *International Journal of Remote Sensing*, *7*(5), 627-642.

Muhlbauer, A., T. Hashino, L. Xue, A. Teller, U. Lohmann, R. M. Rasmussen, I. Geresdi, and Z. Pan (2010), Intercomparison of aerosol-cloud-precipitation interactions in stratiform orographic mixed-phase clouds, *Atmospheric Chemistry and Physics*, *10*(17), 8173-8196.

Murray, B. J., S. L. Broadley, T. W. Wilson, J. D. Atkinson, and R. H. Wills (2011), Heterogeneous freezing of water droplets containing kaolinite particles, *Atmospheric Chemistry and Physics*, *11*(9), 4191-4207.

Penner, J. E., D. J. Bergmann, J. J. Walton, D. Kinnison, M. J. Prather, D. Rotman, C. Price, K. E. Pickering, and S. L. Baughcum (1998), An evaluation of upper troposphere NOx with two models, *Journal of Geophysical Research-Atmospheres*, *103*(D17), 22097-22113, doi:10.1029/98JD01565

Penner, J.E., M. Andreae, H. Annegarn, L. Barrie, J. Feichter, D. Hegg, A. Jayaraman, R.Leaitch, D. Murphy, J. Nganga, and G. Pitari, (2001), *Aerosols, their Direct and Indirect Effects, Intergovernmental Panel on Climate Change, Report to IPCC from the Scientific Assessment Working Group (WGI)*, 289-348, Cambridge University Press.

Penner, J. E., Y. Chen, M. Wang, and X. Liu (2009), Possible influence of anthropogenic aerosols on cirrus clouds and anthropogenic forcing, *Atmospheric Chemistry and Physics*, *9*(3), 879-896.

Phillips, V. T. J., P. J. DeMott, and C. Andronache (2008), An empirical parameterization of heterogeneous ice nucleation for multiple chemical species of aerosol, *Journal of the Atmospheric Sciences*, *65*(9), 2757-2783.

Platnick, S., M. D. King, S. A. Ackerman, W. P. Menzel, B. A. Baum, J. C. Riedi, and R. A. Frey (2003), The MODIS cloud products: Algorithms and examples from Terra, *Ieee Transactions on Geoscience and Remote Sensing*, *41*(2), 459-473.

Prenni, A. J., P. J. DeMott, C. Twohy, M. R. Poellot, S. M. Kreidenweis, D. C. Rogers, S. D. Brooks, M. S. Richardson, and A. J. Heymsfield (2007), Examinations of ice formation processes in Florida cumuli using ice nuclei measurements of anvil ice crystal particle residues, *Journal of Geophysical Research-Atmospheres*, *112*(D10), doi:10.1029/2006JD007549

Pruppacher, H. R., and J. D. Klett, 1997: *Microphysics of Clouds and Precipitation*. 2nd ed. Kluwer Academic, AA Dordrecht, The Netherlands.

Rasch, P. J., W. D. Collins, and B. E. Eaton (2001), Understanding the Indian Ocean Experiment (INDOEX) aerosol distributions with an aerosol assimilation, *Journal of Geophysical Research-Atmospheres*, *106*(D7), 7337-7355, doi:10.1029/2000JD900508

Reddy, M. S., and O. Boucher (2004), A study of the global cycle of carbonaceous aerosols in the LMDZT general circulation model, *Journal of Geophysical Research-Atmospheres*, *109*(D14), doi:10.1029/2003JD004048

Richardson, M. S., et al. (2007), Measurements of heterogeneous ice nuclei in the western United States in springtime and their relation to aerosol characteristics, *Journal of Geophysical Research-Atmospheres*, *112*(D2), doi:10.1029/2006JD007500

Rossow, W. B., and R. A. Schiffer (1999), Advances in understanding clouds from ISCCP, *Bulletin of the American Meteorological Society*, *80*(11), 2261-2287.

Rotman, D. A., et al. (2004), IMPACT, the LLNL 3-D global atmospheric chemical transport model for the combined troposphere and stratosphere: Model description and analysis of ozone and other trace gases, *Journal of Geophysical Research-Atmospheres*, *109*(D4), doi:10.1029/2002JD003155

Rotstayn, L. D., B. F. Ryan, and J. J. Katzfey (2000), A scheme for calculation of the liquid fraction in mixed-phase stratiform clouds in large-scale models, *Monthly Weather Review*, *128*(4), 1070-1088.

Salzmann, M., Y. Ming, J. C. Golaz, P. A. Ginoux, H. Morrison, A. Gettelman, M. Kramer, and L. J. Donner (2010), Two-moment bulk stratiform cloud microphysics in the GFDL AM3 GCM: description, evaluation, and sensitivity tests, *Atmospheric Chemistry and Physics*, *10*(16), 8037-8064.

Santachiara, G., L. Di Matteo, F. Prodi, and F. Belosi (2010), Atmospheric particles acting as Ice Forming Nuclei in different size ranges, *Atmospheric Research*, *96*(2-3), 266-272.

Schaefer, V. J. (1949), The formation of ice crystals in the laboratory and the atmosphere, *Chemical Reviews*, 44, 291-320.

Scott, N. A., A. Chedin, R. Armante, J. Francis, C. Stubenrauch, J. P. Chaboureau, F. Chevallier, C. Claud, and F. Cheruy (1999), Characteristics of the TOVS pathfinder Path-B dataset, *Bulletin of the American Meteorological Society*, *80*(12), 2679-2701.

Seifert, A., C. Köhler, and K. D. Beheng (2011), Aerosol-cloud-precipitation effects over Germany as simulated by a convective-scale numerical weather prediction model, *Atmospheric Chemistry and Physics Discussions*.

Shaw, R. A., A. J. Durant, and Y. Mi (2005), Heterogeneous surface crystallization observed in undercooled water, *Journal of Physical Chemistry B*, *109*(20), 9865-9868.

Storelvmo, T., J. E. Kristjansson, and U. Lohmann (2008), Aerosol influence on mixed-phase clouds in CAM-Oslo, *Journal of the Atmospheric Sciences*, *65*(10), 3214-3230.

Storelvmo, T., C. Hoose, and P. Eriksson (2011), Global modeling of mixed-phase clouds: The albedo and lifetime effects of aerosols - art. no. D05207, *Journal of Geophysical Research-Atmospheres*, *116*, 5207-5207, doi:10.1029/2010JD014724

Susskind, J., P. Piraino, L. Rokke, T. Iredell, and A. Mehta (1997), Characteristics of the TOVS Pathfinder Path A dataset, *Bulletin of the American Meteorological Society*, *78*(7), 1449-1472.

Targino, A. C., R. Krejci, K. J. Noone, and P. Glantz (2006), Single particle analysis of ice crystal residuals observed in orographic wave clouds over Scandinavia during INTACC experiment, *Atmospheric Chemistry and Physics*, *6*, 1977-1990.

Vali, G. (1985), Nucleation Terminology, *Bulletin of the American Meteorological Society*, 66(11), 1426-1427.

Wang, L., Y. Q. Wang, A. Lauer, and S. P. Xie (2011), Simulation of Seasonal Variation of Marine Boundary Layer Clouds over the Eastern Pacific with a Regional Climate Model, *Journal of Climate*, *24*(13), 3190-3210.

Wang, M., and J. E. Penner (2010), Cirrus clouds in a global climate model with a statistical cirrus cloud scheme, *Atmospheric Chemistry and Physics*, *10*(12), 5449-5474.

Wang, M. H., J. E. Penner, and X. H. Liu (2009), Coupled IMPACT aerosol and NCAR CAM3 model: Evaluation of predicted aerosol number and size distribution, *Journal of Geophysical Research-Atmospheres*, *114*, doi:10.1029/2008JD010459

Warren, S.G., C.J. Hahn, J. London, R.M. Chervin and R.L. Jenne, 1986: Global distribution of total cloud cover and cloud type amounts over land. NCAR Tech. Note, *NCAR/TN-273+STR*, 29 pp. + 200 maps.

Warren, S.G., C.J. Hahn, J. London, R.M. Chervin and R.L. Jenne, 1988: Global distribution of total cloud cover and cloud type amounts over the ocean. NCAR Tech. Note, *NCAR/TN-317+STR*, 41 pp. + 170 maps.

Weng, F. Z., and N. C. Grody (1994), Retrieval of cloud liquid water using the special sensor microwave imager (SSM/I), *Journal of Geophysical Research-Atmospheres*, *99*(D12), 25535-25551, doi:10.1029/94JD02304

Xie, S. C., J. Boyle, S. A. Klein, X. H. Liu, and S. Ghan (2008), Simulations of Arctic mixed-phase clouds in forecasts with CAM3 and AM2 for M-PACE, *Journal of Geophysical Research-Atmospheres*, *113*(D4), 16, doi:10.1029/2007JD009225

Young, K. C. (1974), Numerical-simulation of wintertime, orographic precipitation .1.Description of model microphysics and numerical techniques, *Journal of the Atmospheric Sciences*, *31*(7), 1735-1748.

Zhang, M. H., W. Y. Lin, C. S. Bretherton, J. J. Hack, and P. J. Rasch (2003), A modified formulation of fractional stratiform condensation rate in the NCAR Community Atmospheric Model (CAM2), *Journal of Geophysical Research-Atmospheres*, *108*(D1), doi:10.1029/2002JD002523

CHAPTER 3

The effects of hygroscopicity of fossil fuel combustion aerosols on mixed-phase clouds

3.1 Introduction

Soot aerosols produced by fossil fuel and biomass burning contain both black carbon (BC) and organic matter (OM). Both act to absorb solar radiation, thereby changing vertical temperature profiles and decreasing surface radiation. Combustion aerosols can also act as cloud condensation nuclei, causing indirect effects on clouds by decreasing the cloud droplet radius. This causes cooling which counteracts the warming by greenhouse gases. Combustion aerosols can also act as heterogeneous ice nuclei (IN) in mixed-phase clouds [e.g. *Cozic et al.*, 2008], as well as in cirrus clouds [*Koehler et al.*, 2009; *Penner et al.*, 2009]. Their ice effects are much more uncertain, which hinders climate prediction. Due to the abundance of fossil fuel (ff) combustion aerosols, a small change in their ice nucleation ability can produce a large difference in indirect effects. Several studies have noted the sensitivity of aerosol forcing to ice nucleation in mixed-phase clouds [*Lohmann and Hoose*, 2009; *Storelvmo et al.*, 2011; *Storelvmo et al.*, 2008a; *Yun and Penner*, 2012].

During the lifetime of soot aerosols in the atmosphere their hygroscopicity can be altered through coating by sulfate [*Zhang et al.*, 2008]. Several laboratory experiments have investigated the effect of coating on the ability of soot particles to nucleate ice [*DeMott et al.*, 1999; *Mohler et al.*, 2005; *Friedman et al.*, 2011; *Crawford et al.*, 2011]. *DeMott et al.* [1999] conducted ice nucleation experiments on lamp black soot at 213 – 233K with sulfuric acid coating varying from zero to several weight percent. It was found that ice nucleation required the highest supersaturation at almost every temperature when the soot particle was treated with approximately one monolayer of sulfuric acid. However, the critical supersaturation required for ice formation was much lower when BC particles were treated with a multilayer equivalent coverage of sulfuric acid. *Mohler et al.* [2005] investigated ice nucleation of soot particles generated from a Graphite Spark Generator (GSG) at 185 – 240K, and found that internal mixtures of soot and sulfuric acid required higher supersaturation than that of uncoated soot to nucleate ice. The uncoated lamp black soot used by *DeMott et al.* [1999] and the GSG soot used by *Mohler et al.* [2005] have very different ice nucleation properties, with the uncoated GSG soot being a much more efficient ice nuclei [*Kärcher et al.*, 2007]. *Friedman et al.* [2011] found no heterogeneous ice nucleation below water saturation above their experimental detection limit (which was about 0.01-0.1% of the soot particle concentration, or about 10/L) for both coated and uncoated soot particles generated from a mini-CAST Real Soot Generator at 253K and 243K. Above water saturation, ice nucleation could have occurred for both coated and uncoated soot but could not be distinguished from droplet formation. *Crawford et al.* [2011] examined nucleation of ice at 210 – 235K for sulfuric acid coated soot particles generated from a CAST propane burner with various amounts of organic

content. They found that uncoated soot particles with 30% organic mass content freeze before water saturation, and those with 80% and 90% organic mass content are inactive or freeze at water saturation respectively. After coating by sulfuric acid, they all nucleated ice close to the homogeneous freezing conditions of sulphuric acid.

These studies all lead to different conclusions about the effect of adding a soluble coating to soot. One possible reason for the differences in nucleation is the differences in the properties of the bare soot particles, for example, the organic content, porosity, surface area, etc. The amounts of sulfuric acid coating were not quantified in most of these laboratory studies. This hinders the comparability among different laboratory studies, and also the applicability of the results to modeling studies. Furthermore, the results are usually expressed as a freezing onset condition (for example, the ice supersaturation required for activation of 0.1% or 1% the aerosols), which are not directly comparable to the input needed in a numerical model after a typical time step of 30 min. Nevertheless, these studies demonstrated that the addition of a soluble coating can alter the ice nucleation ability of soot particles, which most model studies of aerosol indirect effects (AIE) do not explicitly consider [e.g. *Yun and Penner*, 2012; *Lohmann and Hoose*, 2009; *Storelvmo et al.*, 2011].

Here we adopt recent laboratory studies from *Popovicheva et al.* [2008, 2010, 2011] and *Koehler et al.* [2009], which provide a link between sulfuric acid coating, hygroscopicity,

and ice nucleation efficiencies, and develop a method of differentiating hydrophobic, hydrophilic, and hygroscopic particles and their ice nucleation in models.

Popovicheva et al. [2008, 2010] suggested that the hygroscopicity of soot could be quantified by the amount of water film extended over the soot surface at relative humidity < 80%. Hydrophobic soot never forms a film, while hydrophilic soot does develops a film. Hygroscopic soot develops several layers of water uptake. *Popovicheva et al*. [2011] identified the threshold amount of sulfate coating needed to transform hydrophobic to hydrophilic to hygroscopic soot as 1 monolayer and 3 monolayers. These thresholds are used here. *Koehler et al*. [2009] performed a series of experiments to link soot hygroscopicity to its IN ability, based on *Popovicheva et al*. [2008, 2010]. The frozen fractions of hydrophobic, hydrophilic, and hygroscopic soot were measured at various conditions, which are also used here to differentiate their freezing abilities.

We implemented a 3-ffBC/OM (3-hydrophobic, hydrophilic and hygroscopic) soot scheme in place of a single category scheme (1-ffBC/OM) [*Wang et al.*, 2009]. We present the hydrophobic, hydrophilic and hygroscopic ffBC/OM aerosol fields, as well as the cloud water field and radiative forcing from the original and the new scheme. Finally, an updated total anthropogenic forcing is presented with the new 3-ffBC/OM scheme.

3.2   Methods

The 3-ffBC/OM scheme was implemented into the CAM-IMPACT coupled aerosol transport model and general circulation model [*Wang and Penner*, 2010], as well as an offline radiation model. The coupled model (inline simulation) provides the aerosol fields and meteorology fields for the offline model, and is used to calculate the total anthropogenic forcing. The offline model reads the aerosol and meteorology fields and examines the cloud water fields and mixed-phase cloud anthropogenic forcing without involving feedbacks to the cloud fields from changes in aerosols.

3.2.1   Models

The University of Michigan IMPACT aerosol model has a detailed description of the interaction of sulfate with non-sulfate aerosols through condensation, coagulation, as well as aqueous formation of sulfuric acid in cloud droplets [e.g. *Wang et al.*, 2009]. Although BC and OM are treated as distinct species in the model, they are assumed to be internally mixed [*Liu et al.*, 2005]. The NCAR CAM3 model was updated to include a two-moment microphysics scheme for cloud liquid and ice [*Wang and Penner*, 2010]. In mixed-phase clouds, the *Phillips et al.* [2008] parameterization (PH08) of deposition/condensation/immersion freezing was implemented [*Yun and Penner*, 2012]. The contact freezing parameterization is that of *Young* [1974], with the contact ice nuclei concentration fitted to that recommended by *Young* [1974].

The offline radiation model of *Chen and Penner* [2005] was extended to include mixed-phase clouds. The ice nucleation scheme in mixed-phase clouds is the same as that in the CAM-IMPACT model [*Yun and Penner*, 2012]. The Bergeron-Findeisen process (the conversion of liquid to ice) was also implemented in the offline radiation model, due to its importance to radiative forcing [*Storelvmo et al.*, 2008b]. However, no further processing of ice particles takes place (no sedimentation, coagulation, or precipitation formation). Therefore, the anthropogenic forcing in mixed-phase clouds calculated from the offline radiation model is similar to the 1st indirect effect of aerosols, with the added effect of the Bergeron-Findeisen process.

3.2.2 3-ffBC/OM scheme

The differentiation between hydrophobic, hydrophilic, and hygroscopic ffBC/OM aerosols is based on the number of monolayers of sulfuric acid coating. Freshly emitted ffBC/OM particles are assumed to be hydrophobic. After each time step, the number of monolayers of sulfate coating (n_{coat}) is calculated based on the total mass of sulfuric acid coating, the size of a sulfuric acid molecule, and the average BC/OM size. If $n_{coat}<1$, the particle remains hydrophobic. If $1 \leq n_{coat}<3$, the particle is moved to the hydrophilic category. If $n_{coat} \geq 3$, the particle becomes hygroscopic. The size distributions of the three ffBC/OM species prior to coating by sulfate (and water) are assumed fixed (see *Penner et al.* [1998]). The accommodation coefficient for the condensation of sulfuric acid on

hydrophobic and hydrophilic particles is set to 0.018 [*Zhang et al.*, 2005], while that for hygroscopic particles is 0.65, similar to sulfuric acid surfaces [*Pöschl et al.*, 1998].

The PH08 parameterization was modified to treat the nucleation of ice in mixed-phase clouds by the 3-ffBC/OM categories. Ice nucleation was measured at -40°C as well as at a colder temperature (-51.5°C or -57°C) in *Koehler et al*. [2009]. Due to the coexistence of liquid and ice, water saturation is assumed in mixed-phase clouds in our model. Therefore, we use the frozen fraction measured at -40°C at water saturation to adjust the PH08 parameterization in mixed-phase clouds. For hydrophobic and hydrophilic soot, we use the data for the 200nm particles because this size is close to the volume mean diameter of the BC/OM particles in our model which is 180nm. There are only data for polydisperse particles at -40°C for hygroscopic soot. However, the frozen fractions of the polydisperse particles and 250nm particles are similar at -57°C. So we assumed that differences between the size distribution between the polydispersed particles and our soot particles would not have a large impact on the freezing properties of hygroscopic particles. The frozen fraction of hydrophobic, hydrophilic, and hygroscopic soot measured at -40°C and at water saturation is 0.03%, 2%, and 3%, respectively, while that predicted by PH08 for the same conditions is 0.2%. Therefore, we increased the PH08 frozen fraction by a factor of 10 for hydrophilic ffBC/OM, and reduced it by a factor of 0.15 for hydrophobic ffBC/OM. In doing so, we preserve the temperature dependence specified in PH08.

Freezing for hygroscopic particles followed the "Koop" line for homogeneous freezing of pure dissolved solute at -40°C for a short distance near water saturation. However, the frozen fraction slightly above water saturation was far smaller than that predicted by a homogeneous freezing mechanism. Therefore, we made two assumptions to treat the freezing of hygroscopic particles at higher temperatures. The first is that these particles freeze homogeneously, so we exclude them as a heterogeneous IN (simulation 3BC_noSCO). This is similar to the observation of internally mixed propane burner soot by *Crawford et al*. [2011]. The second is that they freeze heterogeneously, and we scale the frozen fraction of PH08 by a factor of 15 (simulation 3BC_SCO). This is similar to the observation of multi-layer coated lamp black soot by *DeMott et al*. [1999]. The contact freezing treatment was kept the same as in the 1-ffBC/OM scheme, since we want to examine the effect of treating soot ice nucleation using the results of *Koehler et al*. [2009], whose measurement includes deposition/condensation/immersion freezing but no contact freezing. Contact freezing in our model is represented by the *Young* [1974] parameterization fitted to the observation of total number of contact ice nuclei measured by *Blanchard* [1957] [see *Yun and Penner*, 2012]. This treatment makes the contribution from contact freezing to total ice nucleation very small (on the order of 1%).

3.2.3 Experiment set-up

Table 3.1 shows the three offline simulations. In the 1BC simulation, the original PH08 scheme is used and the sum of hydrophobic, hydrophilic, and hygroscopic ffBC/OM is treated as one species. For each configuration, the model is run twice with Present-Day

(PD) and Pre-Industrial (PI) aerosol fields. PI aerosol fields are only applied to ice nucleation in mixed-phase clouds. The in-line model is run using the 3BC_noSCO scheme with PD and PI emission files described in *Penner et al.* [2009]. Aerosol direct effects as well as effects on warm-phase and cirrus clouds are included in the in-line model.

Table 3.1: Offline simulations

Schemes	Description
1BC	1-ffBC/OM scheme
3BC_SCO	3-ffBC/OM scheme and hygroscopic particles as heterogeneous ice nuclei
3BC_noSCO	3-ffBC/OM scheme and no hygroscopic particles as heterogeneous ice nuclei

3.3   Results

3.3.1   Aerosol fields for hydrophobic, hydrophilic, and hygroscopic ffBC/OM

Figure 3.1 shows the PD horizontal distribution of column integrated hydrophobic, hydrophilic and hygroscopic ffBC/OM. Hydrophobic ffBC/OM is confined mainly to regions near emissions. Hydrophilic ffBC/OM is transported farther than hydrophobic
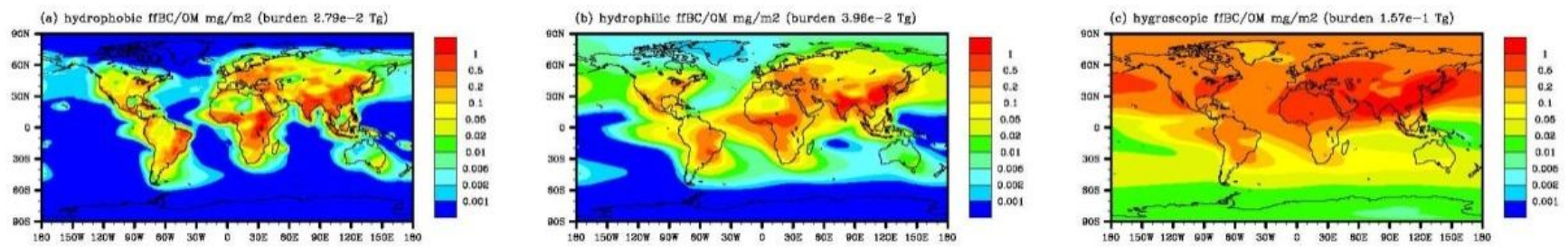
Figure 3.1: PD annual average horizontal distribution of column integrated hydrophobic (a), hydrophilic (b), and hygroscopic (c) ffBC/OM (mg/m^2)

ffBC/OM. Hygroscopic ffBC/OM is even more wide spread. The majority of the ffBC/OM particles are hygroscopic, contributing 69.93% to the total ffBC/OM burden. Hydrophilic and hydrophobic ffBC/OM particles contribute 17.64% and 12.43%, respectively. The lifetime of the ffBC/OM particles increases with hygroscopicity from 0.45 to 0.95 to 4.55 days.

Figure 3.2 shows the change in the hydrophobic, hydrophilic, and hygroscopic ffBC/OM number concentrations from PI to PD due to anthropogenic emissions. Concentrations increase in most places due to higher PD emissions. However, the concentration of hydrophobic ffBC/OM is smaller for the PD in most places of the Northern Hemisphere (NH) (Figure 3.2 a), and the concentration of hydrophilic ffBC/OM is smaller for PD at NH high latitudes (Figure 3.2 b). This is because sulfate emissions increase significantly in the PD in the industrial regions in the NH and more readily coat the surface of the ffBC/OM particles. Therefore, the ffBC/OM particles become hygroscopic more easily and are less likely to remain hydrophilic and even less likely to remain hydrophobic.

3.3.2   Comparison of mixed-phase cloud water field and radiative forcing

Figure 3.3 shows the grid-mean ice number concentration (N_i) change from PI to PD in mixed-phase clouds using the offline model. There is a larger increase in N_i in the NH than in the Southern Hemisphere (SH) for all three experiments. The 1BC case shows increases of order 1/L (1/Liter) throughout the mid-troposphere north of 30°N, while the
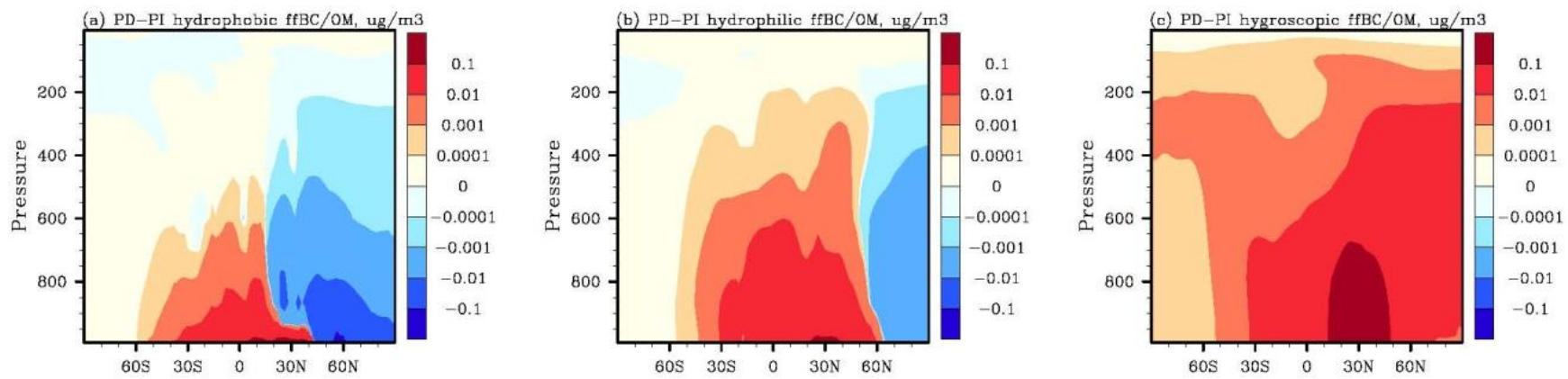
Figure 3.2: PD-PI annual average changes of hydrophobic (a), hydrophilic (b), and hygroscopic (c) ffBC/OM (ug/m^3)
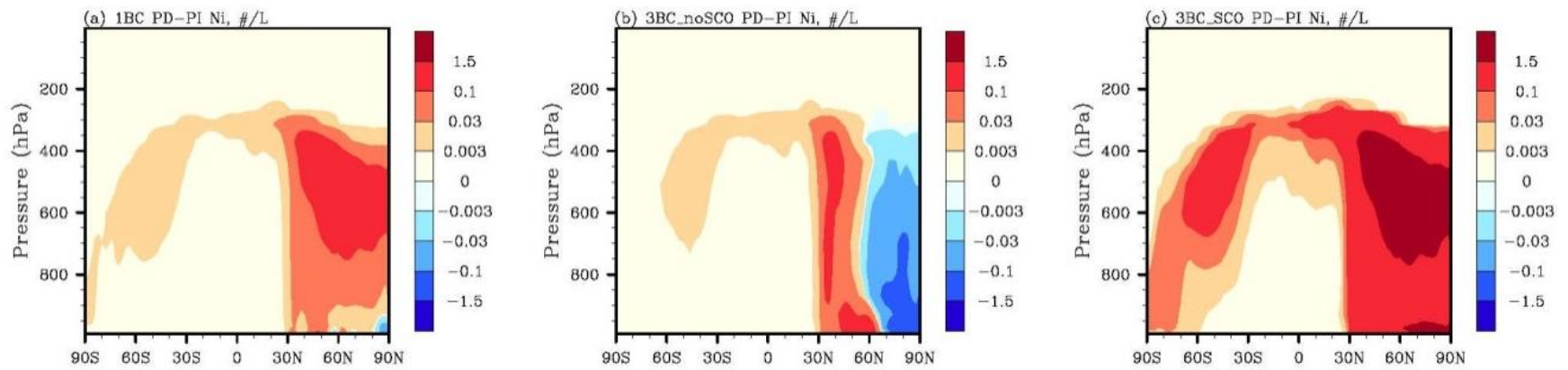
Figure 3.3: PD-PI annual average changes of grid-mean ice number concentration in mixed-phase clouds from 1BC (a), 3BC_noSCO (b) and 3BC_SCO (c) simulations (#/L)

3BC_noSCO case shows decreases north of 60°N, caused by the decrease of hydrophilic ffBC/OM (Figure 3.2 b). The 3BC_SCO case shows much larger increases that also extend to the SH, due to the enhanced effect of hygroscopic ffBC/OM. In general, Ni increases from PI to PD predicted by the 3-ffBC/OM scheme is very different from that predicted by the 1-ffBC/OM scheme. However, the sign of the change depends strongly on the freezing ability of hygroscopic ffBC/OM. When hygroscopic ffBC/OM acts as a heterogeneous IN in mixed-phase clouds, there is a larger increase in *Ni*; when hygroscopic ffBC/OM does not, there is a smaller overall increase.

An increase in *Ni* causes a net conversion of liquid to ice in mixed-phase clouds, as a result of the Bergeron-Findeisen process. Figure 3.4 shows the change in the liquid water mass mixing ratio in all 3 schemes from PI to PD. Liquid cloud mass mixing ratio decreases at most latitudes except north of 60°N in the 3BC_noSCO scheme. The decrease is largest in the 3BC_SCO case and smallest in the 3BC-noSCO case, consistent with the changes in *Ni*.

Table 3.2 shows the anthropogenic forcing in mixed-phase clouds from the three cases. Two aspects contribute to the anthropogenic ffBC/OM forcing. The first is the decrease of ice effective radius associated with the increase of *Ni* (Figure 3.3). Smaller ice effective radius leads to more reflected solar radiation and less long-wave transmission, reducing the net incoming short-wave radiation as well as the net outgoing long-wave radiation at the Top-of-the-Atmosphere (TOA). Therefore, the anthropogenic Short-wave
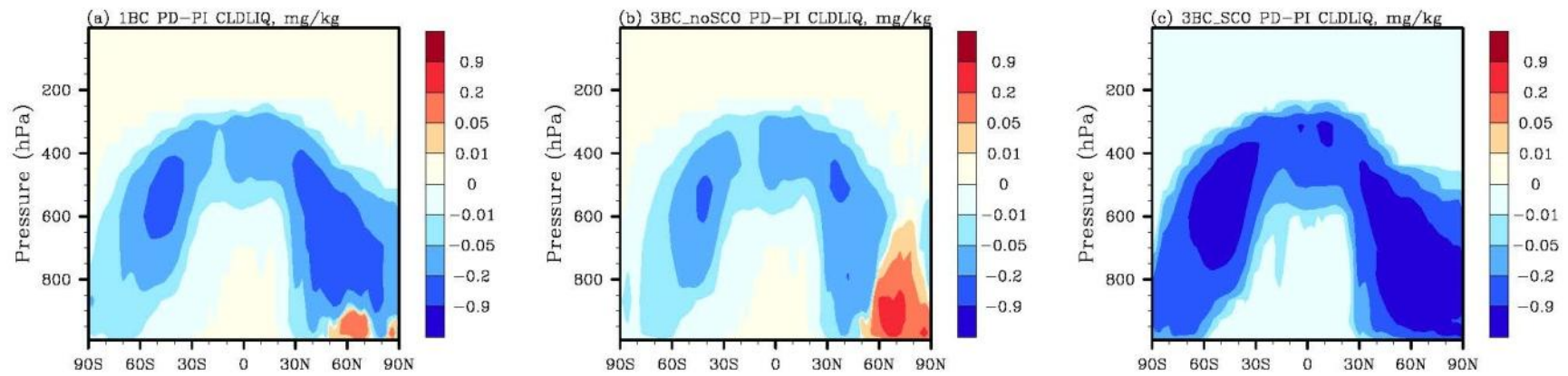
Figure 3.4: PD-PI annual average changes of grid-mean liquid water mass mixing ratio (CLDLIQ) in mixed-phase clouds from 1BC (a), 3BC_noSCO (b) and 3BC_SCO (c) simulations (mg/kg)

(SW) forcing from this effect is negative, and the Long-wave (LW) forcing is positive. The second aspect is the decrease of liquid water mass mixing ratio (Figure 3.4). This results in a smaller liquid water path in the present-day, and therefore a reduced short-wave reflectivity and increased long-wave transmissivity. The result of this change is a positive SW forcing and a negative LW forcing. As shown in Table 3.2, the second effect dominates the sign of the SW and LW forcings.

Table 3.2: Annual average anthropogenic cloud forcings (CF) and whole-sky forcings (W/m^2). The dash line separates offline and inline simulations. Off-line forcings are for mixed-phase clouds, while inline forcings include all effects: warm, mixed-phase, and cirrus clouds and direct effects.

	SWCF	LWCF	Net CF	Net Whole-Sky
1BC	0.188	-0.0173	0.171	0.171
3BC_SCO	1.106	-0.0470	1.059	1.059
3BC_noSCO	0.118	-0.007	0.111	0.111
3BC_noSCO (inline)	2.28	-2.22	0.06	-2.45

The treatment of ffBC/OM with different freezing properties results in significant changes to the offline mixed-phase cloud forcing. When hygroscopic ffBC/OM particles are excluded as IN, there is a 35% decrease in the net anthropogenic forcing compared to the 1BC case. When hygroscopic ffBC/OM particles are included, there is an increase by a factor of 6, due to the large liquid water change in the 3BC_SCO case. The two treatments for hygroscopic soot particles lead to a net offline mixed-phase anthropogenic

forcing that varies by almost a factor of 10, from 0.111 to 1.059 W/m^2.

The total anthropogenic forcing (including sulfate) using the 3BC scheme with the coupled model shows a positive Net CF of 0.06 W/m^2, which is opposite to the sign of the result of this model in *Storelvmo et al*. [2012] (-0.8 W/m^2, manuscript in preparation). The reason is two-fold. The first is that both homogenous and heterogeneous freezing are included in cirrus clouds here, whereas only homogeneous freezing is included in *Storelvmo et al*. [2012]. Including heterogeneous freezing in cirrus clouds suppresses homogeneous freezing, results in decreased cirrus ice number concentrations in the PD, and produces a positive SWCF change from PI to PD, if the decrease in cirrus cloud fraction is not very large. The second is that the anthropogenic emission increase is larger for the emission files used here (described in *Penner et al*. [2009]) than in the emission files used in *Storelvmo et al*. [2012] (which are based on *Dentener et al*. [2006]). With larger aerosol concentrations in PD, there is a larger blocking of the aerosol direct effect (ADE) by clouds which produces a positive PD-PI SWCF, and this effect is enhanced by a larger increase in emissions. The net whole-sky forcing is the same as the CF in the offline simulations because the aerosol and meteorology fields are fixed and no direct effect is included. That for the inline model, however, has all effects including warm cloud, cirrus cloud, and direct effects and is -2.45 W/m^2. However, this number would be smaller if hygroscopic soot particles were allowed to act as IN in mixed phase clouds in the in-line simulation.

3.4   Discussion

Anthropogenic aerosol emissions are thought to produce negative forcing through their indirect effect on warm clouds. This could counteract the warming effect of greenhouse gases and thus has important implications for predicting climate change. However, there are large uncertainties associated with their effects in mixed-phase clouds, which hinders our ability to fully determine the effects of aerosols on climate. Our results show that the net effect of anthropogenic aerosols on mixed-phase clouds is a warming. This warming effect comes from the decrease of optical depth due to the Bergeron-Findeisen process. To estimate the importance of mixed-phase cloud forcing relative to other clouds, we removed the effect of ADE (0.67 W/m^2 estimated using the offline radiation model) from the inline anthropogenic SWCF to estimate the forcing from only the AIE (1.61 W/m^2). As a result, the SW forcing in mixed-phase clouds contributes 7.33~68.7% of the anthropogenic SW forcing in all clouds, and the LW forcing contributes 0.32~2.12% (Table 3.2). The magnitude of the mixed-phase cloud forcing is very sensitive to whether the effect of hygroscopicity is considered, and how it is considered. It is larger when hygroscopic particles are included as IN due to the larger fraction of soot particles acting as ice nuclei. However, we would like to caution our reader here that this forcing range are not to be taken at face value, because there are many other processes that may change BC forcing that are not considered here, for example, the effect of secondary organic coatings. More laboratory experiments are needed to fully determine the freezing properties of hygroscopic ffBC/OM at mixed-phase cloud temperatures to reduce the range of uncertainty.

References

Blanchard, D.C. (1957), The supercooling, freezing and melting of giant waterdrops at terminal velocity in air, in *Artificial Simulation of Rain*, London, Pergamon Press, 233-249.

Chen, Y., and J. E. Penner (2005), Uncertainty analysis for estimates of the first indirect aerosol effect, *Atmospheric Chemistry and Physics*, *5*, 2935-2948.

Cozic, J., S. Mertes, B. Verheggen, D. J. Cziczo, S. J. Gallavardin, S. Walter, U. Baltensperger, and E. Weingartner (2008), Black carbon enrichment in atmospheric ice particle residuals observed in lower tropospheric mixed phase clouds, *Journal of Geophysical Research-Atmospheres*, *113*(D15), 11, doi:D15209 10.1029/2007jd009266.

Crawford, I., et al. (2011), Studies of propane flame soot acting as heterogeneous ice nuclei in conjunction with single particle soot photometer measurements, *Atmospheric Chemistry and Physics*, *11*(18), 9549-9561.

DeMott, P. J., Y. Chen, S. M. Kreidenweis, D. C. Rogers, and D. E. Sherman (1999), Ice formation by black carbon particles, *Geophysical Research Letters*, *26*(16), 2429-2432.

Friedman, B., G. Kulkarni, J. Beranek, A. Zelenyuk, J. A. Thornton, and D. J. Cziczo (2011), Ice nucleation and droplet formation by bare and coated soot particles, Journal of Geophysical Research-Atmospheres, 116, 17203-17203.

Kärcher, B., O. Mohler, P. J. DeMott, S. Pechtl, and F. Yu (2007), Insights into the role of soot aerosols in cirrus cloud formation, *Atmospheric Chemistry and Physics*, *7*, 4203-4227.

Koehler, K. A., P. J. DeMott, S. M. Kreidenweis, O. B. Popovicheva, M. D. Petters, C. M. Carrico, E. D. Kireeva, T. D. Khokhlova, and N. K. Shonija (2009), Cloud condensation nuclei and ice nucleation activity of hydrophobic and hydrophilic soot particles, *Phys Chem Chem Phys*, *11*(36), 7906-7920.

Liu, X. H., J. E. Penner, and M. Herzog (2005), Global modeling of aerosol dynamics: Model description, evaluation, and interactions between sulfate and nonsulfate aerosols, *Journal of Geophysical Research-Atmospheres*, *110*(D18), doi:10.1029/2004jd005674.

Lohmann, U., and C. Hoose (2009), Sensitivity studies of different aerosol indirect effects in mixed-phase clouds, *Atmospheric Chemistry and Physics*, *9*(22), 8917-8934.

Mohler, O., et al. (2005), Effect of sulfuric acid coating on heterogeneous ice nucleation by soot aerosol particles, *Journal of Geophysical Research-Atmospheres*, *110*(D11), doi:10.1029/2004jd005169.

Penner, J. E., Y. Chen, M. Wang, and X. Liu (2009), Possible influence of anthropogenic aerosols on cirrus clouds and anthropogenic forcing, *Atmospheric Chemistry and Physics*, *9*(3), 879-896.

Penner, J. E., C. C. Chuang, and K. Grant (1998), Climate forcing by carbonaceous and sulfate aerosols, *Climate Dynamics*, *14*(12), 839-851, doi:10.1007/s003820050259.

Phillips, V. T. J., P. J. DeMott, and C. Andronache (2008), An empirical parameterization of heterogeneous ice nucleation for multiple chemical species of aerosol, *Journal of the Atmospheric Sciences*, *65*(9), 2757-2783, doi:10.1175/2007jas2546.1.

Popovicheva, O. B., E. D. Kireeva, M. A. Timofeev, N. K. Shonija, and V. P. Mogil'nikov (2010), Carbonaceous aerosols of aviation and shipping emissions, *Izvestiya Atmospheric and Oceanic Physics*, *46*(3), 339-346.

Popovicheva, O. B., N. M. Persiantseva, E. D. Kireeva, T. D. Khokhlova, and N. K. Shonija (2011), Quantification of the Hygroscopic Effect of Soot Aging in the Atmosphere: Laboratory Simulations, *Journal of Physical Chemistry A*, *115*(3), 298-306, doi:10.1021/jp109238x.

Popovicheva, O. B., N. M. Persiantseva, V. Tishkova, N. K. Shonija, and N. A. Zubareva (2008), Quantification of water uptake by soot particles, *Environmental Research Letters*, *3*(2), 12, doi:02500910.1088/1748-9326/3/2/025009.

Pöschl, U., M. Canagaratna, J. T. Jayne, L. T. Molina, D. R. Worsnop, C. E. Kolb, and M. J. Molina (1998), Mass accommodation coefficient of H(2)SO(4) vapor on aqueous sulfuric acid surfaces and gaseous diffusion coefficient of H(2)SO(4) in N(2)/H(2)O, *Journal of Physical Chemistry A*, *102*(49), 10082-10089, doi:10.1021/jp982809s.

Storelvmo, T., C. Hoose, and P. Eriksson (2011), Global modeling of mixed-phase clouds: The albedo and lifetime effects of aerosols - art. no. D05207, *Journal of Geophysical Research-Atmospheres*, *116*, 5207-5207.

Storelvmo, T., J. E. Kristjansson, and U. Lohmann (2008a), Aerosol influence on mixed-phase clouds in CAM-Oslo, *Journal of the Atmospheric Sciences*, *65*(10), 3214-3230, doi:10.1175/2008jas2430.1.

Storelvmo, T., J. E. Kristjansson, U. Lohmann, T. Iversen, A. Kirkevag, and O. Seland (2008b), Modeling of the Wegener-Bergeron-Findeisen process-implications for aerosol indirect effects, *Environmental Research Letters*, *3*(4), 45001-45001, doi:10.1088/1748-9326/3/4/045001.

Wang, M., and J. E. Penner (2010), Cirrus clouds in a global climate model with a statistical cirrus cloud scheme, *Atmospheric Chemistry and Physics*, *10*(12), 5449-5474, doi:10.5194/acp-10-5449-2010.

Wang, M. H., J. E. Penner, and X. H. Liu (2009), Coupled IMPACT aerosol and NCAR CAM3 model: Evaluation of predicted aerosol number and size distribution, *Journal of Geophysical Research-Atmospheres*, *114*, doi:10.1029/2008jd010459.

Young, K. C. (1974), Numerical-simulation of wintertime, orographic precipitation .1. Description of model microphysics and numerical techniques, *Journal of the Atmospheric Sciences*, *31*(7), 1735-1748.

Yun, Y., and J. E. Penner (2012), Global model comparison of heterogeneous ice nucleation parameterizations in mixed phase clouds, *Journal of Geophysical Research-Atmospheres*, *117*, 7203-7203.

Zhang, D., and R. Y. Zhang (2005), Laboratory investigation of heterogeneous interaction of sulfuric acid with soot, *Environmental Science & Technology*, *39*(15), 5722-5728, doi:10.1021/es050372d.

Zhang, R. Y., A. F. Khalizov, J. Pagels, D. Zhang, H. X. Xue, and P. H. McMurry (2008), Variability in morphology, hygroscopicity, and optical properties of soot aerosols during atmospheric processing, *Proceedings of the National Academy of Sciences of the United States of America*, *105*(30), 10291-10296, doi:10.1073/pnas.0804860105.

CHAPTER 4

A global evaluation of the potential effect of marine organic

aerosols as heterogeneous ice nuclei

4.1 Introduction

Ocean covers about 70% of the Earth's surface and marine aerosols are thus an important component in the global aerosol field. Sea salt typically dominates the total marine aerosol burden, however recent measurements have found that organic aerosols contribute a significant portion (e.g. 63%) to the submicron aerosol mass during the phytoplankton blooms [*O'Dowd et al.*, 2004; *Cavalli et al.*, 2004]. Marine organic aerosols (MOA) can be of primary or secondary origin. Primary MOAs are directly ejected from the ocean surface through bubble bursting process and are composed of whole cell or fragments of phytoplankton, polysaccharides, and proteins [*Hawkins and Russell*, 2010]. Secondary MOAs are produced within the atmosphere from the oxidation of emitted biogenic volatile organic compounds (VOCs) such as isoprene, monoterprenes, and amines [*Meskhidze et al.*, 2011].

Marine organic aerosols have been shown to influence cloud microphysical properties over the remote ocean by acting as cloud condensation nuclei (CCN) in both observation and model studies [*O'Dowd et al.*, 2004; *Meskhidze and Nenes*, 2006, *Roelofs*, 2008]. However, the effects of MOA acting as ice nuclei (IN) have had little study. Several observational studies report that marine aerosols may act as ice nuclei. *Bigg* [1973] (B73 hereafter) used long term measurements of ice nuclei concentrations in the marine boundary layer over Australia and the Antarctic Ocean. He found the highest ice nuclei concentrations in the subtropical convergence zone along the 40S parallel, where marine biological activities are strong due to nutrient upwelling. *Schnell* [1975] and *Schnell and Vali* [1976] found that sea water which is rich in phytoplankton is a good source of ice nuclei, with some of them active at temperatures as high as -4°C. These findings were later confirmed by *Schnell* [1977] who found that high concentrations of ice nuclei in sea water were associated with high concentrations of biological materials, and *Rosinski et al*. [1987] who found that ice nuclei have a patchy distribution over the up-welling regions of Pacific Ocean where the supply of nutrients brought to the surface during upwelling is able to promote phytoplankton growth. More recently, *Knopf et al.* [2011] identified the marine phytoplanktonic diatom *Thalassiosira pseudonana* as an efficient ice nuclei in the deposition mode at typical cirrus onset conditions and in the immersion mode at mixed-phase cloud temperatures. *Demott et al.* [2012] measured the ice nucleation activity of laboratory generated sea spray aerosols, and found the lowest IN concentrations with high organic aerosol loading, but IN concentrations increased following additions of bacteria and nutrients and after cells fed on these nutrients.

Due to the considerable contribution of MOA to total marine aerosol and their ice nucleation properties, they have the potential to effectively influence marine cloud microphysics. Ice nucleation not only affects the ice number concentration and ice particle effective radius, but also liquid water clouds due to the Bergeron-Findeisen process. Therefore, MOA can effectively change the cloud phase, cloud optical depth, and cloud radiative forcing. Most previous models do not explicitly consider aerosol properties when predicting ice number concentrations, since they typically parameterize ice number as a function of temperature or ice supersaturation. *Yun and Penner* [2012] found that after switching from an aerosol independent ice nucleation parameterization to an aerosol dependent one, and adjusting the contact freezing parameterization of *Young* [1974] to fit the *Blanchard* [1957] observation, the ice water path in the Southern Hemisphere (SH) decreased by about 20 g/m^2. The adjustment to the *Blanchard* [1957] observation was done by fitting observed contact ice nuclei concentration measured in winter Massachusetts at ground level, which was 0.2 cm^3 at -4C. This restricted the contact ice nuclei to be 0.2% of dust and 0.02% of black carbon and organic carbon (section 2.3.9). Part of the reason for the decrease in the ice water path is that only dust, black carbon, and terrestrial organic carbon are considered to be ice nuclei in the aerosol dependent parameterization, as is the case in other aerosol dependent parameterizations up to now [*Chen et al.*, 2008; *Khvorostyanov and Curry*, 2004; *Diehl et al.*, 2006]. This could result in an under-prediction of ice water in the SH where the ocean coverage is high, and thereby lead to a bias in the present-day cloud radiative forcing.

Furthermore, marine organic aerosol is an integral part of the natural background aerosols. Correct representation of the natural background aerosols is necessary to estimate anthropogenic aerosol perturbations. However, the effects of marine organic aerosols as ice nuclei have not yet been evaluated on a global scale. In this study, we implement an aerosol microphysics and ice nucleation parameterization for MOA in a coupled general circulation model and global aerosol transport model, and examine their effects as heterogeneous ice nuclei in mixed-phase clouds.

4.2   Methods

4.2.1   Model

The coupled CAM3+ and aerosol transport model IMPACT were used in this study. The CAM3+ model has been updated to include a double moment cloud microphysics scheme [*Wang et al.*, 2010] that predicts both the mass and number concentration of cloud liquid and ice. Heterogeneous ice nucleation in mixed-phase clouds is treated using *Phillips et al.* [2008] and the adjusted *Young* [1974] parameterization. The *Eidhammer et al.* [2010] modification to *Phillips et al.* [2008] has been incorporated. The IMPACT aerosol transport model considers emissions and gas/aqueous phase chemistry for SO_2; formation, nucleation, coagulation, and condensation of H_2SO_4; and emission, dry deposition, and wet deposition for all other major aerosols types (organic aerosols, black carbon, dust, and sea salt). The model has also been updated to include a 3 fossil fuel soot scheme that

treats fossil fuel soot ice nucleation according to its hygroscopicity [*Yun et al.*, 2012].

The detailed description of the coupled model can be found in *Yun and Penner* [2012]

and *Wang et al.* [2009].

4.2.2 Emission of marine organic aerosols

In this study, marine organic aerosols were implemented as a separate aerosol species in

the coupled model. The emission of the marine biogenic aerosols was parameterized as a

function of the sea salt emissions. Two methods for the calculating sea salt emissions and

two for calculating the marine organic mass fraction of sea salt emissions were tested.

The first method for calculating sea salt emissions is the same as that used by *Meskhidze*

et al. [2011] and uses the *Martensson et al.* [2003] scheme for particles < 2.8 μm and the

Monahan et al. [1986] parameterization for sea salt sizes larger than 2.8 μm.

$$
\begin{cases}
\dfrac{dF}{dlogD} = 0.0384 \times 10^{-4} \, U_{10}^{3.41} \, (A^k T + B^k) & D < 2.8 \text{ μm} \\[2mm]
\dfrac{dF}{dr} = 1.373 \, U_{10}^{3.41} \, r^{-3}(1 + 0.057 r^{1.05}) \times 10^{1.19 e^{-B^2}} & D > 2.8 \text{ μm}
\end{cases} \tag{4.1}
$$

Here the left hand side of the equations is sea salt flux density in units of particles m^{-2} s^{-1}

μm^{-1}. U_{10} is the wind speed at 10m above the sea surface (m s^{-1}), T is temperature in

degrees Kelvin, $B = (0.380 - \log r)/0.650$, r is the radius at relative humidity of 80%

117

(μm), and D is the dry diameter (μm). A^k and B^k are parameters prescribed according to size interval (Equation (5) and Table 1 in *Martensson et al.* [2003]).

The second method implemented to describe the sea salt emission flux density is that proposed by *Jaegle et al.* [2011], who added a flux-density dependence on the sea surface temperature (SST) to the parameterization implemented by *Gong* [2003].

$$\frac{dF}{dr} = 1.373 \, U_{10}^{3.41} \, r^{-A} \, (1 + 0.057 \, r^{3.45}) \times 10^{1.607e^{-B^2}}$$

$$\times \left(0.3 + 0.1 \times T_c - 0.0076 \times T_c{}^2 + 0.00021 \times T_c{}^3\right)$$

$$A = 4.7(1 + \Theta r)^{-0.017r^{-1.44}}, B = [0.433 - logr]/0.433 \tag{4.2}$$

Here T_c is temperature expressed in °C, Θ is an adjustable parameter which was set to 30 by *Gong* [2003]. Both methods parameterize the sea salt emissions as a function of wind speed, particle size, and temperature. The major difference between the two methods is that the *Martensson et al.* [2003] parameterization was fit to laboratory simulations in order to improve the submicron particle emissions, while *Jaegle et al.* [2011] attemped to reduce the bias between the aerosol optical depth in her model and that measured by MODIS and AERONET by introducing a temperature dependency that increased sea salt emissions in the tropics and decreased them at the mid- and high latitudes. Although the

Martensson et al. [2003] also has temperature dependency, at least for D<2.8 μm, it is much weaker than that derived by *Jaegle et al.* [2011].

The marine organic mass fraction was parameterized using either the *Gantt et al.* [2011] parameterization or the modified *Vignati et al.* [2010] parameterization. The *Gantt et al.* [2011] parameterization is as follows:

$$OM_{SSA}(chl\text{-}a, U_{10}, D)$$

$$= \frac{\frac{1}{1 + exp(-2.63[chl\text{-}a] + 0.18U_{10})}}{1 + 0.03\,exp(6.81D)}$$

$$+ \frac{0.03}{1 + exp(-2.63[chl\text{-}a] + 0.18U_{10})} \qquad (4.3)$$

Here OM_{SSA} is the mass fraction of sea salt that is organic, *chl-a* is the ocean surface chlorophyll-a concentration (mg m^{-3}), and U_{10} is the horizontal wind speed at 10 m height, given in units of m s^{-1}. The original *Vignati et al.* [2010] parameterization was derived for the sum of all submicron sea salt aerosols and does not include any information on size distribution. It was modified by *Meskhidze et al.* [2011] to include size dependency as follows:

119

$$OM_{SSA}(chl\text{-}a, D) = \frac{0.435[chl\text{-}a] + 0.138}{1 + 0.03exp(6.81D)} + 0.03 \times (0.435[chl\text{-}a] + 0.138) \qquad (4.4)$$

The major difference between the two parameterizations is that the modified *Vignati et al.* [2010] parameterization does not depend on wind speed, while the *Gantt et al.* [2011] parameterization depends on all three parameters: the chlorophyll-a concentration, particle size, and wind speed.

The wet scavenging efficiency of MOA is calculated by calculating the activated fraction using *Abdul-Razzak and Ghan* [2000, 2002] parameterization. The kappa factor used in this calculation for MOA is assumed to be the same as that of natural organic aerosols in the IMPACT model, which is 0.14. MOA are predicted for the same four size bins as sea salt, namely, 0.05 to 0.63 μm, 0.63 to 1.26 μm, 1.26 to 2.5 μm, and 2.5 to 10 μm. The size distribution within each size bin is also the same as sea salt, which is represented by a superposition of two lognormal distributions (*Liu et al.* [2005]). The density of MOA is assumed to be 1g/cm^3 [*Cavalli et al.*, 2004].

4.2.3   Ice nucleation efficiency of marine organic aerosols

In order to derive the ice nucleation efficiencies of MOA for each size bin, we used long-term measurements of IN concentrations in the marine boundary layer over Southern

Hemisphere centered on Australia presented by B73. *Burrows et al.* [2012] developed a parameterization for marine IN emissions by multiplying the sea spray emissions by an ocean biological variable (chlorophyll or particulate organic carbon), and a scaling factor. The scaling factor is calculated as a product of five factors, each has a large uncertainty. The value for the scaling factor is chosen to lead to good agreement with B73 observations. Here we apply a different method than *Burrows et al.* [2012]. The membrane filter technique is used for ice nuclei measurement in B73. Particles were collected with a membrane filter on the forward mast of the ship, stored, and later analyzed for IN content in the laboratory by raising the humidity to water saturation. The empirical *Phillips et al.* [2008] parameterization relies on data collected from the continuous flow diffusion chamber (CFDC) method. The chamber draws sampled air between two horizontal temperature-controlled plates. The major problem with the membrane filter technique is that the large number of hygroscopic particles trapped with ice nuclei compete for the available water vapor and thus prevent the humidity at the filter surface from reaching its theoretical value. Therefore, the membrane filter technique could underestimate the IN concentration by a factor of 14±4 compared to the CFDC method [*Hussain and Kayani*, 1988]. The exact difference between the two methods also depends on the Aitken mode aerosol concentration, since a larger Aitken mode aerosol concentration generally means a larger concentration of hygroscopic particles [*Hussain and Kayani*, 1988]. Therefore, we did not directly use the measured IN concentration from B73 to constrain the ice nucleation efficiency of MOA. Instead, we used the ratio of the ice nuclei concentration measured with the same technique at different locations. *Schnell and Vali* [1976] have calculated the average ice nuclei

121

concentration over Australia and the Antarctic Ocean (40°S latitude band) as measured by B73. At -15°C at water saturation, the ratio of ice nuclei number concentration between the two regions (Australia:40S) was 1:3 as reported by *Schnell and Vali* [1976].

We will still use *Phillips et al.* [2008] to parameterize the ice nucleation ability of MOA. In addition, we constrain the *Phillips et al.* [2008] parameterization by fitting this 1:3 ratio between Australia and 40°S latitude band. The ice nuclei concentration at the two regions is calculated by multiplying the aerosol number concentration by the ice nucleation fraction for each aerosol group. Therefore, the ice nuclei concentration ratio that we try to fit is summarized in the following equation:

$$(COTR_{Au} \times Fotr + CMOA_{Au} \times Fmoa) \times 3 = COTR_{40} \times Fotr + CMOA_{40} \times Fmoa$$

(4.5)

COTR is the other aerosol (besides MOA, i.e. dust, BC/OM) number concentration at Australia (Au) and the 40°S latitude band (40). CMOA is the MOA number concentration for the same regions. All of the aerosol number concentrations (dust, black carbon, organic carbon and MOA) are taken from the CAM-IMPACT simulations. *Fotr* is the frozen fraction of non-MOA aerosol at -15°C at water saturation, as predicted using the *Phillips et al.* [2008] parameterization. Fmoa is the MOA frozen fraction for the same condition and is the only unknown variable here. We set an upper limit for Fmoa of

122

100%. With equation (4.5), we can calculate the frozen fractions of MOA at -15°C at water saturation, which are used to constrain the *Phillips et al.* [2008] parameterization. The calculated MOA nucleation efficiency at -15°C at water saturation is 3.75% by number for the smallest size bin (0.05-0.63 µm), and 100% for all of the larger size bins. The efficiency differs by size because larger aerosol has larger surface area and therefore a larger frozen fraction according to the *Phillips et al.* [2008] parameterization. The frozen fractions of MOA are fairly large. However, large frozen fractions are possible, since measurements of ice nucleation of marine diatoms by *Knopf et al.* [2011] showed that at 240K and RH of 95%, about 63% of aqueous NaCl droplets containing marine diatoms will freeze in 9s. In addition, large particles are subject to gravitational settling, and therefore have very low number concentrations at mixed-phase cloud altitudes (around 400-600 hpa). The uncertainties in this derived ice nucleation efficiency are associated with the predicted aerosol number concentration and the predicted ice nucleation efficiency from the Phillips parameterization. The model predicted dust concentration and black carbon concentration is smaller than the observations by *Wolff and Cachier* [1998] at Halley, Antarctica by about a factor of 2 annually (see comparison in *Wang et al.*, [2009]). The *Phillips et al.* [2008] parameterization has been shown to over-predict ice nucleation by dust and soot at warm subzero temperatures. At -15°C, the over-prediction is about a factor of 10 [*Phillips et al.*, 2012]. Comparisons of model predicted marine organic concentrations to field campaigns have been carried out by *Lapina et al.* [2011]. The model predicted marine organic concentrations were shown to be larger than observations by as much as a factor of 6. *Lapina et al.* [2011] used the *Jaegle et al.* [2011] sea salt emission parameterization and two different

parameterizations of the MOA fraction (*Spracklen et al.* [2008] and *Langmann et al.* [2008]), but since their submicron MOA emissions are close to those predicted from our model (section 4.4.1) our model would have a similar over-prediction in comparison to observations. Taking the under prediction of dust and BC concentrations, the over prediction of dust and BC ice nucleation, as well as the over prediction of marine organic concentrations into account, the "true" MOA frozen fraction might be different than our derived value by a factor of 1.2. Below, we test the sensitivity of the simulated ice/liquid water path and cloud radiative forcing to the derived MOA ice nucleation efficiency by increasing and decreasing the efficiencty by a factor of 10, which covers the range of uncertainty in our input parameters.

MOA is also added as contact ice nuclei in the adjusted Young contact freezing treatment. However, contact ice nuclei are not constrained by B73 since the measurement method does not account for contact freezing. MOA is not included in the aerosol direct effect and aerosol indirect effect in warm and cirrus ice clouds.

4.3   Experimental Set-up

A total of six sensitivity simulations were performed (Table 4.1). The No_MOA case is the original set-up as the Phi_YCT_Less case in *Yun and Penner* [2012], but with the modified Phillips parameterization. The Reference case treats sea salt emissions the same as *Meskhidze et al.* [2011] and the fraction of sea salt emissions that is MOA according to

Gantt et al. [2011]. *Meskhidze et al.* [2011] uses the *Martensson et al.* [2003] sea salt emission function for sea salt size smaller than 2.8 μm and *Monahan et al.* [1986] function for sea salt sizes larger than 2.8 μm. The Sslt_Emis case changes the sea salt emission function to the *Gong* [2003] parameterization with SST dependence as described by *Jaegle et al.* [2011]. The MOA_Frac case changes the fraction of sea salt that is MOA to the modified *Vignati et al.* [2010] parameterization described by *Meskhidze et al.* [2011]. To test the uncertainty in the derived ice nucleation efficiency of MOA, the Frz_Less and Frz_More cases decrease and increase the ice nucleation efficiency by a factor of 10, respectively. All simulations are run for 5 years and 4 months. The first 4 months are treated as model spin-up and are excluded from the analysis.

Table 4.1: Sensitivity simulations

Simulation	Description
No_MOA	No MOA
Reference	*Meskhidze et al.* [2011] sea salt emission, *Gantt et al.* [2011] MOA fraction
Sslt_Emis	Sea salt emission changed to *Jaegle et al.* [2011]
MOA_Frac	MOA fraction changed to modified *Vignati et al.* [2010]
Frz_Less	Ice nucleation efficiency of MOA decreased by a factor of 10
Frz_More	Ice nucleation efficiency of MOA increased by a factor of 10

4.4   Results

4.4.1   Marine Organic Aerosol emission, burden, and lifetime

Figure 4.1 shows the MOA emission rates from the sum of bin1 (0.05-0.63 µm) and bin2 (0.63-1.26 µm) from the Reference, Sslt_Emis, and MOA_Frac cases. We focus on the two smallest size bins since they can be more easily transported to the height of mixed-phase clouds compared to the larger size bins. Changing the sea salt emission function from *Meskhidze et al.* [2011] to *Jaegle et al.* [2011] reduces the bin1 and bin2 MOA emission rates in all source regions. This is due to the smaller submicron sea salt emission rates predicted from *Gong* [2003] compared to *Martensson et al.* [2003]. The emission rates are larger around 40-50S and north of 20N, and smaller near the tropics with the modified *Vignati et al.* [2010] MOA fraction function compared to *Gantt et al.* [2011]. The modified *Vignati et al.* [2010] function does not have the inverse dependence on wind speed that *Gantt et al.* [2011] does. Therefore, at the high wind speeds in the extra tropical regions, the MOA fraction is not reduced. At the low wind speeds in the tropics, the MOA fraction is not enhanced over that provided by the *Gantt et al.* [2011] parameterization.
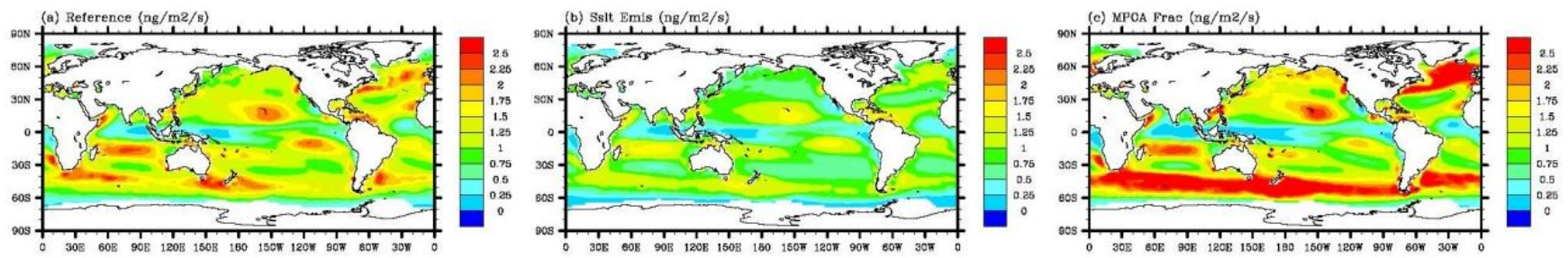
Figure 4.1: bin 1 and bin2 MOA emission rates from Reference, Sslt_Emis, and MOA_Frac cases.

Table 4.2 lists the global annual emissions, burdens, and lifetimes of the MOA aerosols in each size bin predicted from the Reference, Sslt_Emis, and MOA_Frac cases. The mass of emissions of MOA decreases from the first size bin to the 2nd and then increases with larger aerosol size for all three cases. The larger emission for the first size bin is due to the larger emission rate of sea salt for smaller sizes. Compared to the reference case, the *Jaegle et al.* [2011] sea salt emission function produces smaller emissions for the first two size bins, but larger emissions for the larger sizes. The modified *Vignati et al.* [2010] MOA fraction function produces larger MOA emissions at all size bins. With the OM/OC ratio of 1.4 assumed by *Liu et al.* [2005], the submicron (< 1 μm) MOA emission for the Reference, Sslt_Emis, and MOA_Frac cases are 8.24, 5.59, and 9.29 TgC/yr, respectively. This is close to the predicted submicron MOA emission from *Lapina et al.* [2011] (8.2-8.9 TgC/yr). The value for Reference case (11.53 Tg/yr) is larger than that predicted by *Meskhidze et al.* [2011] (9.4 Tg/yr) with the same sea salt and MOA fraction functions. One possible reason is the larger wind speed between 40-60S in the CAM3 model compared to that in CAM5, which was the model used by *Meskhidze et al.* [2011]. The burdens of MOA for each of the three cases follows the changes to the emission rates. The lifetimes of different size bins are similar (around 1.3 days), except for the largest size bin (which is around 0.5 days). The lifetimes are not significantly changed among the different cases.

Table 4.2: MOA emission, burden and lifetime in each size bin.

Sizes (µm)	Reference	Sslt_Emis	MOA_Frac
Emission (Tg/yr)			
0.05-0.63	9.56	6.31	10.87
0.63-1.26	3.36	2.57	3.62
1.26-2.5	6.67	8.72	8.24
2.5-10	13.03	20.92	16.35
total	32.61	38.51	39.08
Burden (Tg)			
0.05-0.63	0.0363	0.0238	0.0412
0.63-1.26	0.0126	0.0096	0.0136
1.26-2.5	0.0242	0.0307	0.0296
2.5-10	0.0194	0.0313	0.0227
total	0.0924	0.0954	0.1071
Lifetime (Day)			
0.05-0.63	1.367	1.358	1.365
0.63-1.26	1.355	1.352	1.352
1.26-2.5	1.305	1.268	1.294
2.5-10	0.535	0.538	0.500
total	1.021	0.892	0.987

4.4.2 Contribution from MOA vs. other aerosols to ice nucleation

It is informative to compare the contribution of MOA to ice number concentration with that of other aerosols, to gain some insight into the relative importance of MOA as ice nuclei. Figure 4.2 shows the predicted ice number concentration from dust, black and organic carbon (BOC), and MOA for deposition/condensation/immersion (DCI) freezing and contact freezing in the Reference simulation. For DCI freezing, the contribution from dust and BOC is largest in the Northern Hemisphere mid-troposphere, since most of the emissions are in the NH (Figure 2.2). Although there is also a region of high ice number concentration in the SH mid-troposphere, the magnitude is much smaller. However, the ice number concentration from DCI freezing of MOA is larger in the Southern Hemisphere, consistent with the MOA emission distribution as shown in Figure 4.1. The distribution of ice number concentration derived from MOA is different from that of the other two aerosol groups. The maxima of ice particles formed from DCI freezing of MOA aerosol are located lower in the troposphere and more toward the poles. The reason can be explained by the distribution of the ice nucleating aerosols. Dust and BOC are both emitted assuming a uniform mixing ratio within the boundary layer, while MOA, is only emitted in the lowest model layer (as is sea salt). This means that there is less vertical transport of the MOA aerosols than for dust and BOC. Therefore, the maxima of the ice number concentration formed from MOA DCI freezing is shifted to lower altitudes. For DCI freezing, MOA is the dominant ice nuclei species, especially in the Southern Hemisphere, with dust next and BOC last. Burrows et al. (2012) also found that

130

marine ice nuclei play a dominant role in determining ice nuclei concentrations over the

Southern Ocean.
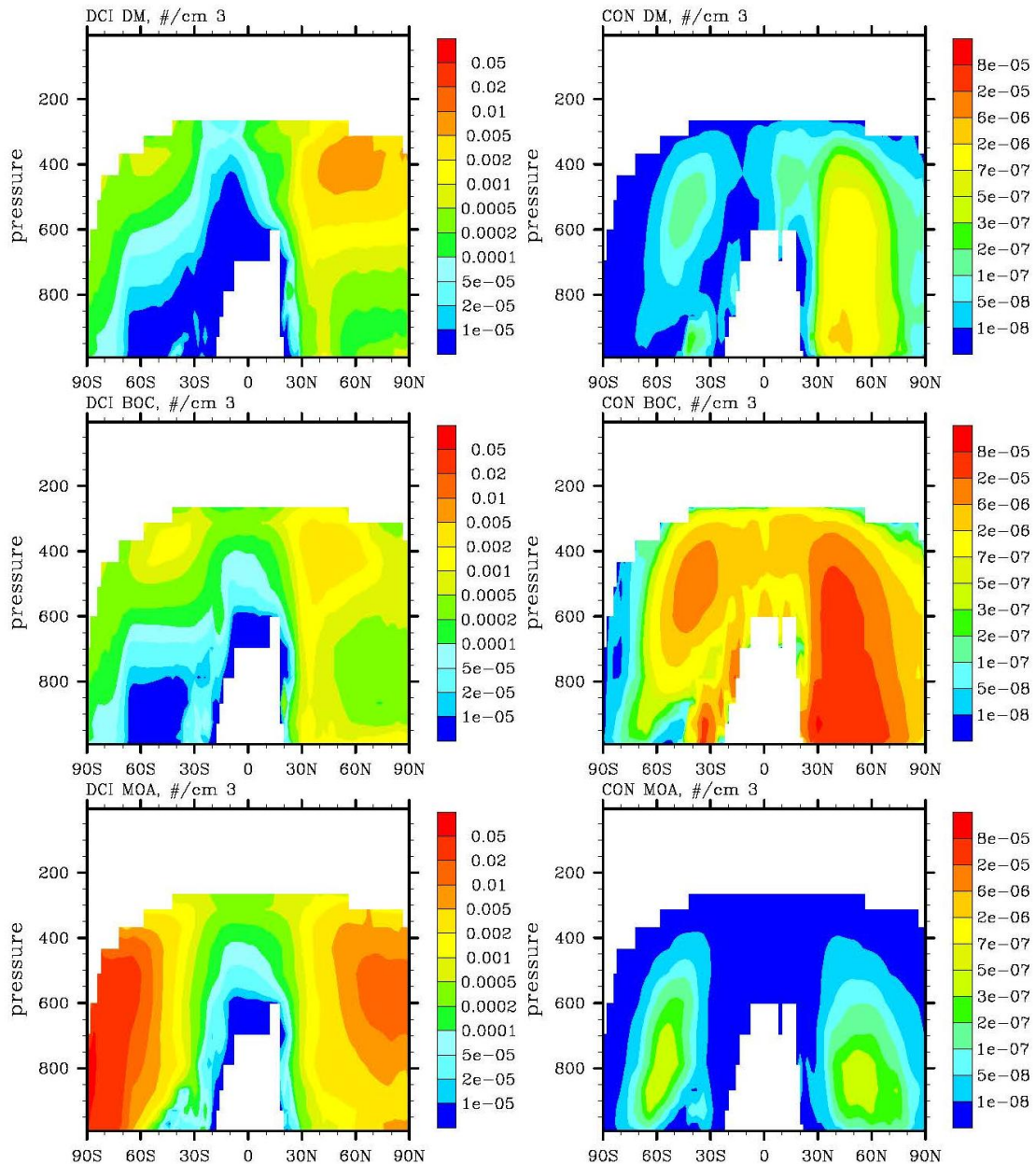
Figure 4.2: Ice number concentration from dust (DM), black and organic carbon (BOC), and MOA for deposition/condensation/immersion (DCI) freezing (left column), and contact freezing (right column) in the Reference case.

The ice number concentration from contact freezing is distributed differently than that from DCI freezing. Since contact freezing requires the presence of liquid droplets to collide with aerosol particles, the distribution of the ice number concentration formed from contact freezing depends on droplet availability. As in the case of DCI freezing, the contribution of dust and BOC to the ice number concentration formed from contact nucleation is larger in the Northern Hemisphere, while that from MOA is comparable in the NH and SH. BOC still dominates contact freezing due to their large number concentration, dust is the second, while MOA is the least important for contact freezing. Comparing DCI and contact freezing side by side, the ice number formed from DCI freezing is about three orders of magnitude more than that formed from contact freezing. This means DCI freezing dominates the ice formation process in this case. Therefore, the formation of ice particles is dominated by the MOA aerosol.

4.4.3 Cloud liquid/ice water field and radiative forcing

The ice water paths (IWP) of all the six simulations are compared to the ISCCP observation (Figure 4.3). As we stated in the introduction, the No_MOA case without MOA as heterogeneous ice nuclei under predicts IWP along the 40-70S latitude band. In the cases where MOA are included as heterogeneous ice nuclei, the IWP in this region increases and compares better with observations. For the sensitivity studies, the

132

Sslt_Emis case produces slightly smaller IWP compared to the Reference case, while the

IWP from the MOA_Frac case is slightly larger. When the ice nucleation efficiency of
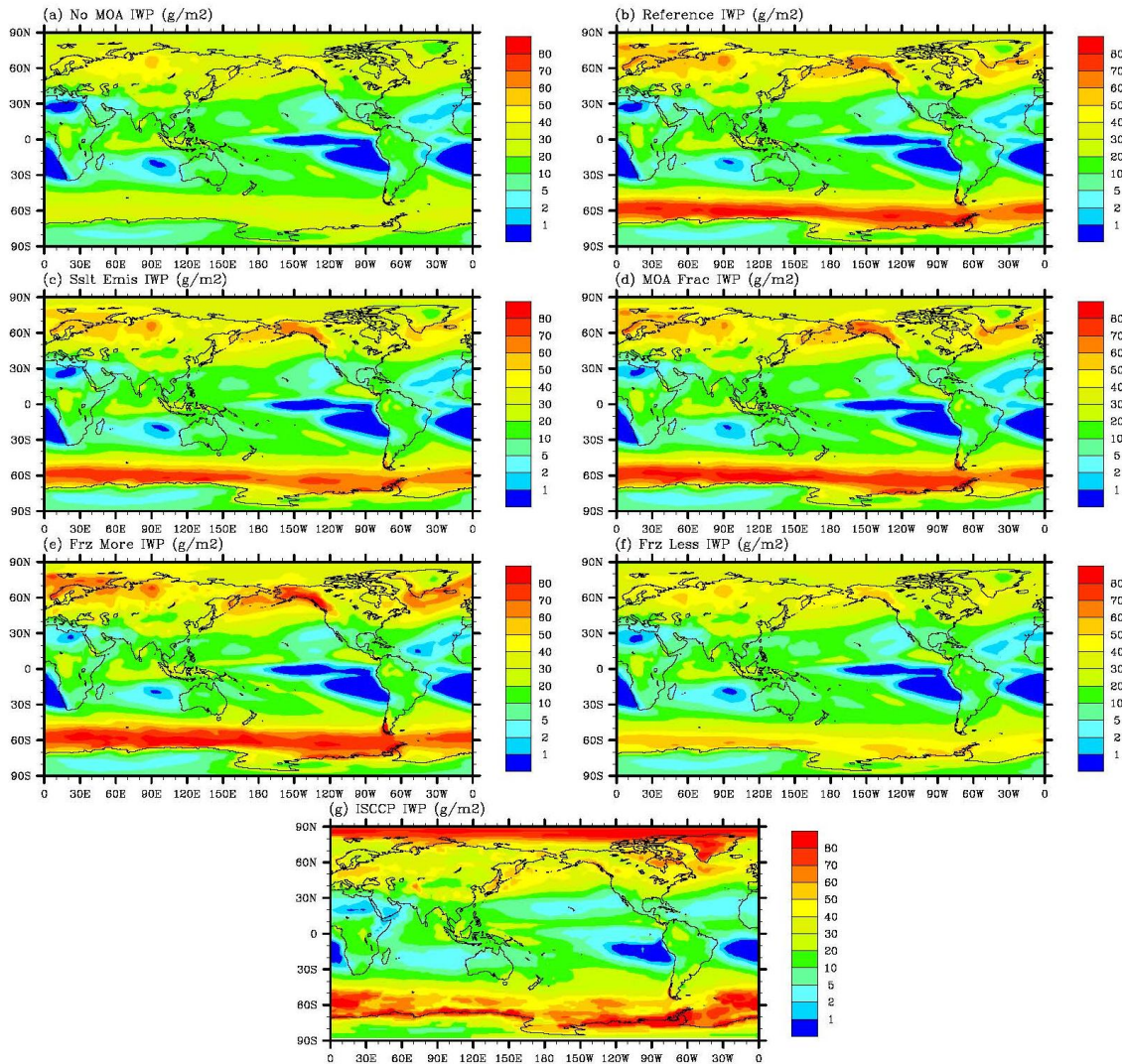
Figure 4.3: IWP from all six sensitivity simulations in Table 4.1 as well as the ISCCP IWP.

MOA is increased by a factor of 10, the ice water path is increased in both the Southern and Northern Hemisphere 40-70 degree latitude band, and also in the tropics. When the ice nucleation efficiency of MOA is decreased by a factor of 10, the ice water path is decreased and is only slightly larger than the No_MOA case.

Figure 4.4 shows the zonal averages of mixed-phase cloud ice/droplet number concentration, mixed-phase cloud ice/droplet size, ice/liquid water path, shortwave/longwave cloud forcing, and comparison to satellite observations. We first examine the effects of changing the MOA emissions. The ice number concentration is larger in the MOA_Frac case than in the Sslt_Emis and Reference case (Figure 4.4a) due to the larger MOA emission rate change (Figure 4.1). This results in smaller ice crystal effective size (Figure 4.4c) due to the limitation of water vapor. Droplet number and droplet size (Figure 4.4b, and d) are both reduced because of stronger Bergeron-Findeison process. IWP is only slightly larger in the MOA_Frac case. LWP is smaller and is dominant in determining the changes to cloud forcings, since the droplets are smaller and more numerous. SWCF and LWCF are both slightly smaller in absolute value in the MOA_Frac case. Next, we examine the effect of changing the ice nucleation efficiency of MOA. As shown in Figure 4.4a, the increase of ice number concentration is less than a factor of 10 between the Reference case and the Frz_More case, since the ice nucleation efficiency is capped at 100%. The IWP is only incrementally increased from
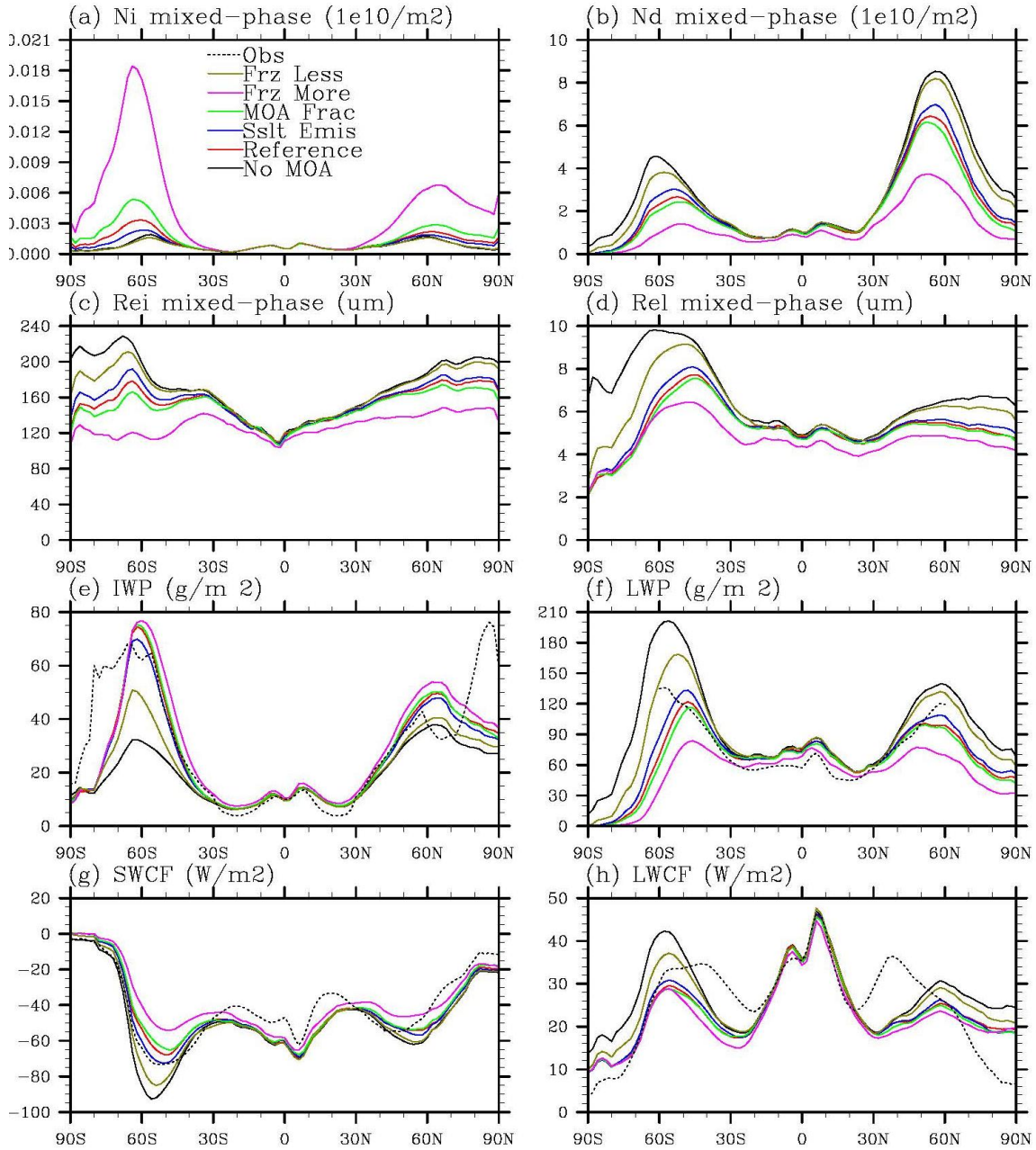
Figure 4.4: Zonal and annual mean vertically integrated mixed-phase ice crystal number concentration (Ni) and cloud droplet number concentration (Nd), effective ice crystal radius (Rei) and cloud droplet radius (Rel) in mixed-phase clouds, ice water path (IWP), liquid water path (LWP), shortwave cloud forcing (SWCF), longwave cloud forcing (LWCF) from the six Present-Day model experiments described in Table 4.1. Black dotted lines refer to CERES data for LWCF and SWCF (http://ceres.larc.nasa.gov), MODIS data for LWP (http://modis.gsfc.nasa.gov/), and ISCCP data for IWP (http://isccp.giss.nasa.gov/).

the Reference case to the Frz_More case, as shown in Figure 4.4c. However, the reduction of IWP is as large as 25 g/m^2 when the ice nucleation efficiency is reduced by a factor of 10.

Generally, varying the ice nucleation efficiency of MOA produces larger changes in IWP than changing the MOA emission rates through using different parameterizations. Therefore, experimental studies that quantify the ice nucleation efficiency for the MOA aerosols are needed for more accurate estimate of their effect on IWP.

The increase of ice number concentration from the inclusion of MOA as heterogeneous ice nuclei results in a decrease of both the cloud droplet number concentration (Figure 4.4b) and droplet radius (Figure 4.4d), due to the Bergeron-Findeisen process. The liquid water path (LWP) is also reduced (Figure 4.4f). The reduced LWP leads to smaller shortwave and longwave cloud forcings (SWCF, LWCF) in the absolute value, as shown in Figure 4.4g and h. In general, the simulations with MOA as heterogeneous ice nuclei at the standard derived ice nucleation efficiency (Reference, Sslt_Emis, and MOA_Frac) compare better to satellite observations of IWP, LWP, SWCF, and LWCF. The simulations with MOA ice nucleation efficiencies increased or decreased by a factor of 10 (Frz_More and Frz_Less) either overestimate or underestimate these variables compared to satellite observations.

Table 4.3 summarizes the global means of mixed-phase cloud ice number concentration, ice/liquid water paths, and cloud forcings for all the simulations as well as for satellite observations. After MOA are added as heterogeneous ice nuclei, the global mean IWP increases from 16.13 g/m^2 in the No_MOA case to 21.83 g/m^2 in the Reference case, comparing better to the observed value of 21.2 g/m^2. The global mean LWP also decreased by 20.74 g/m^2, which is within the range of satellite observations. The absolute value of Net cloud forcing (NCF) decreased by 1.81 W/m^2. For the sensitivity tests, the NCF change produced by the addition of MOA ice nuclei ranges from 0.17 to 5.54 W/m^2, depending mainly on the different MOA ice nucleation efficiencies. The NCF difference between the simulations with different MOA emission rates is 1.08W/m^2, only one fifth of the total uncertainty range.

Table 4.3: global means of mixed-phase cloud ice number (mNi), vertically integrated liquid/ice water paths and cloud radiative forcing. The observation data are the same as those in Table 1.2 in Chapter 2.

Simulation	mNi (10^{10} m^{-2})	IWP (g m^{-2})	LWP (g m^{-2})	SWCF (W m^{-2})	LWCF (W m^{-2})	NCF (W m^{-2})
No_MOA	0.00097	16.13	94.85	-55.34	28.82	-26.52
Reference	0.00230	21.83	74.11	-50.63	25.92	-24.71
Sslt_Emis	0.00175	20.99	77.26	-51.56	26.25	-25.31
MOA_Frac	0.00327	22.10	72.23	-49.99	25.76	-24.23
Frz_More	0.00909	24.53	59.88	-45.39	24.41	-20.98
Frz_Less	0.00107	17.96	87.78	-54.19	27.84	-26.35
Obs		21.2	50 to 87	-47 to -54	22 to 30	

The addition of natural aerosol heterogeneous ice nuclei will also change the effect of anthropogenic aerosols, since cloud properties are most sensitive to the addition of aerosols when the background concentration is low [*Platnick and Twomey*, 1994]. To examine the effect of including MOA as heterogeneous ice nuclei to the anthropogenic aerosol forcing, we also conduct pre-industrial runs for the No_MOA case and the Reference case. Table 4.4 summarizes the Present-Day (PD) minus Pre-Industrial (PI) changes of ice/liquid water path, cloud radiative forcing, and top of atmosphere (TOA) forcing. The PD-PI change of IWP from the Reference case is less than half of that from the No_MOA case. Consequently, the LWP and cloud forcing changes from the Reference case are also smaller. The net cloud forcing is reduced by 0.33 W/m^2, from -0.36 to -0.03 W/m^2. Since the aerosol direct effect, and the indirect effect in cirrus and warm clouds are unchanged, the change in the TOA forcing with and without MOA is similar to that of the cloud forcing, namely 0.3 W/m^2. Therefore, including MOA as a natural source of heterogeneous ice nuclei decreased the anthropogenic aerosol forcing.

Table 4.4: PD-PI liquid/ice water path changes and radiative forcing changes.

Simulation	ΔLWP	ΔIWP	ΔSWCF	ΔLWCF	ΔNCF	ΔNFT
No_MOA	-5.02	1.00	2.20	-2.56	-0.36	-2.82
Reference	-3.38	0.48	1.97	-2.00	-0.03	-2.52

4.5   Conclusions

Marine organic aerosols were implemented as a new natural aerosol species into the coupled CAM3+ and aerosol transport model IMPACT. Their effects as heterogeneous ice nuclei in mixed-phase clouds were tested. The ice nucleation efficiency of MOA is derived so that the observed ice nuclei concentration ratio between Australia and 40S by *Bigg* [1973] was reproduced. Sensitivity studies for the MOA emission rates were carried out by altering the sea salt emission parameterization, and the MOA fraction function. The uncertainty in the derived MOA ice nucleation efficiency was also tested by increasing and decreasing the ice nucleation efficiency by a factor of 10.

Changing the sea salt emission function from *Meskhidze et al.* [2011] to *Jaegle et al.* [2011] reduces the bin1 and bin2 MOA emission rates in all ocean regions. Changing the MOA fraction function from *Gantt et al.* [2011] to the modified *Vignati et al.* [2010] function increased the MOA emission rate from 40-50S and north of 20N, and decreased it near the tropics. The submicron MOA emission rate from the Reference, Sslt_Emis, and MOA_Frac cases are about 11.53, 7.82, and 13.0 Tg/yr, respectively. The burden of total MOA for the three cases is 0.0924, 0.0954, and 0.1071 Tg, respectively.

In contrast to dust and BOC which contribute to ice nucleation mostly in the Northern Hemisphere, the contribution of MOA to ice nucleation is similar in the Northern and Southern Hemisphere. MOA also contributes to more ice formation than does dust or

BOC, thus is the most important ice nuclei in the Reference case. With the addition of MOA as heterogeneous ice nuclei in mixed-phase clouds, the comparison of IWP to ISCCP observations is improved significantly. The global mean IWP increases from 16.13 g/m^2 in the No_MOA case to 21.83 g/m^2 in the Reference case, comparing better to the observation value of 21.2 g/m^2. The increase of ice number concentration from the inclusion of MOA as heterogeneous ice nuclei results in a decrease of both the cloud droplet number concentration and droplet radius, due to the Bergeron-Findeisen process. The global mean LWP also decreases by 20.74 g/m^2, into the range of satellite observations. The decrease of LWP leads to smaller absolute values for the SWCF and LWCF . The absolute value of NCF decreased by 1.81 W/m^2.

In general, the simulations with MOA as heterogeneous ice nuclei using the standard derived ice nucleation efficiency (Reference, Sslt_Emis, and MOA_Frac) compare better to satellite observations of IWP, LWP, SWCF, and LWCF. The simulations with MOA ice nucleation efficiencies increased or decreased by a factor of 10 (Frz_More and Frz_Less) either overestimate or underestimate these variables compared to satellite observations. Varying the ice nucleation efficiency of MOA produces larger changes in forcing than changing the MOA emission rates through using different parameterizations. Reducing the ice nucleation efficiency of MOA by a factor of 10 reduced the ice nucleating effect of MOA greatly.

The addition of MOA as natural aerosol heterogeneous ice nuclei also reduced the magnitude of anthropogenic aerosol forcing. The PD-PI change of IWP from the Reference case is less than half of that from the No_MOA case. Consequently, the LWP and cloud forcing changes from Reference case are also smaller. The PD-PI NCF is reduced by 0.33 W/m^2, from -0.36 to -0.03 W/m^2.

This study evaluates effect of marine organic aerosols to climate through acting as heterogeneous ice nuclei in mixed-phase clouds. Significant changes to IWP and anthropogenic AIE were found when marine organic aerosols are included as ice nuclei. However, results are sensitive to the ice nucleation efficiency of MOA. Further study that quantifies the ice nucleation properties of MOA are needed for a more accurate estimate of their effect.

References

Abdul-Razzak, H., and S. J. Ghan (2000), A parameterization of aerosol activation 2. Multiple aerosol types, *Journal of Geophysical Research-Atmospheres*, *105*(D5), 6837-6844.

Abdul-Razzak, H., and S. J. Ghan (2002), A parameterization of aerosol activation - 3. Sectional representation, *Journal of Geophysical Research-Atmospheres*, *107*(D3).

Blanchard, D.C., 1957: The supercooling, freezing and melting of giant waterdrops at terminal velocity in air, in *Artificial Simulation of Rain*, London, Pergamon Press, 233-249.

Bigg, E. K. (1973), Ice nucleus concentrations in remote areas, *Journal of the Atmospheric Sciences*, *30*(6), 1153-1157.

Burrows, S. M., C. Hoose, U. Pöschl, and M. G. Lawrence: Ice nuclei in marine air: bioparticles or dust?, *Atmospheric Chemistry and Physics Discussion*, 12, 4373-4416.

Cavalli, F., et al. (2004), Advances in characterization of size-resolved organic matter in marine aerosol over the North Atlantic, *Journal of Geophysical Research-Atmospheres*, *109*(D24).

Chen, J. P., A. Hazra, and Z. Levin (2008), Parameterizing ice nucleation rates using contact angle and activation energy derived from laboratory data, *Atmospheric Chemistry and Physics*, *8*(24), 7431-7449.

Demott, P., R. Sullivan, K. Prather, T. C. Hill, G. D. Franc, A. Bertram, R. Mason, T. Guasco, D. Collins, L. Cuadra-Rodriguez, A. Ault, and V. Grassian (2012), Ice nuclei production from sea spray, paper presented at 31st Conference on American Association on Aerosol Research, Am. Assco. Aer. Res., Minneapolis, Min.

Diehl, K., M. Simmel, and S. Wurzler (2006), Numerical sensitivity studies on the impact of aerosol properties and drop freezing modes on the glaciation, microphysics, and dynamics of clouds, *Journal of Geophysical Research-Atmospheres*, *111*(D7).

Gantt, B., N. Meskhidze, M. C. Facchini, M. Rinaldi, D. Ceburnis, and C. D. O'Dowd (2011), Wind speed dependent size-resolved parameterization for the organic mass fraction of sea spray aerosol, *Atmospheric Chemistry and Physics*, *11*(16), 8777-8790.

Gong, S. L. (2003), A parameterization of sea-salt aerosol source function for sub- and super-micron particles, *Global Biogeochemical Cycles*, *17*(4).

Hawkins, L. N., and L. Russell (2010), Polysaccharides, Proteins, and Phytoplankton Fragments: Four Chemically Distinct Types of Marine Primary Organic Aerosol Classified by Single Particle Spectromicroscopy, *Advances in Meteorology*, doi:10.1155/2010/612132.

Hussain, K., and S. A. Kayani (1988), A comparison of the static and flow methods for the detection of ice nuclei, *Atmospheric Research*, 22, 125-136.

Jaegle, L., P. K. Quinn, T. S. Bates, B. Alexander, and J. T. Lin (2011), Global distribution of sea salt aerosols: new constraints from in situ and remote sensing observations, *Atmospheric Chemistry and Physics*, *11*(7), 3137-3157.

Khvorostyanov, V. I., and J. A. Curry (2004), The theory of ice nucleation by heterogeneous freezing of deliquescent mixed CCN. Part I: Critical radius, energy, and nucleation rate, *Journal of the Atmospheric Sciences*, *61*(22), 2676-2691.

Knopf, D. A., P. A. Alpert, B. Wang, and J. Y. Aller (2011), Stimulation of ice nucleation by marine diatoms, *Nature Geoscience*, *4*(2), 88-90.

Langmann, B., C. Scannell, and C. O'Dowd (2008), New Directions: Organic matter contribution to marine aerosols and cloud condensation nuclei, *Atmospheric Environment*, *42*(33), 7821-7822, doi:10.1016/j.atmosenv.2008.09.002.

Lapina, K., et al. (2011), Investigating organic aerosol loading in the remote marine environment, *Atmospheric Chemistry and Physics*, *11*(17), 8847-8860.

Liu, X. H., J. E. Penner, and M. Herzog (2005), Global modeling of aerosol dynamics: Model description, evaluation, and interactions between sulfate and nonsulfate aerosols, *Journal of Geophysical Research-Atmospheres*, *110*(D18), doi:10.1029/2004JD005674

Martensson, E. M., E. D. Nilsson, G. de Leeuw, L. H. Cohen, and H. C. Hansson (2003), Laboratory simulations and parameterization of the primary marine aerosol production, *Journal of Geophysical Research-Atmospheres*, *108*(D9).

Meskhidze, N., and A. Nenes (2006), Phytoplankton and cloudiness in the Southern Ocean, *Science*, *314*(5804), 1419-1423.

Meskhidze, N., J. Xu, B. Gantt, Y. Zhang, A. Nenes, S. J. Ghan, X. Liu, R. Easter, and R. Zaveri (2011), Global distribution and climate forcing of marine organic aerosol: 1. Model improvements and evaluation, *Atmospheric Chemistry and Physics*, *11*(22), 11689-11705.

Monahan, E. C., and I. G. O'Muircheartaigh (1986), Whitecaps and the passive remote sensing of the ocean surface, *International Journal of Remote Sensing*, 7(5), 627-642.

O'Dowd, C. D., M. C. Facchini, F. Cavalli, D. Ceburnis, M. Mircea, S. Decesari, S. Fuzzi, Y. J. Yoon, and J. P. Putaud (2004), Biogenically driven organic contribution to marine aerosol, *Nature*, *431*(7009), 676-680.

Phillips, V. T. J., P. J. DeMott, and C. Andronache (2008), An empirical parameterization of heterogeneous ice nucleation for multiple chemical species of aerosol, *Journal of the Atmospheric Sciences*, *65*(9), 2757-2783.

Phillips, V. T. J., P. J. DeMott, C. Andronache, K. A. Pratt, K. A. Prather, R. Subramanian, and C. Twohy (2012), Improvements to an empirical parameterization of

heterogeneous ice nucleation and its comparison with observations, *Journal of the Atmospheric Sciences*, in press.

Platnick, S., and S. Twomey (1994), Determining the susceptibility of cloud albedo to changes in droplet concentration with the advanced very high-resolution radiometer, *Journal of Applied Meteorology*, *33*(3).

Roelofs, G. J. (2008), A GCM study of organic matter in marine aerosol and its potential contribution to cloud drop activation, *Atmospheric Chemistry and Physics*, *8*(3), 709-719.

Schnell, R. C. (1975), Ice nuclei produced by laboratory cultured marine phytoplankton, *Geophysical Research Letters*, 2(11), 500-502.

Schnell, R. C. (1977), Ice nuclei in seawater, fog water and marine air off coast of Nova Scotia: summer 1975, *Journal of the Atmospheric Sciences*, *34*(8), 1299-1305.

Schnell, R. C., and G. Vali (1976), Biogenic ice nuclei .1. terrestrial and marine sources, *Journal of the Atmospheric Sciences*, *33*(8), 1554-1564.

Spracklen, D. V., S. R. Arnold, J. Sciare, K. S. Carslaw, and C. Pio (2008), Globally significant oceanic source of organic carbon aerosol, *Geophysical Research Letters*, *35*(12), doi:L1281110.1029/2008gl033359.

Vignati, E., M. C. Facchini, M. Rinaldi, C. Scannell, D. Ceburnis, J. Sciare, M. Kanakidou, S. Myriokefalitakis, F. Dentener, and C. D. O'Dowd (2010), Global scale emission and distribution of sea-spray aerosol: Sea-salt and organic enrichment, *Atmospheric Environment*, *44*(5), 670-677.

Wang, M., and J. E. Penner (2010), Cirrus clouds in a global climate model with a statistical cirrus cloud scheme, *Atmospheric Chemistry and Physics*, *10*(12), 5449-5474.

Wang, M. H., J. E. Penner, and X. H. Liu (2009), Coupled IMPACT aerosol and NCAR CAM3 model: Evaluation of predicted aerosol number and size distribution, *Journal of Geophysical Research-Atmospheres*, *114*.

Wolff, E. W., and H. Cachier (1998), Concentrations and seasonal cycle of black carbon in aerosol at a coastal Antarctic station, *Journal of Geophysical Research-Atmospheres*, *103*(D9), doi:10.1029/97jd01363.

Young, K. C. (1974), Numerical simulation of wintertime, orographic precipitation .1. description of model microphysics and numerical technique, *Journal of the Atmospheric Sciences*, *31*(7), 1735-1748.

Yun, Y., and J. E. Penner (2012), Global model comparison of heterogeneous ice nucleation parameterizations in mixed phase clouds, *Journal of Geophysical Research-Atmospheres*, *117*, 7203-7203.

Yun, Y., J. E. Penner, and O. Popovicheva (2012), The effects of hygroscopicity of fossil fuel combustion aerosols on mixed-phase clouds, *Atmospheric Chemistry and Physics Discussion*, 12, 19987-20006, doi:10.5194/acpd-12-19987-2012, 2012.

144

CHAPTER 5

Summary and future work

5.1   Summary

Aerosols are liquid or solid particles suspended in the air. They can be of natural origin such as dust and pollen, or anthropogenic origin such as sulfate and black carbon (BC). In contrast to the greenhouse gases such as CO_2, they are likely to cool the climate. However, the magnitude of the cooling effect is poorly constrained, with the largest estimate almost cancelling or "hiding" the warming effect of CO_2. Therefore, the quantification of the aerosol effect is one of the most important topics in climate change research. Aerosols can affect climate directly by scattering and absorbing solar and infrared radiation, and indirectly by forming liquid or ice particles in warm, ice or mixed-phase clouds (clouds that contain both liquid and ice particles). The aerosol direct effect has become relatively well constrained as a result of a large amount of research. The aerosol indirect effect, especially which occurs in mixed-phase clouds is still poorly quantified, largely due to the lack of understanding of the ice forming processes. At the temperature range in mixed-phase clouds, ice formation always occurs with the aid of an aerosol particle acting as an ice nucleus, i.e. by heterogeneous ice nucleation. However,

most ice nucleation parameterizations in global climate models do not depend on the character and amount of aerosols, but are only a function of temperature or super-saturation.

In the first part of this dissertation, one parameterization for deposition/condensation/immersion ice nucleation and one for contact freezing in mixed-phase clouds that depend on the aerosol size distribution and chemical composition are introduced into a coupled general circulation model and aerosol transport model (CAM-IMPACT). The present-day cloud liquid and ice water fields and the top of the atmosphere cloud radiative forcing are analyzed and compared to observations to see the effect of different heterogeneous freezing treatments. The first question raised in section 1.5 can be answered using the coupled model with different ice nucleation parameterizations.

1. How does an aerosol-dependent ice nucleation parameterization change the predicted distribution of the cloud ice and water field, the cloud radiative forcing, and anthropogenic aerosol effect?

The new aerosol-dependent DCI freezing parameterization (Phillips parameterization) changes the spatial distribution of the cloud water field. Significant changes are found in the cloud ice water fraction, and in the middle cloud fractions. The new DCI freezing

parameterization predicts more ice crystals in the middle troposphere and lower troposphere mid-latitudes in the NH, and fewer ice crystals in the high-latitude NH and most of the SH. This leads to smaller IWP in the SH. The fact that the IWP agree fairly well with satellite observations in the NH shows that the Phillips DCI freezing parameterization is able to correctly predict ice water contents using an online calculation of aerosol fields. The under-prediction of IWP in the SH, however, suggests the possibility that there are missing sources of ice nuclei in the SH.

The smaller IWP leads to a less efficient Bergeron-Findeisen process resulting in a larger liquid water path (LWP), shortwave cloud forcing (SWCF), and longwave cloud forcing (LWCF). When using the aerosol-dependent DCI freezing parameterization, the possibility for a given grid box to have low ice fraction is increased, while that for a given grid box to have a mixture of ice and liquid in decreased than when using non-aerosol-dependent Meyers parameterization.

We also investigated the difference between two contact freezing parameterizations. It is found that contact freezing parameterizations have a greater impact on the cloud water field and radiative forcing than the two DCI freezing parameterizations we compared. The Phillips contact IN parameterization predicts three orders of magnitude less contact IN than the Young parameterization. Using Phillips contact IN parameterization, the contributions from dust and BC/OM are relatively equal, while using the Young parameterization, the contribution from BC/OM is much larger than that from dust. When

using the Phillips contact freezing parameterization, the possibility for a given grid box to have low ice fraction is also increased compared to that using the Young parameterization.

The above changes to the probability distribution of ice fractions further affect the cloud optical thickness observed at middle cloud altitudes. When using the Phillips DCI freezing parameterization and contact freezing parameterization, the optical thickness of middle clouds is increased. As a result, the cloud fractions of altostratus and nimbostratus clouds are increased, and that of altocumulus clouds are decreased compared to using the Meyers parameterization, or the Young parameterization. Therefore, the comparison of altostratus and nimbostratus clouds to ISCCP is improved, while the comparison of altocumulus clouds to ISCCP is worsened.

The net solar flux at top of atmosphere (FSNT), and net long-wave flux at the top of the atmosphere (FLNT) changes by up to 8.73 W/m^2 and 3.52 W/m^2, respectively, due to the use of different DCI and contact freezing parameterizations in mixed-phase clouds. The total climate forcing from anthropogenic BC/OM in mixed-phase clouds is estimated to be 0.16 – 0.93 W/m^2 using the aerosol-dependent parameterizations. A sensitivity test with contact ice nuclei concentration in the original parameterization fit to that recommended by *Young* [1974] gives results that are closer to the new contact freezing parameterization, and produces a smaller anthropogenic aerosol effect of 0.71 W/m^2 in mixed-phase clouds.

Fossil fuel black carbon and organic matter (ffBC/OM) are often emitted together with sulfate, which coats the surface of these particles and changes their hygroscopicity. Observational studies show that the hygroscopicity of soot particles can modulate their ice nucleation ability. Due to the abundance of fossil fuel (ff) combustion aerosols, a small change in their ice nucleation ability can produce a large difference in indirect effects. To address this, in the second part of this dissertation, we implemented a scheme that uses 3 levels of soot hygroscopicity (hydrophobic, hydrophilic and hygroscopic) and used laboratory data to specify their ice nuclei abilities. The 3-ffBC/OM scheme was implemented into the CAM-IMPACT coupled model, as well as an offline radiation model. The coupled model provides the aerosol fields and meteorology fields for the offline model, and is used to calculate the total anthropogenic forcing. The offline model reads the aerosol and meteorology fields and examines the cloud water fields and mixed-phase cloud anthropogenic forcing without involving feedbacks to the cloud fields from changes in aerosols. Therefore, we can answer the second question raised in section 1.5.

2. How does consideration of hygroscopicity of fossil fuel combustion aerosols during the ice nucleation process change the fossil fuel combustion aerosol forcing in mixed-phase clouds?

The new 3-ffBC/OM scheme results in significant changes to anthropogenic forcing in mixed-phase clouds. When hygroscopic ffBC/OM particles are excluded as IN, there is a

35% decrease in the net anthropogenic forcing compared to the 1BC case. When hygroscopic ffBC/OM particles are included, there is an increase by a factor of 6, due to the large liquid water change in the 3BC_SCO case. The two treatments for hygroscopic soot particles lead to a net offline mixed-phase anthropogenic forcing that varies by almost a factor of 10, from 0.111 to 1.059 W/m^2.

Two aspects contribute to the anthropogenic ffBC/OM forcing. The first is the decrease of ice effective radius associated with the increase of Ni. Smaller ice effective radius leads to more reflected solar radiation and less long-wave transmission, reducing the net incoming short-wave radiation as well as the net outgoing long-wave radiation at the Top-of-the-Atmosphere (TOA). Therefore, the anthropogenic Short-wave (SW) forcing from this effect is negative, and the Long-wave (LW) forcing is positive. The second aspect is the decrease of liquid water mass mixing ratio. This results in a smaller liquid water path in the present-day, and therefore a reduced short-wave reflectivity and increased long-wave transmissivity. The result of this change is a positive SW forcing and a negative LW forcing. Since the predicted anthropogenic ffBC/OM forcing is positive, the change in liquid water path dominates the anthropogenic forcing in mixed-phase clouds in our model.

Our results show that the net effect of anthropogenic aerosols on mixed-phase clouds is a warming. The SW forcing in mixed-phase clouds contributes 7.33~68.7% of the anthropogenic SW forcing in all clouds, and the LW forcing contributes 0.32~2.12%. The

magnitude of the mixed-phase cloud forcing is very sensitive to whether the effect of hygroscopicity is considered, and how it is considered. It is larger when hygroscopic particles are included as IN due to the larger fraction of soot particles acting as ice nuclei. More laboratory experiments are needed to fully determine the freezing properties of hygroscopic ffBC/OM at mixed-phase cloud temperatures to reduce the range of uncertainty.

From the first part of this dissertation, it was found that although the new aerosol-dependent formulation reproduces the ice water amount in the Northern Hemisphere (NH) very well compared to satellite observations, the ice water amount in the Southern Hemisphere (SH) is under-predicted significantly. This suggests the possibility that the model is missing a source of ice nuclei in the SH. The existing types of ice nuclei in the model are dust, black carbon, and organic carbon, all of which are from terrestrial sources. Since the land fraction is much smaller in the SH, it is understandable that with the aerosol-dependent ice nucleation parameterization, the ice nuclei concentration in the SH will decrease.

There have been reports in the literature about the potential role of the ocean as an ice nuclei source. Bigg (1973) reported similar number concentration of ice nuclei in the NH and SH. He also showed a band of high ice nucleus concentration along the subtropical convergence zone in the ocean and the Antarctic convergence zone, which are very prolific producers of primary marine plankton (Szyrmer and Zawadzki 1997). Marine

biological materials were later confirmed to be associated with ice nucleation by Schnell (1977), Schnell and Vali (1976), Rosinski et al. (1987), Bigg and Leck (2001), and Brooks et al. (2011). More recently, Knopf et al. (2011) investigated the marine phytoplanktonic diatom *Thalassiosira pseudonana*, and found it to be an efficient ice nucleus at mixed-phase cloud temperatures. These phytoplankton cells and cell fragments can be transported to the atmosphere through the bursting of air bubbles by breaking waves (Cipriano et al. 1981).

This evidence has led to the necessity to evaluate the effects of marine biological organics as ice nuclei. In the third part of this dissertation, marine organic aerosols are implemented as a new natural aerosol species into a coupled CAM- IMPACT. The ice nucleation efficiency of MOA is derived so that the observed ice nuclei concentration ratio between Australia and 40S parallel by *Bigg* [1973] is fulfilled. Sensitivity studies with the MOA emission rates are carried out by altering the sea salt emission parameterization, and the MOA fraction function. The uncertainty with the derived MOA ice nucleation efficiency is also tested by increasing and decreasing the ice nucleation efficiency by a factor of 10. By doing so, the third question raised in section 1.5 could be answered.

3. How does the inclusion of the marine organic ice nuclei change the predicted ice water field, liquid water field, and anthropogenic aerosol forcing?

With the addition of MOA as heterogeneous ice nuclei in mixed-phase clouds, the comparison of IWP to ISCCP observation improved significantly. The global mean IWP increases from 16.13 g/m^2 in the No_MOA case to 21.83 g/m^2 in the Reference case, comparing better to the observation value of 21.2 g/m^2. The increase of ice number concentration from the inclusion of MOA as heterogeneous ice nuclei results in decrease of both the cloud droplet number concentration and droplet radius, due to the Bergeron-Findeisen process. The global mean LWP also decreased by 20.74 g/m^2, into the range of satellite observation. The decrease of LWP leads to smaller SWCF and LWCF in the absolute value. The absolute value of NCF decreased 1.81 W/m^2.

Changing the sea salt emission function from *Meskhidze et al.* [2011] to *Jaegle et al.* [2011] reduces the bin1 and bin2 MOA emission rates in all areas. Changing the MOA fraction function from *Gantt et al.* [2011] to the modified *Vignati et al.* [2010] function increased the MOA emission rate 40-50S and north of 20N, and decreased it near the tropics. The submicron MOA emission rate from the Reference, Sslt_Emis, and MOA_Frac cases are about 11.53, 7.82, and 13.0 Tg/yr, respectively. The burden of total MOA for the three cases is 0.0924, 0.0954, and 0.1071, respectively.

In contrary to dust and BOC which contribute to ice nucleation mostly in the Northern Hemisphere, the contribution of MOA to ice nucleation is similar in both Hemispheres. MOA is also the largest ice nuclei contributor to ice formation in the Reference simulation. In general, the simulations with MOA as heterogeneous ice nuclei at the

standard derived ice nucleation efficiency (Reference, Sslt_Emis, and MOA_Frac) compare better to satellite observations of IWP, LWP, SWCF, and LWCF. The simulations with MOA ice nucleation efficiencies increased or decreased by a factor of 10 (Frz_More and Frz_Less) either overestimate or underestimate these variables compared to satellite observations. Varying the ice nucleation efficiency of MOA produces larger changes in forcing than changing the MOA emission rates through using different parameterizations. Reducing the ice nucleation efficiency of MOA by a factor of 10 reduced the ice nucleating effect of MOA greatly.

The addition of MOA as natural aerosol heterogeneous ice nuclei also reduced the magnitude of anthropogenic aerosol forcing. The PD-PI change of IWP from the Reference case is less than half of that from the No_MOA case. Consequently, the LWP and cloud forcing changes from Reference case are also smaller. The PD-PI NCF is reduced by 0.33 W/m^2, from -0.36 to -0.03 W/m^2.

In summary, MOA is found to be the dominant ice nuclei species compared to dust and soot. Significant changes to IWP and anthropogenic AIE were found when marine organic aerosols are included as ice nuclei. New IWP compared better to ISCCP observation. However, results are sensitive to the ice nucleation efficiency of MOA. Further study that quantifies the ice nucleation properties of MOA are needed for more accurate estimate of their effect.

5.2 Future work

The research on aerosol indirect effect in mixed-phase clouds is still in its infancy stage. Improvements in both the aerosol and cloud treatments in GCMs, as well as in observation are needed to advance our understanding of aerosol-cloud interactions and to decrease the uncertainty in the estimated aerosol indirect effects, which are discussed below.

1. The Phillips ice nucleation parameterization that we introduced in Chapter 2 could be improved to consider different reference scenarios. Currently, the reference scenario is taken from the free troposphere field observation at Colorado. This could serve as a representative condition for the terrestrial free troposphere, with the contribution from dust to total ice nuclei being 2/3, soot being $1/3 - 0.06$, and organic being 0.06. The exact contribution from each aerosol type in each grid cell is the contribution in the reference condition modified by the ratio of aerosol surface area concentration in the grid cell and that in the reference condition. However, in other conditions such as over the oceans, another reference scenario could be built, where the contribution from dust and black carbon should be reduced, while that from the organic increased.

2. Other ice nuclei sources. Ice nucleation abilities of terrestrial biological particles, such as pollen, spores, and bacteria has been recently noted at warm subzero temperatures [*Diehl et al.*, 2001; *Diehl et al.*, 2002; *von Blohn et al.*, 2005; *Pratt et al.*, 2009; *Prenni et*

al., 2009]. Even though their effect on a global scale is suggested to be small [*Hoose et al.*, 2010], they could have strong influence to the local cloud microphysics.

3. Prediction of aerosol number concentration and aerosol size distribution. The aerosol transport model uses a single moment aerosol microphysics scheme for non-sulfate aerosols, which only predicts aerosol mass concentration. Aerosol size distribution is prescribed. Aerosol number concentration is calculated with the predicted aerosol mass and prescribed aerosol size distribution. However, the size distribution and number concentration of aerosols should be determined by their emission and removal mechanism, as well as their interaction with other aerosols. Both the ice nucleation and cloud droplet nucleation prediction schemes rely on the calculated aerosol number concentration. A double moment aerosol microphysics scheme that predicts the aerosol number concentration and size distribution will improve the accuracy of the estimated aerosol indirect effect.

4. Cloud microphysics in convective clouds. Convective cloud is an important component in the hydrology cycle for producing precipitation. Convective detrainment of cloud ice is also a moisture source for the upper troposphere. It has been shown that increased aerosol concentration may affect convective cloud microphysics [*Rosenfeld et al.*, 1999; *Rosenfeld et al.*, 2008]. However, owing to incomplete knowledge of cumulus microphysics and computational limit, the microphysical processes in convective updraft

are ignored or parameterized very crudely in many convection parameterization schemes [*Song and Zhang*, 2011].

5. In this dissertation, we only considered the hygroscopicity change of fossil fuel combustion aerosols through interaction with sulfuric acid. However, coating of organic species may also change the hygroscopicity and ice nucleation properties of aerosols. Organic-rich particles have been shown to require higher ice supersaturation to nucleate ice [*Cziczo et al.*, 2004; *Crawford et al.*, 2011, *Friedman et al.*, 2012]. In future studies, the effect of organic coating on ice nucleation of soot particles should be considered.

6. More in-situ or laboratory measurements on the ice nucleation activity at the mixed-phase cloud temperature range are needed. This could be used to improve the ice nucleation treatment for fossil fuel combustion aerosols and marine organic aerosols in Chapter 3 and Chapter 4.

Other possible improvements include improving the aerosol emission inventory, especially for pre-industrial emission scenario; implementing the aerosol microphysics and cloud microphysics for secondary organic aerosols and nitrate aerosols; implementing the effect cloud entrainment on aerosol indirect effect.

Reference

Crawford, I., et al. (2011), Studies of propane flame soot acting as heterogeneous ice nuclei in conjunction with single particle soot photometer measurements, *Atmospheric Chemistry and Physics*, *11*(18), 9549-9561.

Cziczo, D. J., P. J. DeMott, S. D. Brooks, A. J. Prenni, D. S. Thomson, D. Baumgardner, J. C. Wilson, S. M. Kreidenweis, and D. M. Murphy (2004), Observations of organic species and atmospheric ice formation, *Geophysical Research Letters*, *31*(12), 4, doi:10.1029/2004gl019822.

Diehl, K., S. Matthias-Maser, R. Jaenicke, and S. K. Mitra (2002), The ice nucleating ability of pollen: Part II. Laboratory studies in immersion and contact freezing modes, *Atmospheric Research*, *61*(2), 125-133.

Diehl, K., C. Quick, S. Matthias-Maser, S. K. Mitra, and R. Jaenicke (2001), The ice nucleating ability of pollen - Part I: Laboratory studies in deposition and condensation freezing modes, *Atmospheric Research*, *58*(2), 75-87.

Friedman, B., G. Kulkarni, J. Beranek, A. Zelenyuk, J. A. Thornton, and D. J. Cziczo (2011), Ice nucleation and droplet formation by bare and coated soot particles, *Journal of Geophysical Research-Atmospheres*, *116*, 17203-17203.

Pratt, K. A., P. J. DeMott, J. R. French, Z. Wang, D. L. Westphal, A. J. Heymsfield, C. H. Twohy, A. J. Prenni, and K. A. Prather (2009), In situ detection of biological particles in cloud ice-crystals, *Nature Geoscience*, *2*(6), doi:10.1038/ngeo521.

Prenni, A. J., M. D. Petters, S. M. Kreidenweis, C. L. Heald, S. T. Martin, P. Artaxo, R. M. Garland, A. G. Wollny, and U. Poschl (2009), Relative roles of biogenic emissions and Saharan dust as ice nuclei in the Amazon basin, *Nature Geoscience*, *2*(6), 401-404, doi:10.1038/ngeo517.

Rosenfeld, D. (1999), TRMM observed first direct evidence of smoke from forest fires inhibiting rainfall, *Geophysical Research Letters*, *26*(20), doi:10.1029/1999gl006066.

Rosenfeld, D., U. Lohmann, G. B. Raga, C. D. O'Dowd, M. Kulmala, S. Fuzzi, A. Reissell, and M. O. Andreae (2008), Flood or drought: How do aerosols affect precipitation?, *Science*, *321*(5894), doi:10.1126/science.1160606.

Song, X., and G. J. Zhang (2011), Microphysics parameterization for convective clouds in a global climate model: Description and single-column model tests, *Journal of Geophysical Research-Atmospheres*, *116*, doi:10.1029/2010jd014833.

von Blohn, N., S. K. Mitra, K. Diehl, and S. Borrmann (2005), The ice nucleating ability of pollen: Part III: New laboratory studies in immersion and contact freezing modes including more pollen types, *Atmospheric Research*, *78*(3-4), 182-189, doi:10.1016/j.atmosres.2005.03.008.